Franka Roofs: Can they be a Viable Alternative to the Typical Concrete Roof?

Rebecca Mifsud

Dissertation submitted to the Faculty for the Built Environment, University of Malta in part fulfilment of the requirements for the attainment of the Masters in Structural Engineering.

June 2023

FACULTY/INSTITUTE/CENTRE/SCHOOL Faculty for the Built Environment

DECLARATIONS BY POSTGRADUATE STUDENTS

(a) Authenticity of Dissertation

I hereby declare that I am the legitimate author of this Dissertation and that it is my original work.

No portion of this work has been submitted in support of an application for another degree or qualification of this or any other university or institution of higher education.

I hold the University of Malta harmless against any third party claims with regard to copyright violation, breach of confidentiality, defamation and any other third party right infringement.

(b) Research Code of Practice and Ethics Review Procedures

I declare that I have abided by the University's Research Ethics Review Procedures. Research Ethics & Data Protection form code BEN-2022-00070.

As a Master's student, as per Regulation 77 of the General Regulations for University Postgraduate Awards 2021, I accept that should my dissertation be awarded a Grade A, it will be made publicly available on the University of Malta Institutional Repository.

Acknowledgements

I would like to express my thanks to my tutor Prof. Spiridione Buhagiar B.E.&A. (Hons), M.Sc. (Lond.), D.I.C., Ph.D. (Lond.), F.I.Struct.E., M.A.S.C.E., C.Eng., Perit for his constant guidance, support and insight throughout this dissertation.

I would also like to convey my gratitude to my family for their constant support and understanding throughout my academic studies.

Finally, my appreciation goes to the remarkable friends which I encountered throughout my studies at the University of Malta. Thank you for the laughter, support and shared experiences which I shall cherish throughout my life.

I take full responsibility for any shortcomings in this dissertation

Abstract

When designing contemporary roofing structures, section active systems which primarily rely on bending action tend to be the system of choice. This structural choice manifests itself through the use of reinforced flat concrete slabs. Upon reflection, three observations pertaining to material, geometry and construction emerged.

Firstly, concrete production is resource and energy intensive, accounting for up to 8% of the worlds CO_2 production. Using locally sourced materials could help reduce its demand by encouraging the recycling of local materials and their use in new products such as reconstituted stone.

Secondly, unlike reinforced concrete which can resist both tension and compression resulting from the reinforcement, stone is a brittle material that is only capable of resisting compressive loading. This leads us to the second point being geometry. Maltese architecture has its roots in masonry construction. The above mentioned fundamental properties guided the development of roofing systems on the Maltese islands, resulting in an architecture founded on the use of funicular structures such as arches, vaults and domes. This was one of the primary sources of inspiration for the adopted geometry of the roofing structure devised in this dissertation study.

Lastly, whether a typical cast in-situ concrete roof or an arching masonry system is adopted, both require temporary formwork. Hence, what if the temporary formwork is integrated within the arch, serving as formwork during construction and later becoming an integral part of the structure?

This dissertation adopts the concept of active-bending as the primary method through which an initially flat formwork is actively bent into an arched form corresponding to the Elastica curve which is geometrically similar to an inverted catenary curve. Through the filling of the formwork with voussoirs, the formwork geometrically transforms from the Elastica curve into a segment of a circle. By using physical models which were 3D printed in PLA, this concept was widely explored by testing several different solutions for the integrated formwork, resulting in geometric forms from active-bending and the incorporation of the formwork in the final curved structure. Such geometries ranged from deep arches to shallower ones, eventually translating into the third dimension by creating a vault.

The study proceeds with a finite element analysis of the selected integrated formwork filled with the voussoirs to understand the behaviour of the formwork during the filling process along with the final state of the completed arch, the impacts of material thickness on the formwork integrated arch along with a comparative study between a formwork integrated arch and a traditional masonry arch.

Results from Finite Element Analysis showed that a steel integrated formwork could offer the required flexibility for active bending whilst being stiff enough to withstand the load from the filling process with voussoirs. It could also be noted that an increase in rod thickness of the integrated formwork had a positive impact on the load bearing capacity of the formwork integrated arch, resulting from the activation of the steel formwork which aids the arch in carrying load via bending.

When comparing the formwork integrated arch with a traditional masonry arch with mortar joints, it could be concluded that a significant increase in the load bearing capacity of the arch was noted for the formwork integrated arch along with the improvement in failure mode which was ductile in this case. Such mode of failure is preferred over brittle failure which is sudden.

Through the use of the Funicular Polygon Method, the importance of geometry on the load carrying capacity of the arched roofing structure could be illustrated along with the use of this method as a simplified approach for the analysis of curved structures whose results could then be compared with those from Finite Element.

Keywords: Active-bending, Funicular, Reconstituted Stone, Structure Integrated Formwork, Finite Element Analysis, 3D printing.

Table of Contents

List of Figures

1. Introduction

This chapter shall begin with an introduction to the relevant material and concepts of importance to this study.

1.1. Local Context

Maltese vernacular architecture has been dominated by the use of globigerina limestone as the primary building material since the Neolithic temples (Tonna, 1971). The popularity of this building material was driven predominantly by the following three aspects (Vella I. M., 2019):

a. Local Resources:

Being a small island with limited resources, limestone was the only local available resource that, although heavy and brittle, has excellent workability characteristics due to its softness, which facilitates cutting and trimming.

b. Geographic Limitations:

Being an island, the Maltese could only import goods through vessels. Poor technology and the high costs implied by such transportation, made imports of sizeable and heavy building construction materials challenging. This further pushed towards using the local materials, with limestone being the material of choice.

c. Limited Technology and Resources

Vernacular architecture was heavily shaped by the contextual constraints of the time. Despite the technological limitations, which hindered specific experimentation and development of new structural systems, the reliance on and use of limestone led the architects and builders to become highly skilled and proficient. Detailing and techniques slowly gained over time through experience were of high quality and skill, resulting in an architectural style that defines the Maltese landscape today.

"Masons however make good use of the island's stone for building purposes, or turn it into lime. The Maltese stone is white and remarkable for its softness, it is sawed more easily than wood often huge blocks of stones are prised loose by wedges from the solid rock."

(Vella H. C., 1980)

1.2. The Development of Roofing Systems on the Maltese Islands

Although it has been noted that some roofing structures did use bamboo overlain by a mixture of reed and mud (Tonna, 1971), this is not the case for most buildings where stone was used to create the roofing enclosure.

Perhaps one of the oldest structures where the stone was used to provide an enclosed space was the girna. The girna follows a circular plan with thick stone walls that corbel inwards as the walls move higher up, allowing for a flat slab of stone to span a short distance. Further development followed this system by still making use of corbelled walls yet the roof enclosure consisted of stone slabs (xorok) supported by corbels (kileb) which rest on the corbelled walls. In this manner, the free span of the roof started to increase slowly. Moving slowly to a more

rectangular plan, diaphragm arches (ħnejjiet) were used regularly with corbels on top across which the stone slabs could be spanned.

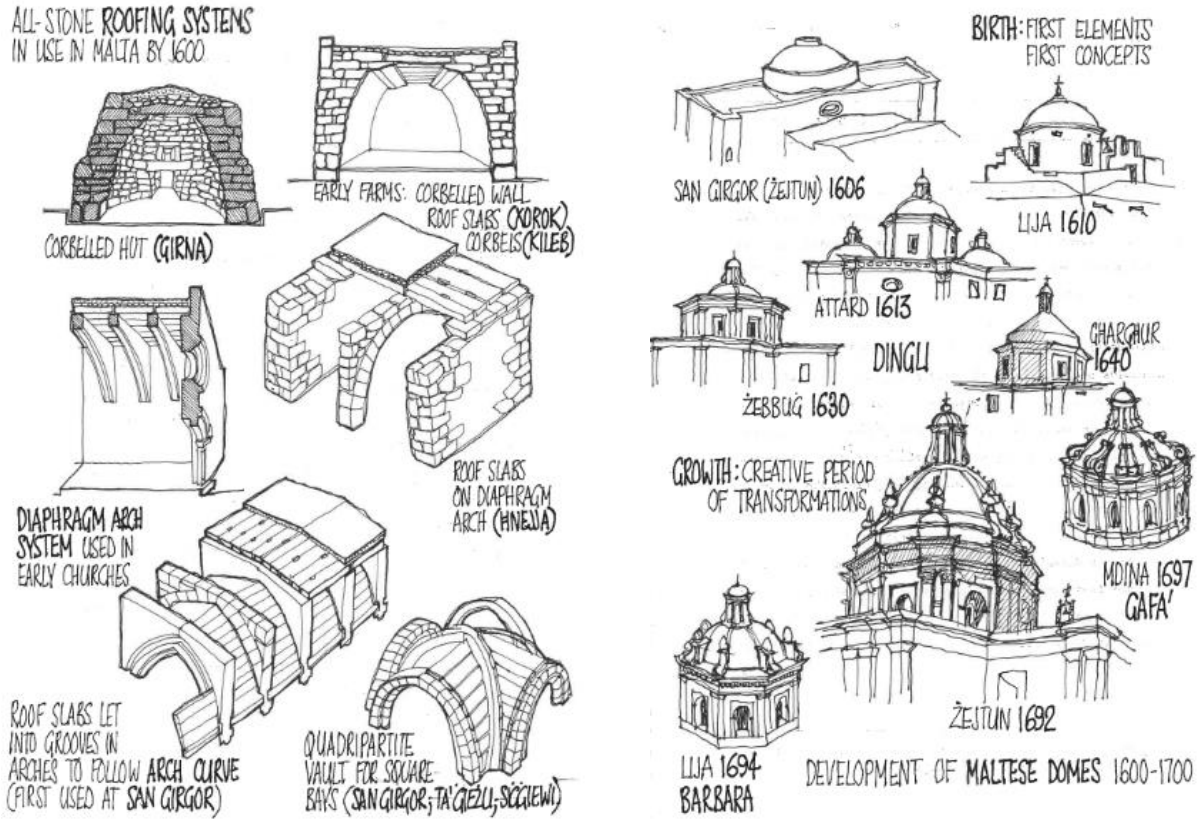

Figure 1.1: Development over the years of Roofing Systems on the Maltese Islands (Tonna, 1971)

With further development and progress, it was realised that using the same roof slabs as in previous applications, these could be embedded in grooved arches, resulting in a curved roof which follows the curvature of the arch. The idea was further expanded by having stone slabs in 2 directions, in each direction supported by arches as displayed in Figure 1.1. The concept of corbelling led to the creation of domes which were used as a roofing structure for most churches around which Maltese villages developed.

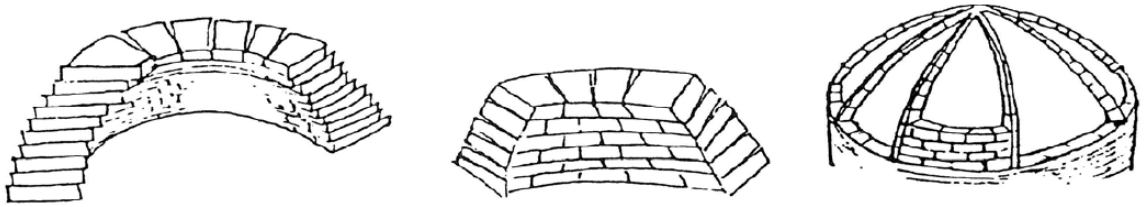

Figure 1.2: Dome Construction (Ghasempourabadi et al., 2012)

With the industrial revolution and technological advancements, new materials such as steel and reinforced concrete could offer new possibilities in the architectural world. Before, stone slabs were spanned across walls or arches, then, the supporting structure was first replaced by timber beams and, further on in time with steel beams (Mallia, 2018).

Figure 1.3: Xorok supported by steel or timber beams

Eventually the stone slabs were replaced with cast-reinforced concrete and precast-reinforced concrete slabs which could span even greater distances, allowing for larger clear spans. However, has the introduction of the new and modern building materials such as steel and concrete led us to abandon the vernacular aspect in contemporary architecture?

1.3. Formwork

Since this dissertation centres around the possibility of reconstituted stone roofing structures in single curvature through bending-active systems, it is important to understand the traditional erection methods used in the construction of traditional masonry roof structures.

Figure 1.4: Formwork for a concrete shell

Although curved structures such as shells and arches are capable of spanning long distances with material savings due to their geometry and light form, the construction process tends to be the discouraging factor for their erection. Curved structures like closed shells, arches and vaults require extensive formwork, also known as centering, if cast in situ or if precast/cut stone voussoirs are used as in Figure 1.5 (Hang et al., 2019). Moreover, such modes of erection are time consuming which is undesirable. Hence, can a modern and efficient solution be found in order to make these curved forms more attractive to execute in the real world?

Figure 1.5: Formwork for a barrel vault (Hang et al., 2019)

1.4. Bending-Active Structures

As defined by (Lienhard et al., 2011), the general definition for bending-active structures is as follows:

Bending-active structures are curved beams and surface structures whose resultant geometry is derived through the "elastic deformation of initially straight or planar elements"

The process through which an initially straight member is elastically deformed is in fact a form of prestress. This is attained via substantial displacements at the nodes in a statically indeterminate system. As a result, large deformations in the member and uniform bending stresses arise. This is what gives the member its prestress. For the member to remain a bending-active element, the deformations must be reversible and hence the induced bending

stresses must always remain below the elastic limit. This is done by choosing a member stiffness which following bending, still follows the linear elastic part of Hooke's Law.

$$\text{Young's Modulus (E)} = \text{Stress } (\sigma) / \text{Strain } (\epsilon) \qquad (1.1)$$

Hence, the member must follow a linear material law which can be graphically expressed through the graph in Figure 1.6 below:

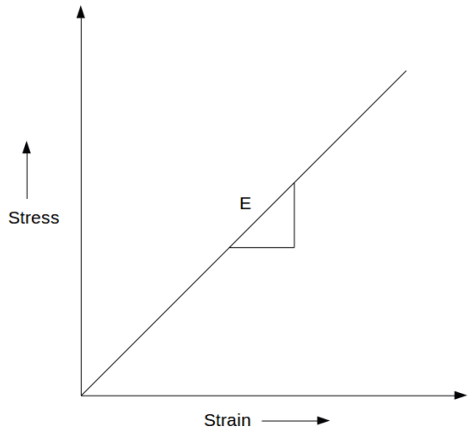

Figure 1.6: Young's Modulus - Linear Material Law

A linear material law was adopted throughout this dissertation whilst the analysis was carried out as geometrically nonlinear. The condensed structural definition of bending-active can be written as:

> *Confined structures which are in a statical indeterminate state having residual bending stresses. (Lienhard et al., 2014)*

The determination of a bending-active geometry can only be obtained either via the use of physical models or else through a form determining software such as the Finite Element Method of Analysis.

1.5. Terminology

Although an in-depth explanation of important terminology can be found within this dissertation, some clarifications shall be made to properly understand the nomenclature used. The term 'integrated formwork' refers to the supporting structure used for the erection of roofs in single curvature which shall become part of the final structure. On the other hand, the use of the term 'the Elastica' refers to the resulting curved geometry from the elastic deformation of an initially straight element. The term 'reconstituted stone' refers to the an engineered type of hard stone made up of limestone construction waste which can be worked in a similar way to quarried globigerina limestone.

1.6. Motivation

This research has been motivated by three main aspects;

First is the material. Most roofing structures are made of concrete, a highly polluting material, accounting for up to 8% of the worlds CO_2 production. Moreover, locally we are facing the problem of high volumes of demolition waste that essentially constitutes globigerina limestone, a deteriorating resource due to its intensive extraction. This could in turn be used for the production of reconstituted stone..

Reconstituted stone could then be used to construct roofing structures. An important consideration to be made revolves around the material properties of reconstituted stone, leading us to the second main aspect of this research, the structure's geometry. Since masonry is strong in compression but weak in tension, a curved roofing structure is adequate to carry loading in compression, leading us back towards traditional concepts of Maltese architecture.

An immediate drawback emerges, leading us to the third aspect; the need for a temporary formwork which on site is expensive and time consuming. Here it is worth noting the already conducted research by (Calleja, 2018) on auxetic structures and their potential application in constructing grid shells. The existing research has arrived at an open roofing structure. The following question arises when combining the above traditional concepts with this research. What if the negative spaces are filled with reconstituted stone elements and the positive spaces become the 'mortar' between the stone, represented by an integrated formwork?

In this way, the formwork is retained as part of the final structure, possibly enhancing and optimising the structural performance of the roofing structure whilst facilitating on-site construction. The intention is to devise a bending-active integrated formwork for creating a feasible roofing structure in single curvature, also known as a developable structure, which could be a viable replacement to the typical flat concrete roof structures.

1.7. Research Objectives

The main objective of this research is to understand whether it is possible to integrate the formwork of a roof under single curvature as part of the final structure and its potential benefits with respect to structural performance and on-site construction.

The project is divided into two main parts;

a. First are several physical geometric studies deriving the overall geometry, the span to-height ratios, and the geometric pattern of the integrated formwork (study 1- study 7).

b. Once the final geometry has been selected, several Finite Element studies shall be carried out to understand the structural behaviour of the integrated formwork within a single curvature roofing structure which shall constitute of two materials; reconstituted stone for the voussoirs and steel for the integrated formwork (study 8 – 11).

The ultimate aim is to understand the structural feasibility of such a proposed system.

1.8. Research Questions

i. *Franka Roofs: Can they be a viable alternative to the typical concrete roof?*

ii. *What is the ideal geometric pattern for the integrated bending-active formwork for a roof in single curvature as part of the final structure and what is its structural feasibility?*

iii. *Which material can undergo bending to create the desired curved geometry whilst being stiff enough once fixed in place to accommodate the loading of the stone?*

iv. *What is the load-bearing capacity of such a curved reconstituted stone roof with the integrated formwork and how does it compare to a traditional masonry curved roof ?*

1.9. Research Method

For a more holistic understanding of the roofing structure's geometry and structural behaviour, numerical analysis via computer software and experimental methods via physical models are used.

Finite Element Analysis is carried out to obtain a detailed mechanical description of the stresses within the geometry, material properties and the interaction between the reconstituted stone voussoirs and the integrated formwork. In parallel, physical models are used for a more visual and perceptive understanding of the problem at hand.

1.10. Layout

In Chapter 1, the relevant theories and principles are first outlined as an introduction to the fundamental aspects of this study. These are followed by the motivations that have led to this research along with the main research objectives and questions. The experimental and numerical research methods adopted to derive the appropriate geometry and structural behaviour are also outlined in this chapter.

Chapter 2 starts by categorising structures by structural action, one of the actions being active-bending as a formation process guided by elastic deformation. This was followed by beam theory and the resulting geometry from elastically bent elements being the Elastica. Different methods for solving its path are outlined mainly geometrical approaches such as the Euler-Poisson equation, analytical software such as Grasshopper 3D and Finite Element Method using (Lusas, 2023). The section proceeds with a moment-to-curvature derivation using similar triangles, followed by a study on suitable materials for bending-active structures. The international and local context of such structures is outlined, followed by the 3 main approaches used to design bending-active structures: behaviour-based, geometry-based, and integral. Modes of erection and the effect of scale on bending-active structures are also included. The text proceeds with an in-depth understanding of funicular forms, mainly focusing on arches, the effect of rise on the lateral thrust, and the importance of geometry and the mortar joint on structural behaviour. A simplified approach for arched analysis was outlined as the Funicular Polygon followed by Heyman's three assumptions and the importance of the rule of middle thirds. The chapter ends with a brief outline of the use of 3D printing in creating prototypes.

In Chapter 3, Gaussian curvature was introduced as a geometrical description of the devised structures in terms of zero curvature, corresponding to developable structures. An insight on the variation in radius of curvature along the Elastica curve was included followed by a tensile

restraining system that can modify the Elastica to attain a constant radius of curvature. Eleven short studies followed this section. The first seven studies deal with creating analytical and physical models to understand the geometrical behaviour of the formwork under deformation and upon loading. The rest of the studies aim to understand the true behaviour of the formwork during the bending stage and the completed arch stage. This was done using the Method of Finite Element Analysis (FEA) along with the Funicular Polygon Method.

Chapter 4 deals with the attained results from the methodology, whilst Chapter 5 concludes this dissertation study by focussing on the main points resulting from each chapter along with a discussion of the research questions identified at the beginning of this dissertation and the attained insights from the results. In this chapter, the dissertation also provides proposals that future researchers can further investigate as a continuation of this study.

2. Literature Review

2.1. The Structural Systems Framework

Throughout the history of structural engineering, understanding and categorising structural systems has been of great importance in developing physics-based analytical structural methods. However, in the present age, such a method of analysis is not the only option for structural design. Advancements in Finite Element software have uncovered a new potential which could not be unravelled with a thinking centred around typology. As a result, structures can be considered as a series of interconnected elements rather than one singular typology.

> *"Engineers are trained in 'model thinking', in knowing all these typologies and then choosing and applying the most appropriate one for a given design task…The introduction of computational design offers the potential to break through these barriers of model thinking (thinking in discrete typologies) in structural engineering."* (Knippers, 2013)

Although the capacity of Finite Element modelling is superior to physics-based modelling, it can be too intricate and lack interactivity when designing a structure. Potential lies in the possible combination of physics-based and Finite Element modelling in a way that they would aid each other. Bending-active structures could add to the discussion in their ability to develop different structural systems resulting from their elastic bending behaviour. Since a unique structural system cannot describe such structures, it would be wise to understand the main structural families so that one can abstractly locate them in the realm of structural action (Lienhard et al., 2014).

2.2. Structural Categorization by Action

Heino Engel made a prominent attempt at structural categorization in the end of the 20th century. He devised a system that categorized structures into a series of families, which can be further subdivided into types and structures (Engel, 1997). Here a simplified approach will be explained as devised by (Lienhard et al., 2011), where seven main structural categories are identified based on structural action. Structural action refers to the mechanism by which a structure receives, transfers, and transmits load.

2.2.1. Section Active Structures

Section active structures will carry and resist the applied loads through bending moments and shear by using their cross-section properties and overall geometry. Such structures include beams, slabs, plates, frames and grillages.

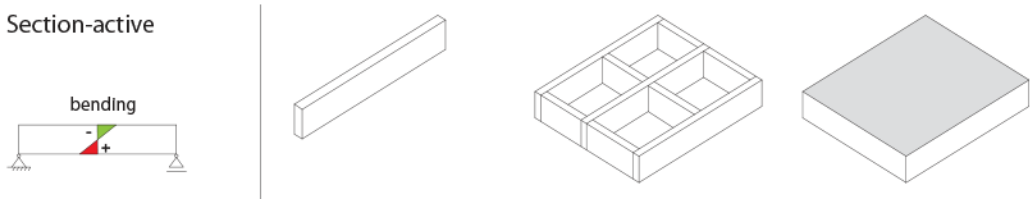

Figure 2.1: Examples of section active structures (Lienhard et al., 2014)

2.2.2. Vector Active Structures

Straight and linear elements form vector active structures joined together via pin joints in a triangulated manner. This creates a stable geometric form that efficiently carries load axially, with the members within the structure either in pure tension or compression. These structures have in common properties with form active structures yet differ in their end conditions since vector active structures have no lateral thrust. Examples of such structures include 2D planar or curved trusses and Space Frames.

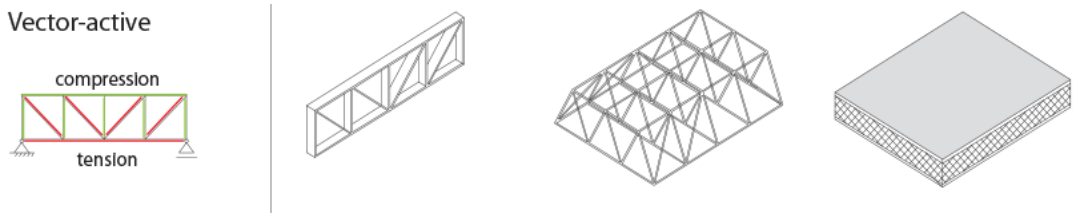

Figure 2.2: Examples of vector active structures (Lienhard et al., 2014)

2.2.3. Surface Active Structures

Surface active structures will carry load mainly through surface tension, surface compression and shear stresses with negligible bending. Such structures tend to be built from reinforced concrete with steel mesh. Examples of such structures include folded plates, plate structures which carry loading within their plane and shell structures.

Figure 2.3: Examples of surface active structures (Lienhard et al., 2014)

2.2.4. Form Active Structures

Form active structures carry structural loading either through pure compression or pure tension. This eliminates shear and moments in such structures. Hence such structures rely heavily on their form and geometry to allow forces to flow along lines of thrust. Examples of such structures working in pure tension include tensile structures such as cable nets, pneumatic structures and membrane structures, while those working in pure compression include funiculars such as arches, vaults and domes.

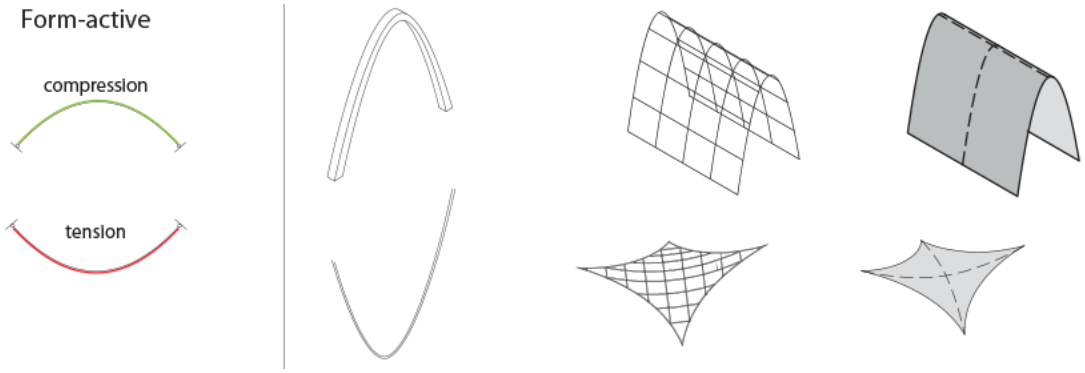

Figure 2.4: Examples of form active structures (Lienhard et al., 2014)

2.2.5. Height Active Structures

Height active structures are predominantly defined by their verticality. Such structures can use a combination of the above discussed categories to transfer loading (refer to sections 2.2.1 – 2.2.4). Examples include tall and slender structures such as multi-storey buildings and towers.

2.2.6. Hybrid Structures

As the title implies, such structures transfer loading through a combination of mechanisms by linking two primary systems into a coupled system. Typical examples of such combinations include section active with form active structures and the combination of vector active with surface active structures

Figure 2.5: Examples of hybrid structures (Lienhard et al., 2014)

2.2.7. Understanding Bending-Active Structures

As the introduction explains, bending-active structures are the resulting geometries from elastically bent elements that are initially straight. In this section, bending-active structures shall be further explored.

2.2.7.1. Why Bending Active-Systems?

An attractive property of bending-active systems is the simplicity by which they attain a curved geometry by applying a horizontal load at the supports of an initially straight element. When it comes to the real world, the manufacture of straight elements is simpler, whilst when it comes to transportation, straight elements will take up less space volumetrically, possibly allowing for longer elements to be transported.

On site, the transported elements can be easily pre-assembled on the ground and then erected in place by active-bending of the structure. In this modern age driven by economics, the efficient use of materials, ease of prefabrication, transportation, assembly and construction are all factors which make a project desirable and plausible. Hence, using bending-active structures offers a flexible and aesthetic design whilst being feasible in the real world (Gengnagel et al., 2014).

2.2.7.2. Bending-Active Structures as a Formation Process

Rather than being categorized as a defined structural system, bending-active systems are more of a formation process through which their geometric and loading properties are formed during the process of elastic bending.

Bending-active structures carry loading through bending and normal actions and hence can be classified as a sub-group of section active structures. In their final state, once fixed in place,

they can achieve true arching action; hence, their behaviour becomes similar to that of surface active and form active structures.

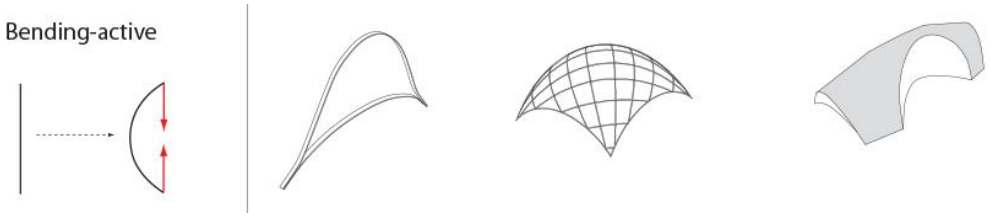

Figure 2.6: Examples of bending active structures (Lienhard et al., 2014)

2.3. An Introduction to the Mechanical Behaviour of Bending-Active Structures

2.3.1. Elastic Kinetics/Compliant Mechanisms

Let us first understand the basics categories and branches of classical mechanics in order to be able to categorize the mechanical behaviour of bending-active structures;

Statics can be defined as the branch of mechanics concerned with the way forces act on stationary rigid bodies.

Dynamics can be defined as the branch of mechanics concerned with the way forces act on moving rigid bodies.

Kinematics can be defined as the branch of mechanics concerned with the movement of bodies whilst neglecting the forces which would have led to such a movement.

Kinetics can be defined as the branch of mechanics concerned with the movement of bodies yet unlike in kinematics, is concerned with the forces which lead to movement.

The member will experience elastic deformation in Bending-Active Structures due to the applied force leading to movement. Hence since there is a transfer of forces/displacement from one point to another as the member deforms elastically, Kinetics or more accurately, Elastic Kinetics are the branch under which bending-active structures fall. Elastic Kinetics are also known as compliant mechanisms in mechanical engineering. Hence it could be deduced that bending-active structures are compliant mechanisms that allow for reversibility from an original state to a prestressed state (Lienhard et al., 2014).

2.4. General Definitions

The definitions below have been added for a complete understanding of specific terms and structural concepts;

a. Nonlinearity

In a linear relationship, if the inputs of an equation are multiplied by a factor n, the output is expected to increase by a factor n. This relationship results in a straight line plot in the form of y=mx+c. In a nonlinear relationship, this linearity and proportionality are absent and will result in a curved plot where at least one term has a power greater than 1. Non-linearity can manifest itself in many ways, such as the nonlinear behaviour of materials which leads to plasticity (not the case in bending-active structures), boundary conditions nonlinearity which can be reviewed

in bending-active structures and nonlinearity in geometry which is the most important relationship in bending-active structures and hence should always be taken into account.

b. Nonlinearity in Geometry

Nonlinearity in Geometry arises as a result of large deformations which go against small deflection theory. Geometric nonlinear theory uses static equilibrium on the deflected member, resulting in resultant forces of a linear proportion and a nonlinear deformation dependant proportion. Due to the consideration of equilibrium on the deformed member, changes to the stiffness matrix K are to be expected. This is due to the imposed stresses arising in the deformed shape, which create geometric stiffness (can be referred to as initial stress-stiffness).

c. Geometric Stiffness/ Stress Stiffening

Geometric stiffness is a property which varies with two main factors: structural geometry and loading. If a member is loaded in tension, this will increase member stiffness as the internal member forces act in the opposite direction of the applied load. Conversely, if a member is loaded in compression, the member will experience a reduced stiffness as the direction of the resulting internal forces is the same as the applied force. Hence the longitudinal component of a force is the one that will increase/decrease structural stiffness as it will either pull the system causing it to extend or else draw the member causing it to contract. The former is also referred to as stress stiffening. Stress or tension stiffening will translate into a stiffening effect on the geometrical stiffness matrix K, which is considered in nonlinear structural analysis software such as Ansys, Lusas, etc.

d. Prestress

Prestressing is a system resulting from geometric nonlinearity that leads to stress stiffening, which increases the stiffness of the member yet does not affect its load bearing capability. In the case of bending-active structures, the type of prestress is mechanical, as it results from induced displacements.

e. Residual Stress

Residual stress can be defined as the remaining stress within a material when all the external loads/forces have been eliminated. Residual stresses can result from prestressing forces, stresses arising from elastic bending and others. These residual stresses such as structural stiffness, stability and eigen buckling frequencies can impact a structure's behaviour

f. Eigenvalues, Eigenvectors and Eigenfrequencies

Eigenvalues are scalar quantities which can be mathematically represented by equation 2.1 where λ and x are the eigenvalues and eigenvectors respectively whilst the magnitude of the eigenvalues is attained through equation 2.2:

$$\underline{\underline{A}}\underline{x} = \lambda \underline{x} \qquad (2.1)$$

$$\det\left(\underline{\underline{A}} - \lambda \underline{\underline{E}}\right) = 0 \qquad (2.2)$$

Eigenvalues are useful as they can be used to find the natural frequencies of vibration of a structural system. These are also known as eigenfrequencies. Making use of the linearised eigenproblem where K and M are the stiffness and mass matrices respectively, the frequency of vibration w can be found by taking the square root of the eigenvalue λ whilst the vibration mode shape is determined through the eigenvector x. These relationships can be represented mathematically as:

$$\underline{\underline{K}} \cdot \underline{x} = \lambda \cdot \underline{\underline{M}} \cdot \underline{x} \qquad \text{with } \lambda = \omega^2 \tag{2.3}$$

2.5. An Introduction to Bending Theory

To understand bending theory, derivations and explanations shall consider a simple beam of uniform cross-section. Bending can be defined as the resulting deformation of a vertically loaded element, in this case, a simply supported beam. Under such loading, a stress gradient will result in the beam, with compressive stresses forming at the top and tensile stresses at the bottom. As a result, a neutral plane will form between the top and bottom stresses also known as the neutral axis. The member's resistance to bending is known as the section modulus (I) and is the distance between the neutral axis and the extreme ends of the member's section.

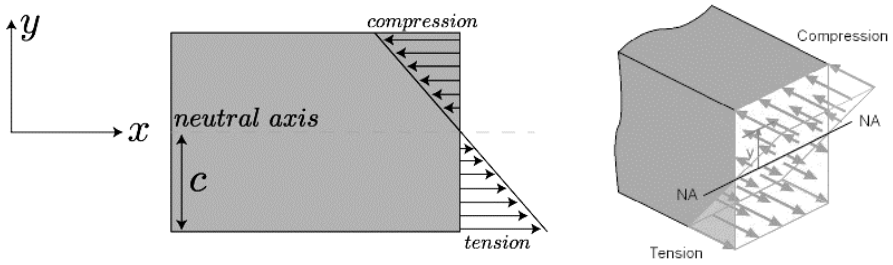

Figure 2.7: Typical Bending Stress Diagram

2.5.1. Nonlinear Beam Theory

The most known bending beam models in the field of structures are the Euler-Bernoulli Model and Timoshenko Model, which shall be briefly explained in sections 2.5.1.1 and 2.5.1.2. These models shall explain the structural behaviour of the bending-active formwork.

2.5.1.1. Beam Model 1: The Euler-Bernoulli Model

This model, sometimes also referred to as the classical beam model, is based on two main assumptions (The Bernoulli-Euler Beam Theory, 2023):

Assumption 1: Plane sections remain plane

If, we were to take an arbitrary cut through a beam following bending, the plane would be flat and perpendicular to the neutral axis just as it was before bending. This assumption remains relevant unless the beam becomes very short and deep. Otherwise, the Timoshenko model is more accurate.

Assumption 2: The slope of the deformed beam is small

If slope angles are small, the displacement Δx at a location x along the beam will result in a slope θ as follows:

$$\theta = \frac{d\Delta}{dx} \tag{2.4}$$

Moreover, if θ is small, then squaring the slope value will result in an even smaller value closer to 0. Moreover, since angles are small, the rise over run ratios when converted to angles will be approximately equivalent to:

$$\begin{aligned} \sin\theta &\approx \theta \\ \cos\theta &\approx 1 \end{aligned} \tag{2.5}$$

This approximation is most accurate for slopes up to five degrees. From these two assumptions we arrive at the simplified differential equation of bending as follows:

$$M = EI\frac{d^2\Delta}{dx^2} \tag{2.6}$$

2.5.1.2. Model 2: The Timoshenko Model

Like the Euler-Bernoulli Model, Timoshenko agrees with the assumption that plane sections remain plane, yet in his model, the planes are no longer perpendicular to the neutral axis but rather rotate about it. This assumption considers the effects of rotational bending and deformations from shear. If these considerations are neglected, then the equations of Euler-Bernoulli and Timoshenko would be identical (Li, 2023).

$$\frac{\mathrm{d}w}{\mathrm{d}x} = \varphi - \frac{1}{\kappa AG}\frac{\mathrm{d}}{\mathrm{d}x}\left(EI\frac{\mathrm{d}\varphi}{\mathrm{d}x}\right). \tag{2.7}$$

This term considers the effects of rotational bending and deformations from shear

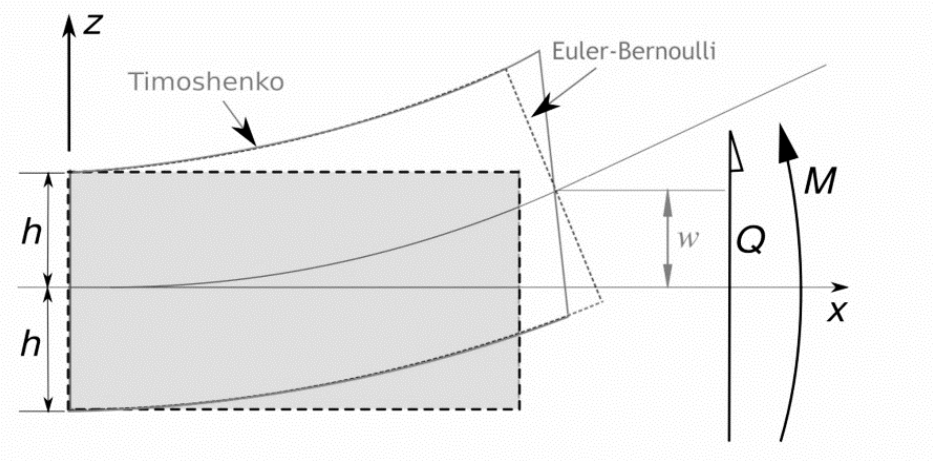

Figure 2.8: Superimposition of the Euler-Bernoulli and Timoshenko Models (Nguyen, 2017)

2.5.1.3. Comparing the Beam Models and considering Nonlinearity

The approach taken by Timoshenko gives a more accurate model especially for deeper members. However, most structural members are relatively shallow in depth compared to their length (e.g. a 150mm deep beam for a 3000mm span); hence, both theories will offer sufficient results (Fertis, 2006).

Although the Euler-Bernoulli model has a second order nonlinear differential equation for larger deformations, this does not give straightforward answers due to its high complexity. Such an equation would be as equation 2.8:

$$\frac{1}{r} = \frac{y''}{\left[1 + (y')^2\right]^{3/2}} = -\frac{M}{EI} \qquad (2.8)$$

Although complex to solve, this equation proves that curvature (r) is always directly proportional to the bending moments for both small and large deformations. If we were to solve the above equation, we would arrive at the *Elastica*.

2.5.2. The Elastica

This section will give an in-depth overview of the Elastica's origins, behaviour and geometry.

2.5.2.1. The Elastica and its origins

As described by (Lienhard et al., 2013), the **Elastica** describes the "elastic deformation curve of a slender single span beam in its post-buckling state." Yet unlike in beams where a uniform curvature is assumed to correspond to small deflection, curvature in the Elastica is non-uniform (Lee, 2019).

The concept of the Elastica first appears in the 13th century by Jordanus de Nemore claiming that "when the middle is held fast, the end parts are more easily curved." He also remarks that the solution for such a problem is a circle yet this is incorrect. Although a circle can solve the Elastica, it is not the case for the stated claim nor all the possible Elastica curves.

Several centuries later, in 1638 Galileo continued on the work done by de Nemore and came up with a mathematical formulation for the problem. If one considers the equilibrium of moments, the Elastica can be formulated by three fundamental concepts; moments, curvature and the relationship between moments and curvature. If we consider an ideal elastic strip, this should lead to a linear relationship. This mathematical study was founded by analysing a cantilever beam loaded at one end. Through this, he could conclude that the ratio of the moment at "c" to the moment of resistance is of the same proportion as the ratio of length CB to half the depth BA. From this, the ratio of resistance to breaking must also be in the same proportion as the ratio of length CB to half the depth BA as in Figure 2.9. These simple relationships allowed Galileo to arrive to other correlations such that there is a scaling relationship which shall be discussed in section 2.9 (C.Truesdell, 1970).

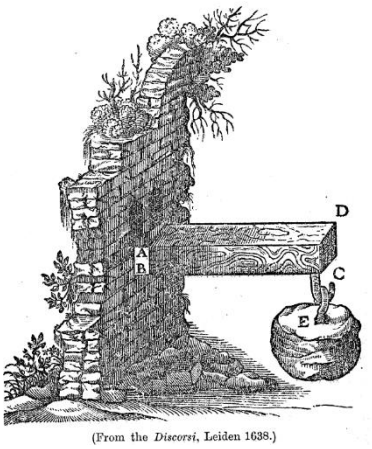

Figure 2.9: Cantilever beam loaded at one end (C.Truesdell, 1970)

In 1678, Hooke came up with the mathematical theory which states that the applied load is directly proportional to the extension. Nowadays, this theory is known as Hooke's Law. At this time, Hooke also briefly addressed the elastic strip problem yet was still unaware of how the curvature of a singular fibre relates to bending moments and how the fibres influence each other.

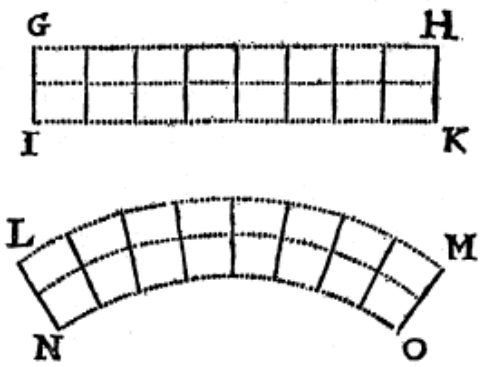

Figure 2.10: The elastic strip problem (C.Truesdell, 1970)

James Bernoulli was sceptical of the linear relationship of Hooke's law and hence aimed to consider nonlinearity in displacement. In 1691 James Bernoulli formulated the exact Elastica problem as follows: Considering every node of curve AB, the product of curvature radius and the perpendicular distance BC is a constant. This means that the radius of curvature is inversely proportional to distance BC.

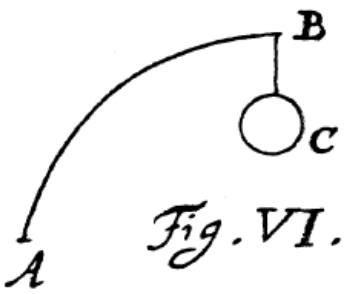

Figure 2.11: Formulation of the Elastica problem by Bernoulli (Levien R. , 2008)

In 1694 he published the exact solution, yet this publication did not attract much interest. It was in 1742 that Daniel Bernoulli rekindled the problem of the Elastica and continued on the work of James Bernoulli. Following communication with Euler, Bernoulli managed to build on the previous work of Euler and by making use of variational techniques, managed to arrive at a complete family of Elastica curves. Although he acknowledges that infinite types of Elastica curves exist, he created a classification of 9 possible species as follows:

Euler's species #	Euler's Figure	Euler's parameters	λ	comments
1		$c = 0$	$\lambda = \infty$	straight line
2	6	$0 < c < a$	$0.5 < \lambda$	
3		$c = a$	$\lambda = 0.5$	rectangular elastica
4	7	$a < c < a\sqrt{1.651868}$	$.302688 < \lambda < .5$	
5	8	$c = a\sqrt{1.651868}$	$\lambda = .302688$	lemnoid
6	9	$a\sqrt{1.651868} < c < a\sqrt{2}$	$.25 < \lambda < .302688$	
7	10	$c = a\sqrt{2}$	$\lambda = .25$	syntractrix
8	11	$a\sqrt{2} < c$	$0 < \lambda < .25$	
9		$a = 0$	$\lambda = 0$	circle

Figure 2.12: Mathematical Classification of the Elastica Curves (Levien R., 2008)

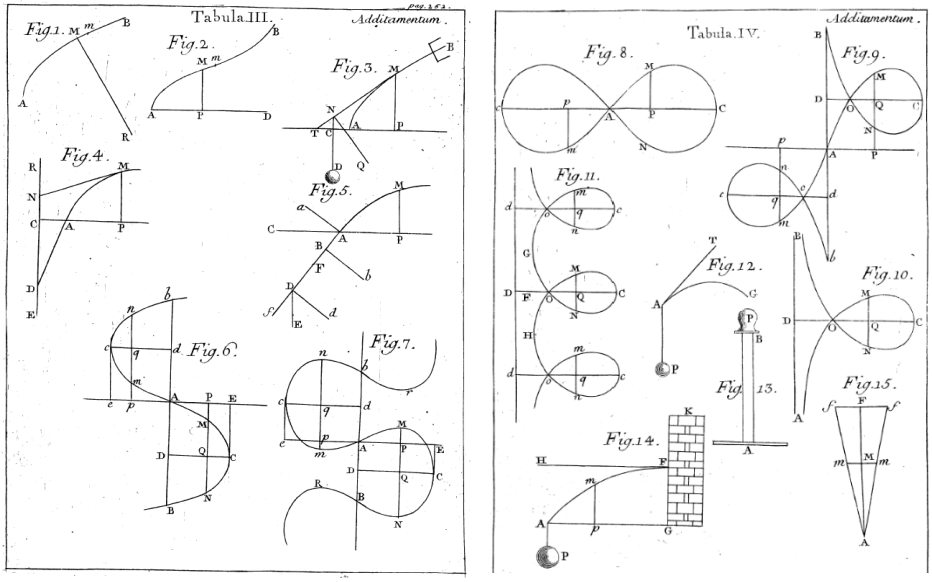

Figure 2.13: Geometrical Classification of the Elastica Curves (Levien, 2008)

Through the use of parameters a, c and λ one can mathematically solve this variational problem and determine the gradient of every point of the path taken by the Euler-poisson equation (equation 2.9) (Levien R., 2008):

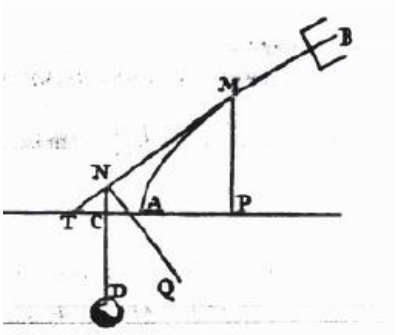

Figure 2.14: A sketch by Euler of a fixed rod at B subjected to a load CD of lever arm c (length of CA) (Goss, 2003)

$$\frac{dy}{dx} = \frac{(a^2 - c^2 + x^2)}{\sqrt{(c^2 - x^2)(2a^2 - c^2 + x^2)}} \tag{2.9}$$

Where c is distance AC on Figure 2.14, corresponding to the lever arm and a is a parameter resulting from the following correlation (Goss, 2003);

$$a = \frac{Ek^2}{T}. \tag{2.10}$$

Where:
E = Modulus of Elasticity of the Material
K^2 = I = Second moment of area
T = Applied axial force

The Elastica can be tackled through various methods such as the method of mechanical equilibrium, as an elliptical integral solution (as in section 2.5.2.3) and as a calculus of variation (as Euler) problem. The study of the Elastica is an important sector in understanding of splines in a mathematical manner.

2.5.2.2. The Elastica in Structural Terms

For our scope, we are interested in understanding the Elastica in terms of structural mechanics so as to apply it in the design of bending active structures. Now the Elastica can be explained in different manners, yet here reference will be made to the following three approaches:

Complex Techniques

Approach 1: The Elastica as the post-buckling curve

Approach 2: The Elastica as the path that creates the lowest bending energy in the system

Finite Elemen

Approach 3: The Elastica as an equilibrium of forces in a physical and static arrangement.

Approaches 1 & 2 require sophisticated mathematical techniques (e.g. elliptical integrals) to solve. If we consider approach 2, which considers the Elastica as the path that creates the lowest bending energy in the system, we can better understand the link between the form/curvature taken (the Elastica) by a bending-active structure and its mechanical behaviour. The form adopted by a constrained loaded system is not random nor by chance. Depending on the applied loads the system intends to bear, the system will deform accordingly to best carry the loading whilst requiring the least potential energy to keep such a form. Such an approach allows engineers to develop aesthetic yet structurally efficient structures. This relationship can be mathematically represented by equation 2.11 (Lienhard et al., 2014):

`

$$\tilde{E}[\kappa(x_0)] = \frac{1}{2}\int_0^l EI \cdot \kappa(x_0)^2 dx_0 \tag{2.11}$$

$\kappa(x_0)$	local curvature
$\tilde{E}$	total bending energy [J] = $[\frac{kg \cdot m^2}{s^2}]$
E	Youngs modulus [N/mm²]
l	Length of the deformed beam[m]

The behaviour of the Elastica can be summarized by two different end conditions (Levien R. L., 2009)*:*

Condition 1: Unconstrained

If unconstrained, the Elastica corresponds to Euler's species 1 (Figures 2.12 & 2.13) where curvature c=0 and λ= infinity. This results in a straight line path and hence has 0 bending energy.

Condition 2: Constrained

If constrained, typically with boundary conditions corresponding to a pin-pin configuration, curvature c is no longer 0 and λ will vary depending on the resulting form such as circle, rectangular Elastica etc. The bending energy will be a value greater than 0 yet will be the lowest possible for such a form.

Figure 2.15: The 2 main conditions of the Elastica

To solve *approaches 1 & 2* we require advanced mathematical techniques and hence, a grasshopper script was used in section 2.5.2.3. The resulting solution is geometrical based, hence not the only property required to bend active structures. As a result, *approach three* was later adopted in the study where form finding of curves that result in the lowest bending energy was done through nonlinear Finite Element Analysis.

2.5.2.3. The Geometric Approach: Determining the Coordinates of the Elastica using Elliptical Integrals

Based on a geometric study, elliptical integrals can arrive at the x and y coordinates of every point of the Elastica curve. The following derivation was devised by (Pacheco & Piña, 2007) and (Valiente, 2004) on the previous studies of the Elastica done by Euler.

Consider a rod of uniform cross-section as shown in the below diagram with parameters L (length), b (width) and h (height).

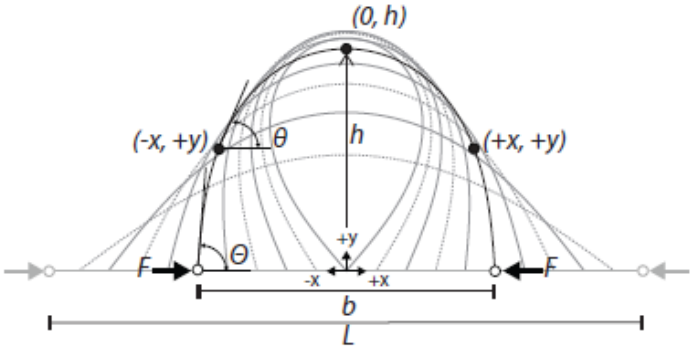

Figure 2.16: Elastica curves to derive its coordinates

These three parameters (L,b,h) can be correlated to parameter m which is usually in the range of 0<m<1. Parameter m is needed to calculate the elliptical integrals E(m) and K(m). K(m) and E(m) are the complete elliptical integrals of the first and second kind respectively. Hence this correlation can be summarized by the following three equations:

$$\frac{b}{L} = 2\frac{E(m)}{K(m)} - 1 \tag{2.12}$$

$$\frac{h}{L} = \frac{\sqrt{m}}{K(m)} \tag{2.13}$$

$$\frac{h}{L} = \frac{\sqrt{m}}{K(m)} \tag{2.14}$$

Furthermore, the m parameter which is unique to every configuration of the Elastica, can be expressed in terms of the tangential angle at the pin support of the Elastica path by parameter Θ as follows:

$$\Theta = 2\sin^{-1}\left(\sqrt{m}\right) \tag{2.15}$$

Using the m and Θ parameters, the cartesian coordinates (x and y) can be obtained. To arrive at these coordinates, one should first assume a set of y-values starting from 0 up to h, corresponding to the curve's highest point. Using these y-values, the corresponding rotations θ could be found (Valiente, 2004).

$$y = \frac{0.5L\sqrt{2}\,\sqrt{\sin(\Theta - \frac{\pi}{2}) - \sin(\theta)}}{K(m)} \tag{2.16}$$

$$\theta = \sin^{-1}\left(\sin\left(\Theta - \frac{\pi}{2}\right) - \left(K(m)\frac{y}{0.5L\sqrt{2}}\right)^2\right) \tag{2.17}$$

Once the y-coordinates and rotations θ are found, the corresponding x-coordinates are obtained from the equation below;

$$\pm x = \sqrt{\frac{EI}{2F}}\int_{\theta}^{-\frac{\pi}{2}} \frac{\sin\omega}{\sqrt{\sin(\Theta - \frac{\pi}{2}) - \sin\omega}}\,d\omega \tag{2.18}$$

Force F is the axial load applied at the supports which can be quantified by the below equation (Pacheco & Piña, 2007);

$$F = EI\left(2\frac{K(m)}{L}\right)^2 \tag{2.19}$$

Substituting (eq. 2.19) in equation (eq. 2.18) eliminates the flexural rigidity term EI, and hence the resulting equation gives a purely geometric relationship as follows;

$$\pm x = \frac{0.5L}{\sqrt{2}\,K(m)}\int_{\theta}^{-\frac{\pi}{2}} \frac{\sin\omega}{\sqrt{\sin(\Theta - \frac{\pi}{2}) - \sin\omega}}\,d\omega \tag{2.20}$$

(McElwain, 2014) took the above derived mathematical explanation and created a grasshopper script which relates parameters such as the length, rise and span in the expected form of the Elastica. The script runs on an iterative process, trying to find the correct value of m for the inputted parameters. This allows for a quick visualisation of the Elastica function.

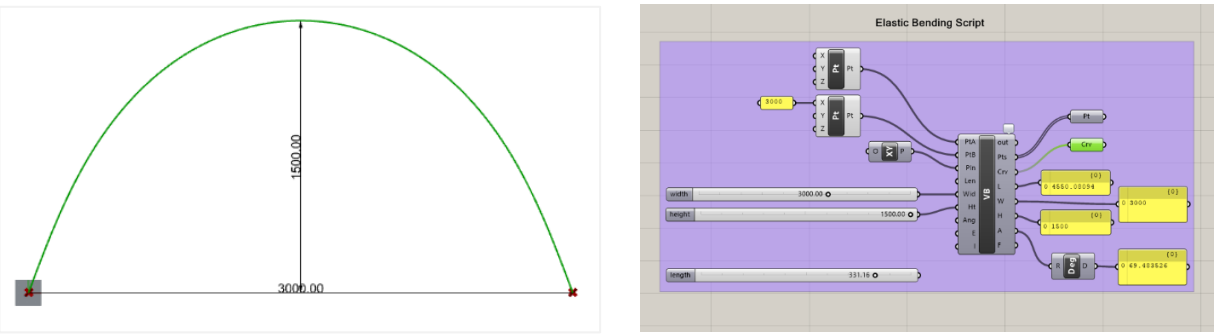

Figure 2.17: Left: Visual Representation of the Grasshopper Elastica script on Rhino; Right: Grasshopper script of the Elastica

2.5.2.4. Structural Behaviour of the Elastica

As briefly mentioned, the Elastica can be defined as the path that creates the lowest bending energy in the system. The corresponding initial stress resulting from such bending impacts the total stress a structure can withstand. The total stress a structure can withstand consists of the sum of the initial stress from bending and the additional applied stress resulting from loading (Gengnagel et al., 2014).

$$\text{Total Allowable Bending Stress } (\sigma m,rd) = \text{Initial Bending Stress (Residual Stress } \sigma(xo) \text{)} + \text{Additional Applied Stress} \quad (2.21)$$

Hence a high initial bending stress will lead to a structure which can carry a lower load over a similar structure with low initial stress. The initial stress resulting from this bending action can be determined through equation 2.28.

2.5.2.5. How to Lower the Initial Bending Stress?

a. *Select a material with a low elastic modulus*
b. *Lower the depth of the material*
c. *Increase the radius of curvature*

A deeper section profile is needed to reduce stress and deformations from applied loading. However, these properties are in conflict as we require a flexible material that still needs stiffness. Considering the above, if a material has a moderate/high stiffness it requires a higher force to deform in the required shape. Hence, a high initial stress (residual stress), and higher stiffness is beneficial in having an overall stiffer structural system which will exhibit lower deformations upon additional applied stresses (Gengnagel et al., 2014).

2.5.3. Relationship between Moment and Curvature

The Euler-Bernoulli law described above by equation 2.8 manifests a moment-to-curvature relationship. However, this correlation can also be deduced through the use of similar triangles. Below is the procedure for such a derivation (Lienhard et al., 2014):

a. Consider a section of a deflected beam as follows:

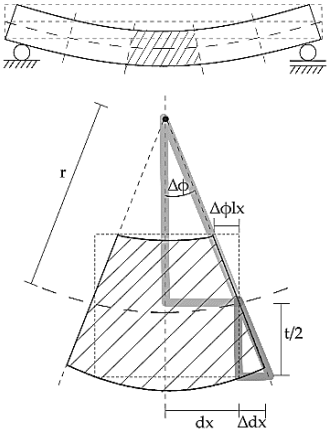

Figure 2.18: Derivation considering a typical section of the beam

b. By Similar Triangles:

$$\frac{r(xo)}{dx} = \frac{t/2}{\Delta dx} \qquad \frac{t/2}{r(xo)} = \frac{\Delta dx}{dx} \tag{2.22}$$

c. Arranging and including Hooke's Law:

$$\frac{t/2}{r(xo)} = \frac{\Delta dx}{dx} = \varepsilon = \frac{\sigma}{E} \tag{2.23}$$

d. But

$$M = \sigma W = \frac{\sigma I}{t/2} \qquad \sigma = \frac{M(xo)\, t/2}{I} \tag{2.24}$$

$$\frac{t/2}{r(xo)} = \frac{\Delta dx}{dx} = \varepsilon = \frac{\sigma}{E} = \frac{M(xo)\, t/2}{EI}$$

e. Hence arriving at the moment of curvature relationship:

$$\frac{1}{r(xo)} = \frac{M(xo)}{EI} \qquad r(xo) = \frac{EI}{M(xo)} \tag{2.25}$$

f. Recall that:

$$M(xo) = \frac{\sigma I}{t/2} \qquad \frac{I}{M(xo)} = \frac{t/2}{\sigma} \tag{2.26}$$

g. Hence the minimum radius is:

$$r(xo) = \frac{Et}{2\sigma(xo)}$$

$$rmin(xo) = \frac{Et}{2\sigma rd} \qquad (2.27)$$

h. The corresponding initial stress caused by bending (residual stress) is:

$$\sigma(xo) = \frac{E\,t}{2r(xo)} \qquad (2.28)$$

i. And the corresponding strain is:

$$\sigma = E\varepsilon$$

$$\varepsilon(xo) = \frac{t}{2r(xo)} = \frac{\Delta l}{l} \qquad (2.29)$$

j. Considering the segment of the arc below having an angle of α, the arc length can be obtained through simple mathematics as follows:

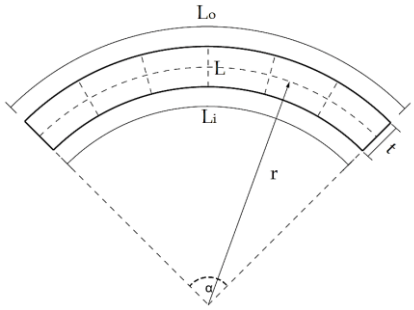

Figure 2.19: Segment of an arch

$$L = \frac{\alpha \times 2\pi r}{360} = \frac{\alpha \pi r}{180} \qquad (2.30)$$

2.6. Materials for Bending-Active Structures

2.6.1. Overview of Materials

Bending-active structures require materials which allow for large elastic deformations and are hence capable of maintaining high strain values without undergoing permanent deformation whilst having sufficient stiffness to retain their aspiring geometry, especially if loaded. This means that internal stresses in the material must never exceed the elastic limit. This creates a challenge or the designer when deciding on the material for a geometry resulting from bending-active action (Brancart et al., 2014).

Hence the ideal material would have low bending stiffness (flexible) whilst offering high strength values as explained in section 2.5.2.5. In the building and construction industry, typical materials used are steel, timber and FRP's (fibre reinforced polymers) which are more recent and modern materials. Timber is a material that offers a sufficient elastic range for bending-active structures. Although relatively stiff, steel has a high strength-to-weight ratio, making it desirable for such a purpose. FRP's are promising materials for bending- active structures since they have low bending stiffness and density values whilst achieving high strengths.

When selecting the structural material, rather than looking at a singular parameter, the combination of properties must be considered , with the most critical being the Young's Modulus of the Material (E) and the maximum allowable bending stress ($\sigma_{m,rd}$). Below are the maximum allowable bending stresses as summarized by (Lienhard et al., 2014) for typical construction materials:

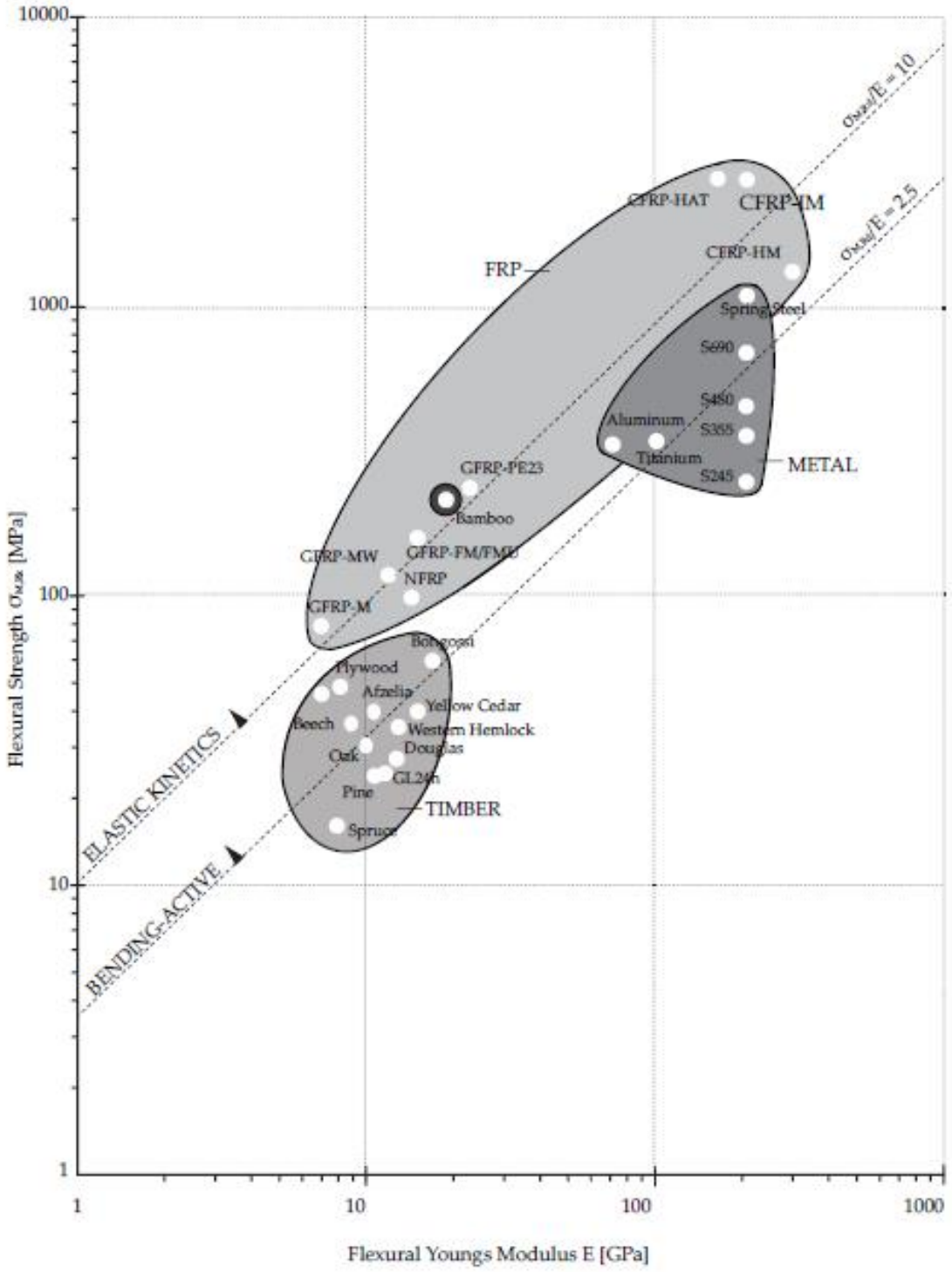

Figure 2.20: Graph of the Maximum allowable bending stresses for different materials on a logarithmic scale (Brancart et al., 2014)

Metals:			
Type	Flexural Strength [MPa]	Flexural Youngs Modulus [GPa]	Ratio
S245	245	210	1.17
S355	355	210	1.69
S450	450	210	2.14
S690	690	210	3.29
Spring Steel	1100	210	5.24
Titanium	340	102	3.33
Aluminum	330	70	4.71
Timber:			
Type	Flexural Strength [MPa]	Flexural Youngs Modulus [GPa]	Ratio
Spruce	16	8	2
Pine	24	11	2.18
Douglas	30	12	2.5
Western Hemlock	35	13	2.69
Yellow Cedar	40	15	2.67
Oak	30	10	3
Beech	35	10	3.5
Afzelia	40	11	3.64
Bongossi	60	17	3.53
GL24h	24	11.6	2.07
GL28h	28	12.6	2.22
GL32h	32	13.7	2.34
GL36h	36	14.7	2.45
Birch Plywood (6.4 mm)	50.9	12.737	4
Brich Plywood (18 mm)	40.2	10.048	4
Combi-Plywood (6.4 mm)	50.8	12.69	4
Combi-Plywood (18 mm)	35.8	8.95	4
Softwood Plywood (6.4 mm)	29.1	9.462	3.08
Softwood Plywood (18 mm)	23	7.464	3.08
Bamboo	213	19.129	11.13
FRP:			
Type	Flexural Strength [MPa]	Flexural Youngs Modulus [GPa]	Ratio
CRFP-HAT	2800	165	16.97
CRFP-IM	2800	210	13.33
CRFP-HM	1350	300	4.5
P E 23	300	23	13.04
GRFP-M	80	7	11.43
GRFP-MW	120	12	10
GRFP-FM/FMU	160	15	10.67
NRFP	101	14.38	7.02

Figure 2.21: Values for the Maximum allowable bending stresses for different materials corresponding to the graph in figure 2.20 (Brancart et al., 2014)

Further claims that the ideal ratio of the Flexural Strength ($\sigma_{m,rd}$) to the Flexural Young Modulus (E) for Bending-Active structures should be greater than 2.5. (Lienhard et al., 2014)

$$\frac{\sigma m,rd}{E} > 2.5 \qquad (2.31)$$

Moreover, a relationship between curvature (r) and the Young Modulus (E) could be drawn where z is the distance between the section's neutral axis to the outmost fibres.

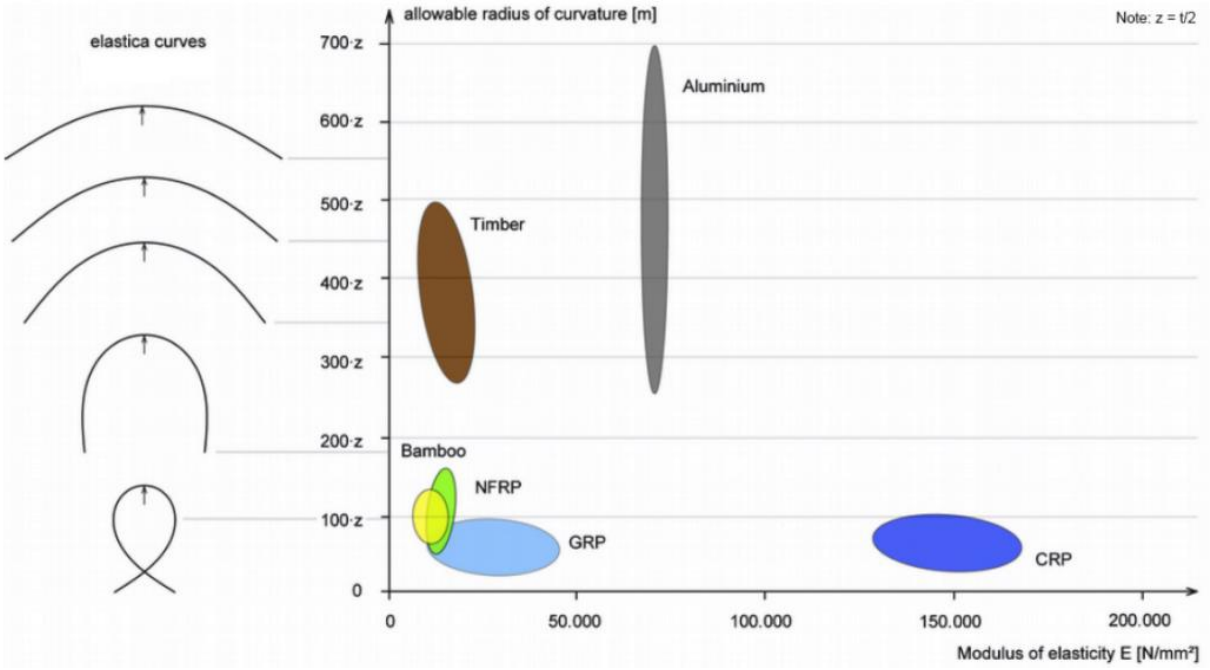

Figure 2.22: Relationship between curvature (r) and the Flexural Young Modulus (E) (Gengnagel et al., 2014)

2.7. Active-Bending in Architecture and Structures - The Influence of Material on Form over the Years

2.7.1. International Context

As established, bending-active structures require materials with high breaking strain values such as softwoods and bamboo. Such a building typology was found in locations where softwoods and bamboo were abundant or in countries that were not yet skilful enough to work with larger pieces of lumber (Lienhard et al., 2014).

With the industrial revolution emerging, new materials such as steel and concrete and the split from the master builder to more specific fields such as urban design, structural engineering, architectural design etc. could be noted. The building industry moved away from the more iterative form-finding approach to defined building typologies as defined at the beginning of the literature review.

Hence the development of form-finding techniques where forces and materials inform the resulting structure was only explored by a few individuals like Frei Otto, Heinz Isler and Félix Candela. Such structures require more time and energy to be derived and hence, especially with the new age of architecture, limited the use of such concepts to a small number of structures. An example is the Mannheim Multihalle designed by Mutschler Carlfried, Langner Joachim and Frei Otto. The structure was bent from a flat state and locked into position, forming a double curvature roof (Brutting et al., 2017).

2.7.2. The Local Scenario

As already discussed in the introduction, our vernacular and contextual buildings have been dictated by the local material of globigerina limestone. Different structural forms were made possible as architects and builders gained further knowledge on the material such as walls, arches, domes, flat roofs etc. However all these developments were centred around one of the essential properties of stone; weak in tension and strong in compression. As a result, the only way that large clear spans could be attained in the past was through curved funicular forms.

2.8. Types of Bending-Active Structures

As explained, bending-active structures are more of a formation process that attain their geometry and properties from elastic bending. Elastic bending is an economical process through which curved forms can be formulated. In bending-active structures, the final form is heavily reliant on the design of the system and the chosen materials. Hence we can further subdivide bending-active systems into 3 design approaches being (1) Behaviour Based Approach, (2) Geometry Based Approach and (3) Integral approach.

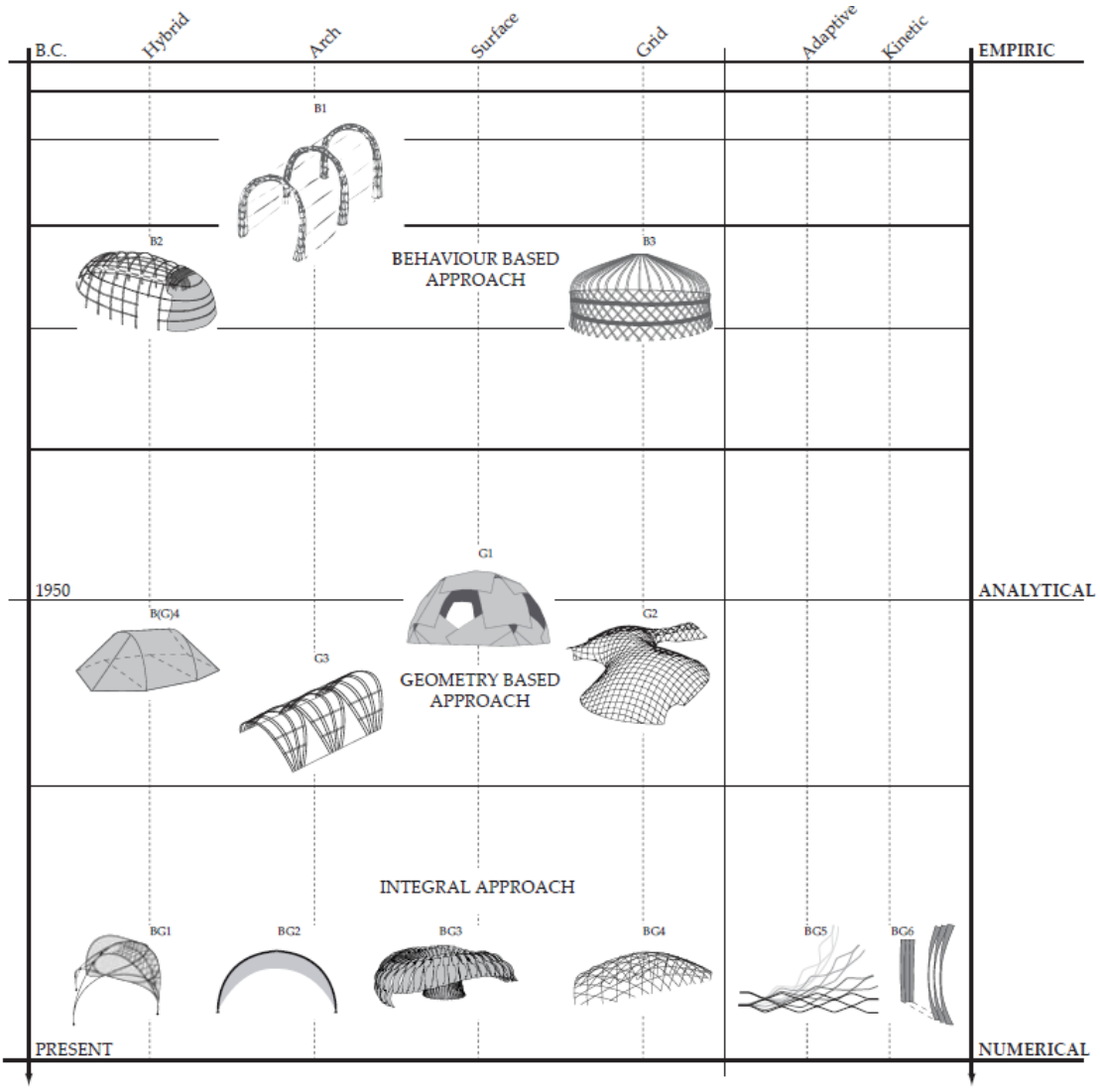

Figure 2.23: A historical time frame of bending active design approaches (Lienhard et al., 2014)
x-axis: Structural types of bending-active structures
y-axis: Historical time frames corresponding to the different design approaches

2.8.1. Behaviour Based Approach

The Behaviour Based Approach is an empirical method in which, through experience and observation, the designers and engineers will predict a structure without going into its analysis and calculations. Through prototyping and physical testing they will attain further knowledge on the structure, allowing them to modify the design and materials until they arrive at the optimal desired design. Hence it is of no surprise that most of the existing projects throughout the history of bending-active structures have made use of this approach as it allows for the creation of a shelter through basic structural understanding (Lienhard et al., 2014).

Looking at real life applications, throughout history, many cultures worldwide have used the concept of elastic deformation to build and construct their vernacular shelters. This resulted in structures which are very similar in form. An example are the Mudhif cane huts (Building a Mudhif, 2023) which can be found in the south of Iraq. These structures makes use of vertical bundles of reed which are anchored to the ground in bucket foundations and joined at the top to create an arch. Another example are the structures created by the Nomadic Turkmen in Iran (Different types of Nomadic Tents in Turkey, 2023) which make use of slender timber elements which are connected together in a pantographic grid at the lower end, elastically bent and joined together at the top.

Figure 2.24: Left: Mudhif cane hut in South Iraq (Building a Mudhif, 2023); Right: Nomadic Turkmen huts in Iran (Different types of Nomadic Tents in Turkey, 2023)

Nowadays, the behaviour based approach is still widely popular and used in combination with new materials that are able of offering high strengths whilst allowing for sufficient elastic bending and deformation such as glass fibre reinforced polymers and aluminium. Typical examples of the use of such a concept and materials are the mountaineering tents which could be easily bent and assembled by hand, creating a quick and temporary shelter. An interesting case study adopting the behaviour based approach is the Water and Wind Café Bamboo bar located in Vietnam which was designed by the architect and engineer, Võ Trong Nghia.

Figure 2.25: Water and Wind Café Bamboo bar by Võ Trong Nghia (Oki, 2023)

2.8.2. Geometry Based Approach

The Geometry Based Approach arrives at a structural shape either through a known geometrical form whose mathematical equation is known, such as a segment of a circle, parabola, elliptical curve etc. or else through physical experimentation through which the form of the attained structure could be approximated as the resulting shape of the bending-active system. Material considerations are accounted for through the use of Euler's moment-to-curvature relationship.

Throughout history, the catenary has been the most popular concept for finding the resulting geometries of bending-active systems. This could be done either through the use of physical models such as a hanging chain model or else through the use of the mathematical equation of the catenary curve which is a hyperbolic cosine curve having the below mathematical equation 2.32 (Svirin, 2023);

$$y = a \cosh \frac{x}{a}. \tag{2.32}$$

(Otto et al., 1985) arrived to the conclusion that the hyperbolic cosine that forms the catenary curve and the Elastica curve are very similar. This information led Frei Otto to carry out further research on elastically bent grid shells. Through the use of physical experimentation, he came up with several prototypes which aided him in the design of the Mannheim Multihalle. Frei Otto along with Mutschler Carlfried and Langner Joachim arrived to the structural form using a hanging model (Dragoș et al., 2014) which was translated into reality through the use of a double-layered timber bending-active structure. This was lifted from its original flat position and left to deform into a grid shell of double curvature (Liddell, 2015). The slotted holes allow for movement in the structure until the desired form is attained and is then fixed in place by tightening the bolts.

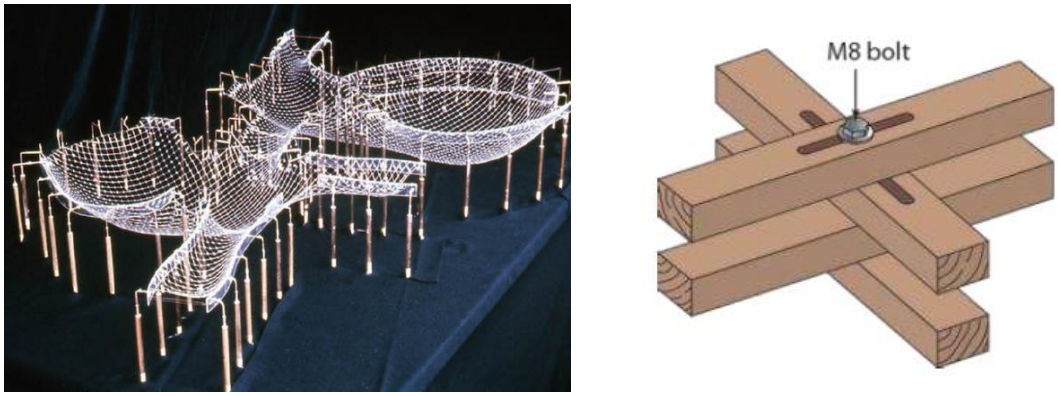

Figure 2.26: Left: Hanging model of the Mannheim Multihalle; Right: Joint Connection of the Mannheim gridshell (Liddell, 2015)

It must be noted that computational modelling tools of that time were finding it challenging to replicate the high amounts of required deformation for bending-active structures as not many grid shells using this approach had been built, hence data was limited (Lienhard et al., 2014). Although the hanging model provided crucial information, it had its limitations as it could not simulate the complex deformations which would occur in real life structures nor the behaviour and stiffness of the material. Moreover it was resource heavy as it required tools such as stereo-photogrammetry to attain the coordinates of the resulting geometry from the physical models.

Recently, this experimental and geometry based approach has been evolving with the use of more sophisticated analytical tools which incorporate mathematical and geometrical data such as the use of variational techniques which have been previously discussed. Programs such as Grasshopper 3D can aid the form-finding process whilst helping optimise the surface and its discretization. The attained forms could then be imported in a structural program for analysis. This improvement in the ease of communication between form and structural behaviour has facilitated the complex design of grid shells. These modern developments are closer to the integral approach, which unifies form and structural function (Liuti et al., 2018).

2.8.3. Integral Approach

The Integral Approach uses computational numerical form-finding techniques such as Finite Element Analysis to understand how the materials of a structure behave under elastic deformation. Such programs will consider the material properties such that the deformed shape attained through the analysis will closely predict the real-life application. These new developments in the modelling and computational fields of structural engineering have made the possibility of more complex structural systems more manageable (Lienhard et al., 2014).

Computational modelling allows the designer to define a geometry and assign its physical properties such as the material, end constraints, etc. followed by structural analysis. Although computer simulations offer a good approximation of the structural behaviour of the predicted structure, physical models are still useful and used. By using both physical models and computational simulation techniques, one can get a complete picture of the structure with each method informing the other (Liuti et al., 2018).

Current research is focussing on developable grid structures consisting of several interconnected elements that can be assembled flat on the ground and then elastically deformed into the final form. The challenge arises in determining the final erected form; hence research is focussing on form finding methods and software to simulate such an erection process. (Douthe et al., 2006) carried out a study where a grid shell built from chs beams placed in an orthogonal layout was elastically deformed in the final form. The structure was tested using a dynamic relaxation programme under nonlinear analysis with applied wind and snow loads. An interesting observation could be drawn from this study where prior to buckling, there is a linear relationship between the load applied, corresponding stresses and deformations whilst the linear elastic range has a relatively high range.

Figure 2.27: A large scale prototype of the grid shell developed by Doubthe, Baverel and Caron

Through the carrying out of these studies, the development in form finding techniques will keep moving forward, each time arriving to solutions which better integrate form and function. The following is a list of typical software currently used for form-finding techniques including; Rhinoceros 3D, Grasshopper 3D, Karamba 3D, Kangaroo Physics, Lusas, Ansys, Oasys GSA etc.

2.8.4. Modes of Erection

Considering the bending-active structures which have been constructed in recent years, the most popular erection methods used were summarized by (Naboni, 2016) as being:

Method 1: The Lift-Up Method

This method is also sometimes referred to as the push-up method. It lifts a structure in place through the use of jacks and cables which at times are used to aid the structural stability during the erection process. Caution must be taken when using this method as it could lead to overstressing in the erection process.

Method 2: The Ease-Down method

The ease-down method first raises the structure using cranes to the highest predicted point and then the perimeter of the structure is pulled downwards to the meet the ground at the location of anchorage.

Method 3: The Inflation Method

This method is the most sensitive of the above mentioned systems as it uses pneumatic cushions to inflate and lift the bending-active system in place. This results in an even distribution of upward force on the structure and hence eliminates the risk of concentrated stresses during its erection.

Method 4: The Compression Method

Through the application of a compression force at the ends of the structure, the compression method results in a buckling force which leads to the deformed form of the structure.

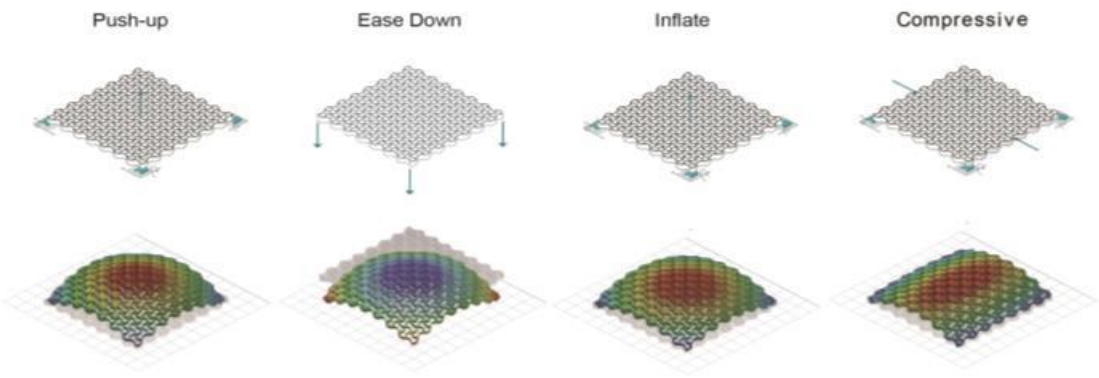

Figure 2.28: Erection modes tested on a sinusoidal pattern (Naboni, 2016)

2.9. Scaling Up of Bending-Active Structures

When prototyping, we tend to build small scale models. But how does their behaviour and properties translate on a larger scale? In this section the Buckingham Pi-theorem shall be used to arrive to scaled relationships. Five variables shall be considered; vertical deflection (Uz), span (L), elastic modulus (E), moment of inertia (I) and vertical udl load (qz). The units of all these variables can be written in terms of two units; Newton (N) and millimetre (mm). These shall be referred to as the (n-rd) terms. With this data, a dimensionless matrix can be set up as follows (Lienhard et al., 2013);

5 Variables: U_z, L, E, I_y, q_z

2 Dimensions: [mm], [N]

5-2 = 3 Pi-Terms

The dimensional Matrix is:

	U_z	L	E	I_y	q_z
$[N]$	0	0	1	0	1
$[mm]$	1	1	−2	4	−1

Figure 2.29: Setting up the dimensionless matrix

Combining the above variables can lead us to three dimensionless pi-terms with pi-term 1 relating deflection and span, pi-term 2 relating span and moment of inertia and pi-term 3 relating loading with length and the elastic modulus. These relationships could be summarized by the below equations in Figure 2.30;

$$\pi_1 = \frac{U_z}{L};\ \pi_2 = \frac{L^4}{I_v};\ \pi_3 = \frac{q_z}{E \cdot L}$$

Figure 2.30: Arriving to the 3 pi-terms

Using these dimensionless pi-terms we can now start making some conclusions relating to scale. A scaling factor (s) will be used to demonstrate the scaling relationship, symbol (m) will refer to the small scale model parameter and symbol (p) will refer to the large scale prototype. Starting with pi-term 2, it can be proved that the systems' dimensions will scale up linearly and hence we can conclude that as the span of a system increases, so do the cross-sectional properties of the structural member.

$$\left(\frac{L^4}{I_y}\right)_m = \left(\frac{(s \cdot L)^4}{I_y}\right)_p \longrightarrow I_{y,p} = s^4 \cdot I_{y,m}$$

$$s^4 \cdot I_m = s^4 \frac{b_m \cdot {h_m}^3}{12} = \frac{s \cdot b_m \cdot (s \cdot h_m)^3}{12}$$

Figure 2.31: Pi-term 2 leading to a linear scaling relationship between span and cross-section properties

Continuing with pi-term 3, it can be shown that for the same material, the vertical loading (qz) will scale up proportionally with span (L).

$$\left(\frac{q_z}{E \cdot L}\right)_m = \left(\frac{q_z}{s \cdot E \cdot L)}\right)_p \longrightarrow q_{z,p}$$

Figure 2.32: Pi-term 3 leading to a linear scaling relationship between span and vertical loading

Lastly if we take pi-term 1 and compare it with pi-terms 2 & 3, it can be concluded that the deformed shape resulting from elastic bending will be of the same geometry yet at a different scale depending on the size of the structure.

$$\frac{U_z}{L} = \phi\left(\frac{L^4}{I_y}, \frac{q_z}{E \cdot L}\right)$$

Figure 2.33: Pi-term 1 leads to a linear scaling of the Elastica curve

However this conclusion excludes the effect of the self-weight of the structure and any residual forces which might arise. In reality there is a cubic relationship between mass and scale. Although such a relationship can be neglected for lightweight structures since the slight mass increase will not impact the structural stiffness, for larger structures the mass increase will impact the overall structural behaviour and cannot be neglected.

$$\text{Scale} \propto \text{Mass}^3 \qquad (2.33)$$

Hence we can conclude this section by the following statement: A bending-active system will linearly scale up both in geometry and properties as discussed above as long as the structure's weight is not too great to lead to structural instability.

2.10. Stiffness of the Elastica Curve

(Lienhard et al., 2013) carried out a study to determine the effect of rise on stiffness by keeping the same span for various rise to span ratios. These were repeated for scale factors 1, 2, 4 and 8. It could be concluded that the Elastica exhibited the highest stiffness and lowest deflection values for the rise to span ratios (f/L) of 15 to 35 percent.

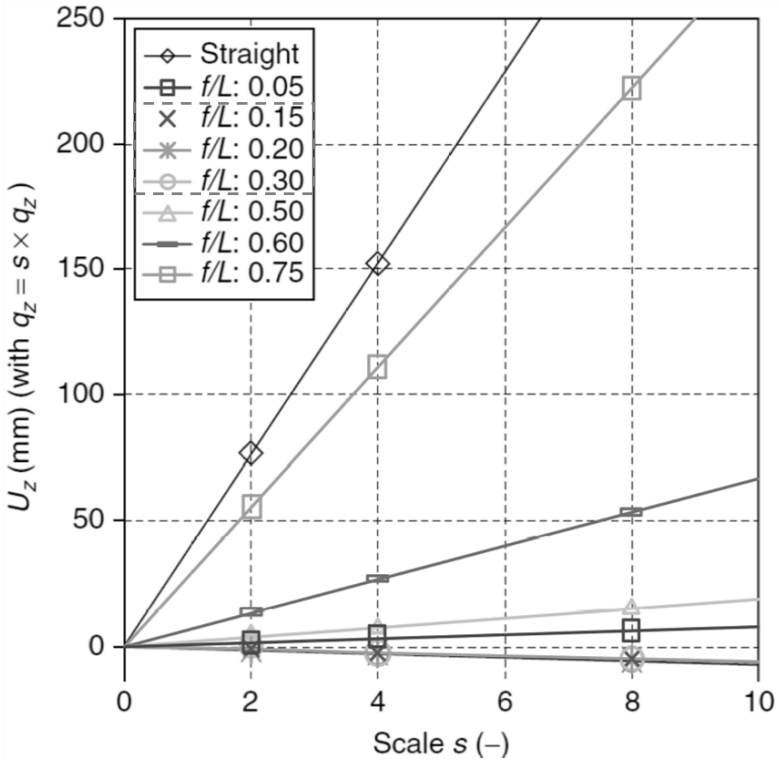

Figure 2.34: Deflection vs scale graph for different rise to span ratios (constant span)

2.11. Moving towards the Traditional: The Mechanics of Arches

2.11.1. The Arch

An Arch is a structural form which uses blocks of stone (voussoirs) spanning across an opening to transfer vertical loading laterally along a line of thrust to the abutments. For the same loading conditions, a shallow arch will experience greater compressive forces and hence a higher resultant at the abutments. Conversely, a deeper arch will experience lower compressive forces and hence a lower resultant force at the abutments. An arch can be compared to an inverted catenary chain whereas in a chain the members transfer loading through tension, in an arch load is transferred through compression (Gobrick, 1995).

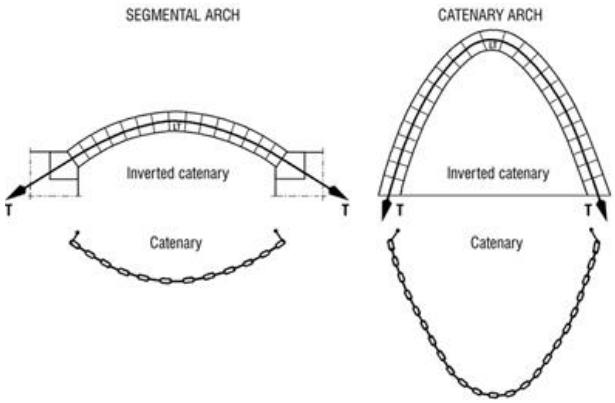

Figure 2.35: Left: Segmental Arch; Right: Catenary Arch (Gobrick, 1995)

2.11.2. Understanding how an Arch Works

When it comes to arches, their behaviour cannot solely be understood through contemporary structural theory where the safety of a structural system is determined through and understanding of stress and strain. The geometry and shape of an arch will tend to be the detrimental factor determining whether an arch will stand or collapse. Hence, geometrical studies have long been carried out to understand how the thrust lines pass within the arch thickness. This does not mean that the crushing of stone cannot occur yet for a typical arch of modest scale with good quality stone; the geometry tends to be more critical over the crushing of stone. Hence the geometry of the arch should follow from the applied loads (Heyman, 1982).

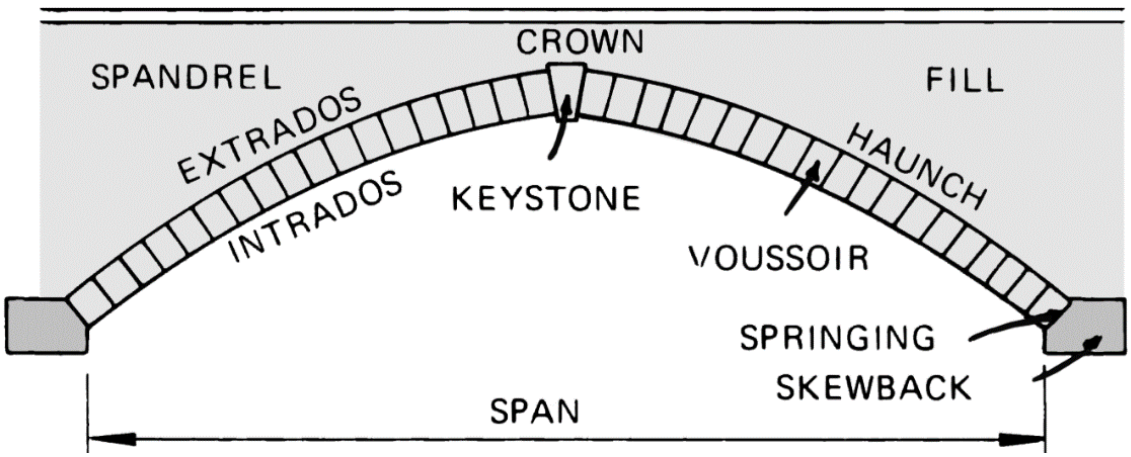

Figure 2.36: Nomenclature used for arches

2.11.3. The Function of Mortar in Arches

Along with the tapering of the voussoirs, mortar aids the structural integrity of the arch by keeping the voussoirs in place and ensuring that the arch's geometry remains as the original form. However, the mortar will still allow for a low degree of deformation in the arch which can occur to ensure the right fitting of the voussoirs whilst ensuring an adequate path for the transmission of the applied loads to the abutments (Repointing stone and brick, 2023).

Mortar also has the important function of creating a smooth surface, enabling the even distribution of loading from one voussoir to the other. In this manner, the creation of concentrated loading that could arise from the uneven cutting of stone would be eliminated, reducing the risk of crushing at such points while allowing for continuous transmission of loading. This aspect is even more important in shallower arches where compressive forces are higher and hence the creation risk of highly concentrated stress points is more likely to occur (Heyman, 1982).

When designing an arch of stone voussoirs with mortar in between, the mortar should always be the weakest link of the two. A soft mortar will ensure that it will fail first prior to the stone voussoir and hence reducing the risk of structural damage to the stone voussoirs. In this manner, any repair works shall only involve the repointing of stone which is much simpler than replacing stone voussoirs (The Different Kinds of Mortar, 2023).

2.11.4. Analysing Lines of Thrust in Arches through the Funicular Polygon Method.

This method solves the forces in an arch through a graphical representation. The Funicular Polygon Method starts by assuming that the loads on an arch are acting on a weightless string. The shape of the deformed string is assumed and sketched as in Figure 2.37.

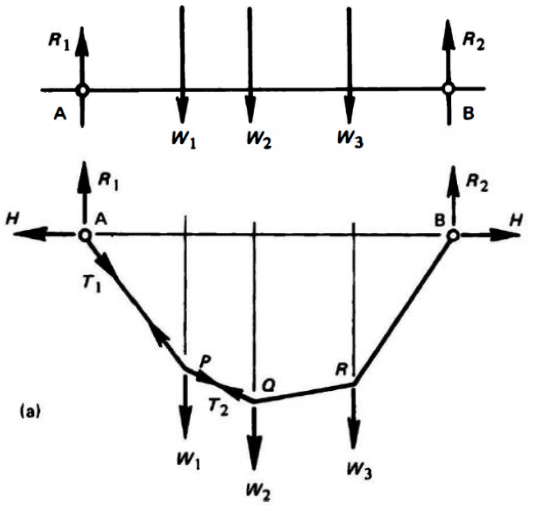

Figure 2.37: Drawing the assumed catenary for the given loading (Heyman, 1982)

Since the structural system is in equilibrium, it can be concluded that the resultant of the vertical forces is equal to 0 and hence the vertical reactions are equal to the applied vertical loads.

$$W_1 + W_2 + W_3 = R_1 + R_2 \qquad (2.34)$$

Taking moments about point A, we can resolve reactions 1 and 2. If we assume a value for the horizontal thrust, H, the Funicular Polygon of the system can be drawn up as follows:

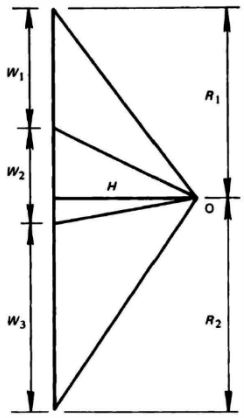

Figure 2.38: Drawing the Funicular Polygon (Heyman, 1982)

Finally, using Pythagoras' Theorem, the internal forces can be found as follows;

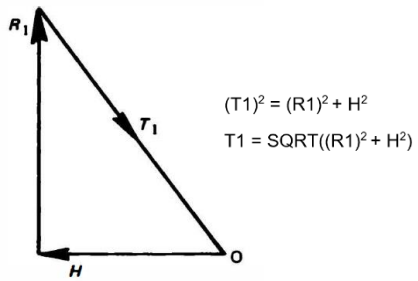

Figure 2.39: Solving the funicular polygon forces using Pythagoras theorem

Now although the value of the horizontal thrust was assumed, it was proven that a higher or lower horizontal value (H) will result in a Funicular Polygon of the same geometry yet the higher horizontal thrust will lead to a shallower Funicular Polygon. This corresponds to the analogy of a string where a longer string will have a deeper sag and hence lower horizontal pull whilst a shorter string will have a lower sag and hence a larger horizontal thrust.

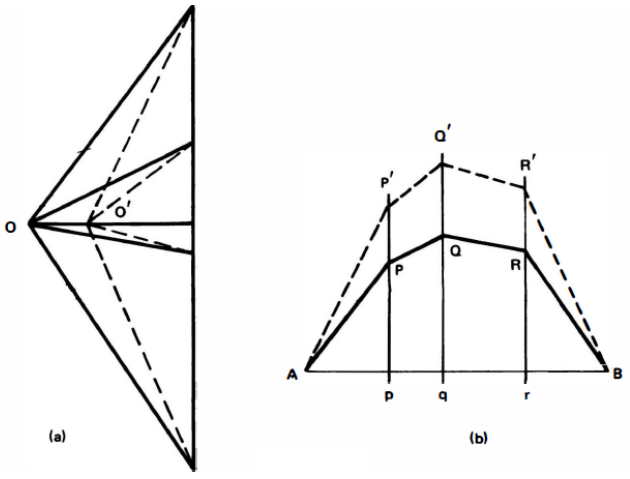

Figure 2.40: Superimposition of lines of thrust resulting from variable horizontal thrusts (Heyman, 1982)

AP'Q'R'B'- Lower horizontal thrust
APQRB - Larger horizontal thrust

2.11.5. Heyman's Three Key Assumptions for Structural Actions

Heyman set **three** important assumptions for the analysis of arches (Heyman, 1982);

1. The *first assumption* claims that sliding failure is not possible as either there is a high degree of interlock between the voussoirs or else friction is greater than the sliding force.

2. The *second assumption* assumes that the arch voussoir can only transfer compressive forces due to the weak mortar joints between the voussoirs. This is a safe and conservative assumption as, in reality, the arch may be able to take some tensile forces due to the interlock between the voussoirs.

3. The *third assumption* assumes that the stone has infinite compressive strength as in general stresses within such construction systems are low and hence the likeliness of crushing is low. However caution must be taken when working with very shallow arches where the compressive force is very high and hence the risk of crushing might be possible.

These assumptions would allow for using elastic theorems such as the Funicular Polygon Method (see section 2.11.4) where internal forces can be expressed by the external loads applied to the structure. (Huerta, 2006) also agrees that this approach is the ideal method for analysis arches. However people like Ricardo Gulli have argued that Finite Element Analysis would offer superior data and analysis when it comes to such structures (López, 2012).

2.11.6. The Rule of the Middle Thirds

This rule can be explained through three main scenarios. A uniform compressive stress is developed when the thrust line falls within the centre of the middle third of the voussoir section. As the line of thrust starts to move away from the centre and exactly approaches the edge of the middle third, the stress exhibits a linear distribution with one edge falling to 0. When the line of thrust goes beyond the middle third of the voussoir, a tensile force develops yet unreinforced masonry cannot withstand such a force and can lead to the opening of voussoir joints. As the line of thrust starts approaching the edge, the area upon which the compressive force of the arch acts diminishes and hence and increase in stress can be recorded. Masonry has a finite value of allowable compressive stress. If this is exceeded, crushing will occur, which can lead to the failure of the arched system. These 3 scenarios were used to demonstrate the importance of the rule of middle thirds (Heyman, 1982).

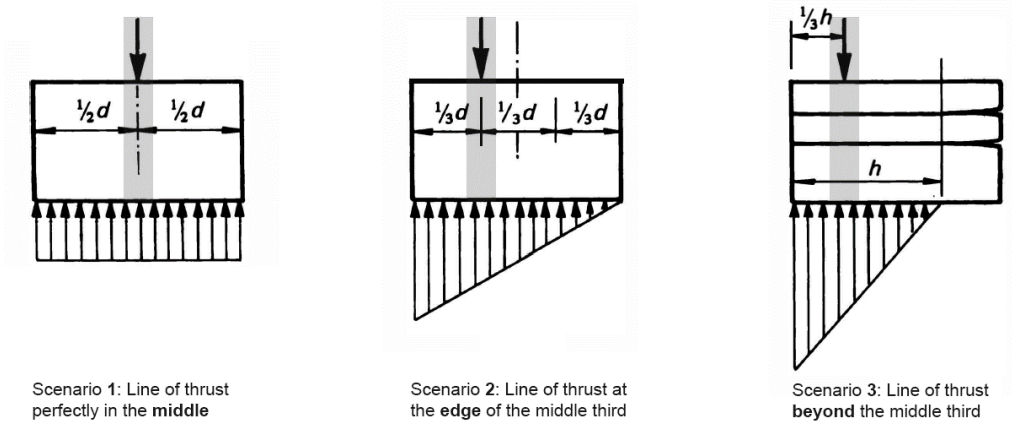

Figure 2.41: 3 Scenarios of loading corresponding to varying lines of thrust (Heyman, 1982)

2.11.7. Geometrical Factor of Safety

As discussed in section 2.11.2, the critical parameter determining masonry arches' stability is the geometry. Hence the corresponding factor of safety tends to be related to this parameter. The safety factor of an arch can be related to the possibility of fitting a line of thrust within the given geometry. A thicker arch can accommodate for a higher number of line of thrust configurations over a thinner arch. Moreover, it is more likely for a line of thrust to fall within the middle thirds in a thicker arch over a thinner one. Corresponding to the rule of middle thirds, the general safety factor adopted for funicular construction is 3.

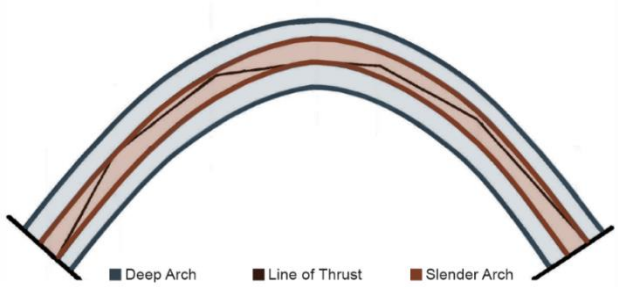

Figure 2.42: Comparison of a Slender and Deep Arch w.r.t the lines of thrust

2.12. 3D Printing Technology

3D printing technology has been a very convenient tool for the fields of architecture and engineering by allowing the designer to test and visualize the envisaged designs. Moreover, 3D printing can produce customised elements that might be too intricate and expensive to manufacture in a traditional workshop. The most commonly used materials to 3D print tend to be plastics like PLA, ABS, TPU etc. Each plastic offers different properties and characteristics, so the designer can opt for the desired type.

In the study by (Zhang et al., 2019), 3D printing was used to construct a formwork made out of resin and TPU which would support stone elements and test the structural behaviour of the formed thin shell. Using Karamba, a structural form was found along with the corresponding principle stress lines which were 3D printed in TPU. TPU is flexible enough to be bent in the desired form yet to retain the shape, the in between grooves were infilled with resin. Under loading, this combination of materials would resist tension through the TPU whilst the resin would offer stiffens and resist any deformations from such a load. Once complete, the stone shell was constructed and the formwork was removed. For the 450mm spanning shell structure having a thickness of 3mm, a load of 1kg could be resisted.

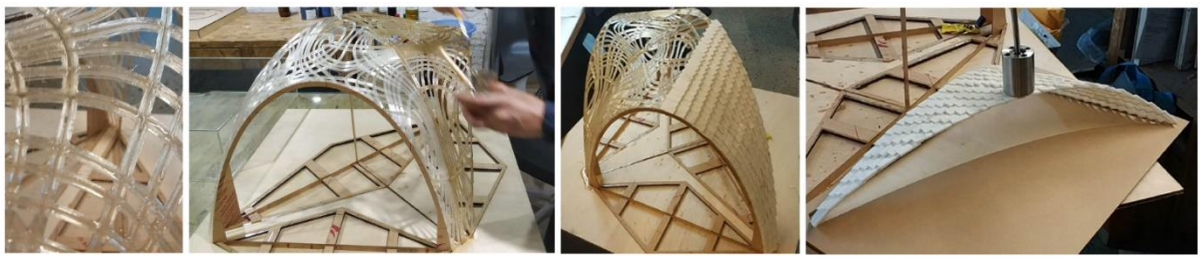

Figure 2.43: The process of 3D printing the stress lines, resining, constructing the stone shell and applying a load of 1kg (Zhang et al., 2019)

However, can the formwork be retained and integrated as part of the structure to enhance the structural behaviour?

2.13. Conclusion

This chapter showed that bending-active structures are more of a formation process which attain their final form through the process of elastic deformation rather than a distinct structural system. An introduction to bending theory has been outlined where it could be concluded that the Euler-Bernoulli model is a sufficient structural model in the approach of elastic deformation.

The resulting geometry of elastically bent elements was long studied in history starting with De Nemore in the 13th century up until the 18th century when Bernoulli following communications with Euler manages to solve the geometrical coordinates of the Elastica by deriving the Euler-Poisson equation based on variational techniques.

These methods involve complex mathematics and hence the solving of the Elastica using this geometrical approach has been attempted through the use of computational software such as Grasshopper 3D. Since such an approach is solely based on geometry, another approach was introduced, the Finite Element Method, which considers the structure's material. It was concluded that bending-active structures should use flexible materials which still offer high strength values upon loading.

The design of bending-active structures could be summarized into 3 main categories:

(i) The Behaviour Based Approach has been the most common method throughout history resulting from its primitive nature of using experience and observation as the sole means of structural judgement.

(ii) The Geometry Based Approach centres around the use of physical prototypes and known geometrical mathematical relationships, resulting in a method which adopts a geometrical approach.

(iii) The Integral Approach which takes elements from the geometry based approach and combines them with sophisticated structural software being the Finite Element Method.

Different modes of erection were outlined followed by the effect of scale on actively bent structures. It could be deducted that the parameters of bending-active systems will scale up linearly apart from mass which shows a cubic relationship with scale.

Traditional forms of construction were included in effort to understand how these can be combined with bending-active structures. The effect of rise on an arch’s lateral thrust was demonstrated by the use of a catenary chain, proving that shallower arches will exhibit a higher lateral force. It was determined that when it comes to funicular structures such as arches, most often, the geometry determines the structural stability of the form. The importance of mortar within an arch was established, its function being mainly to act as a smooth surface between the voussoirs for the even distribution and transmission of compressive forces.

This chapter ends by the elastic method of the Funicular Polygon, a preliminary approach in the analysis of arches. Heyman’s 3 assumptions which assume that sliding failure cannot occur, the arch is under pure compression and that stone has infinite compressive strength were outlined followed by the importance of the rule of middle thirds in relation to the factor of safety of arches. Lastly, 3D printing was briefly outlined as a possible tool in the development of physical models.

3. Methodology

3.1. Introduction

Chapter three shall delve further into the geometrical behaviour of bending-active structures to understand how the resulting form can be used to create an integrated formwork layout which the infilling of voussoirs shall follow. This is done with the aim of attaining a shallow roofing structure that can be a viable alternative to the traditional flat concrete roof.

The studies outlined in Chapter 3 are aimed to arrive at an answer to the research questions which have been defined in Chapter 1 and produced here once again;

i. *Franka Roofs: Can they be a viable alternative to the typical concrete roof?*

ii. *What is the ideal geometric pattern for the integrated bending-active formwork for a roof in single curvature as part of the final structure and what is its structural feasibility?*

iii. *Which material can undergo bending to create the desired curved geometry whilst being stiff enough once fixed in place to accommodate the loading of the stone?*

iv. *What is the load-bearing capacity of such a curved reconstituted stone roof with the integrated formwork and how does it compare to a traditional masonry curved roof ?*

To visually understand the behaviour of bending-active structures and that of the formwork, physical models and geometrical modelling software such as Grasshopper 3D were a crucial part of the iterative process required to attain a holistic understanding of the problem and arrive closer to a solution. As stated in section (1.9), when the integrated formwork is actively bent it has to allow for the insertion of the reconstituted stone voussoirs. It was important to understand the geometrical transition of the devised integrated formwork from the erection stage, where the formwork is actively bent and hence, the geometry is that of the Elastica, to the completed stage, where the voussoirs are inserted into the formwork, and the geometry corresponds to a segment of a circle. Moreover, to understand the behaviour of the integrated formwork when transitioning from a 2D aspect, corresponding to a singular arch, to the 3D aspect, corresponding to the extension of the arch into a vault, physical models help to illustrate the geometrical behaviour through the resulting deformations. Hence studies (1-7) were devised to tackle these aspects.

After having attained a comprehensive understanding of the geometry, a computer software analysis programme was used, hereby being Finite Element Analysis. This was carried out to understand the integrated formwork's influence on the roofing structure's overall behaviour. Through such an analysis, a detailed mechanical description of the stresses within the geometry, material properties and the interaction between the reconstituted stone voussoirs and the integrated formwork can be obtained. This analysis offers an insight on the behavioural changes within the structure between a formwork integrated arch structure in comparison to a similar masonry unreinforced arched structure. This section was tackled by studies (8-10). The Method of the Funicular Polygon is then used as a traditional elastic approach whose results were compared with those emerging from Finite Element Analysis. Hence, the set of studies (1-11) aim to offer a complete understanding of the structure with respect to its geometrical and structural behaviour.

The design process for both the formwork and formwork integrated arch structure made use of all the three design approaches used in the design of bending active structures, which have been outlined in Chapter 2, being the Behaviour Based Approach, Geometry Based Approach and Integral Approach.

3.2. Gaussian Curvature: Geometry of the Bending-Active Structure

The resulting geometry of an actively bent shape can be described in term of the Gaussian curvature. Gaussian curvature (K) of a surface at a given point (A,B) can be mathematically defined as the product of the principal curvatures whilst the gaussian radius of curvature can be mathematically defined as the reciprocal of Gaussian curvature (Mirante, 2015).

$$K = KA \times KB$$
$$K = 1/R$$
$$K = 1/RA \ X \ 1/RB \qquad (3.1)$$

The resultant value of Gaussian curvature can be linked to a Gaussian category. Three Gaussian categories can be defined being;

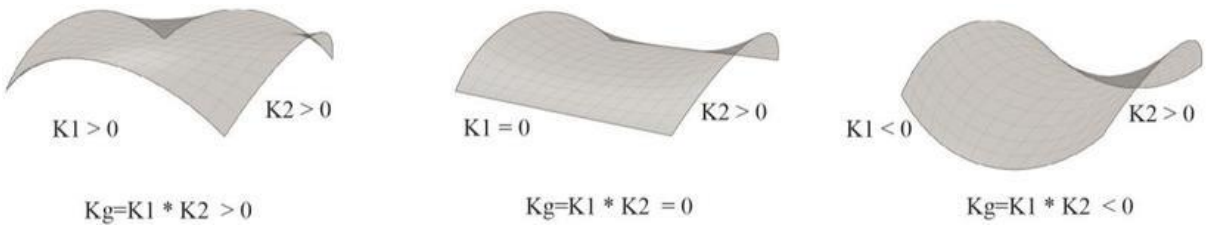

Figure 3.1: Left: Synclastic Surface; Middle: Developable Surface; Right: Anticlastic Surface (Mirante, 2015)

Category 1: Synclastic Surfaces (K>0)

Synclastic surfaces are defined by a positive Gaussian value. These surfaces are associated with segments of spherical forms and hence translate into domes. Domed structures have a long history and their use can be traced back to important historical buildings such as the Pantheon located in the city of Rome.

Category 2: Anticlastic Surfaces (K<0)

Anticlastic Surfaces are defined by a negative Gaussian value. The discovery of these surfaces has been quite recent and has captured the interest of famous architects and engineers like Frei Otto which led him to explore more complex geometries like the saddle shape. Most anticlastic structures are of the modern age with a typical example being the Olympic Velodrome in London, UK.

Category 3: Developable Surfaces (K=0)

Developable Surfaces are defined by a zero Gaussian value. Developable surface are the most relevant for this dissertation study since they can be opened to a flat surface without undergoing any permanent deformation. Throughout history, these surfaces were the most

popular since they are the simplest to understand and develop. Typical examples of developable surfaces include arches and barrel vaults. This study shall focus on a singular arch with the intention of expanding it into a vault

3.3. Shaping Actively Bent Elements

3.3.1. Resulting Geometry from Elastic Deformation

The elastic deformation of an initially straight member results in the Elastica which can be defined by the second order differential equation (equation 2.8) of the Euler-Bernoulli relationship. The resulting curvature will vary along the Elastica path and hence will have a varying radius. Through studies, (Alpermann et al., 2012) could conclude that the central part of the Elastica, coinciding with the point of maximum bending moment, will exhibit a relatively constant radius whilst as you move towards the end restraints of the curve where the bending moment is zero, an infinite increase in radius can be documented. This exhibits an inversely proportional relationship between bending moment and radius.

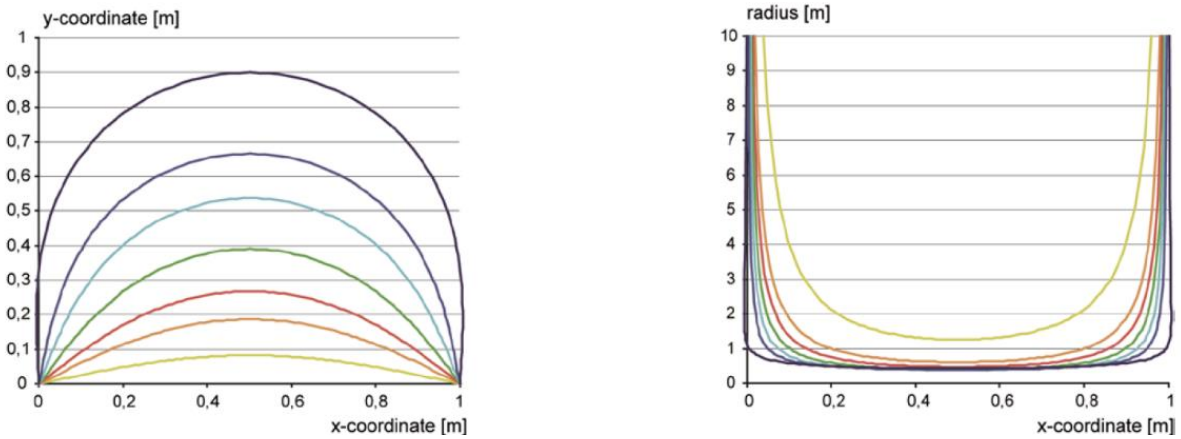

Figure 3.2: Left graph plots the Elastica curve whilst the right plots the corresponding x-coordinates to radius relationship (Alpermann et al., 2012)

3.3.2. Required Geometry from Elastic Deformation

This inconsistency in radius is not ideal for the scope and purpose of this study as:

a. Variable curvature implies that the stress distribution along the bent member is unequal which makes the structure inefficient.

b. Variable curvature means that if the resulting curve were to be divided into an equal amount of voussoirs, each voussoir will have its unique geometry. Again, this is undesirable as it will require the distinct and individual production of every voussoir which defeats the concept of repeatability and modularity.

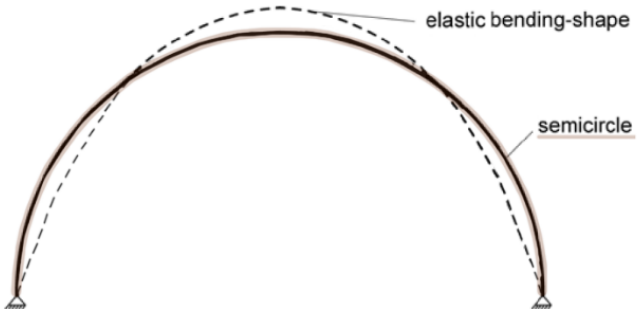

Figure 3.3: Comparing the Elastica with a semicircle (Lienhard et al., 2014)

(Alpermann et al, 2012) suggest the use of tensile restraining elements such as cables to modify the shape from the Elastica to form part of a circle. This was tested out through the use of a preliminary cardboard model whose behaviour was in agreement with the above research.

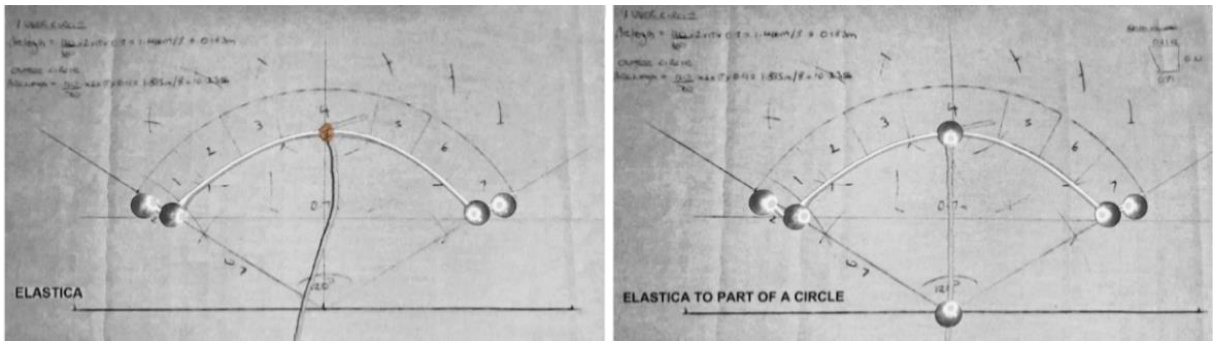

Figure 3.4: Preliminary physical prototype of the Elastica modification to fit in a segment of a circle

The question then arises; Would it be possible to have a bending-active formwork which when elastically bent although geometrically would not form part of a circle, following the insertion of voussoirs will modify in shape into a part of a circle, becoming an integral part of the structure?

3.4. Physical and Computational Studies

A number of short geometrical studies were devised to arrive at the optimal design solution for a funicular structure that uses an integrated formwork. The sequence, along with a brief description of these geometrical and structural studies is summarized below:

1. Study 1: A Comparative study of the Elastica, Catenary and Circular curves founded on a Geometry Based Approach using form-finding software to understand the geometrical differences between the formwork erection stage (the Elastica) and the completed arch stage (segmental arch) which will lead to the understanding of the similarities between the Elastica and the catenary curves.

2. Study 2: A comparative study of the Elastica curve using the 3 main design approaches (behaviour-based, geometry-based and integral approach) to understand if any differences arise and hence test the accuracy of the form finding and Finite Element software.

3. Study 3: First prototype of a 3D printed semi-circular arch with integrated formwork on the basis of the Geometry Based Approach

4. Study 4: Second Prototype of a 3d printed joint formwork an attempt to extend the arch (2D) into a vault (3D)

5. Study 5: Third Prototype of a 3D printed shallow segmental arch with a modified integrated formwork that allows for the vault development on the basis of the Behaviour Based Approach

6. Study 6: Fourth prototype on the basis of prototype 3 of a shallow barrel vault

7. Study 7: Fifth prototype of a flat arch to understand the influence of curvature against a flat structural system

8. Study 8: Finite Element Analysis of the 2 phases of the structure starting with Stage 1: During the Erection process

9. Study 9: Finite Element Analysis of the 2 phases of the structure continuing with Stage 2: Understanding the behaviour of the completed arch

10. Study 10: A comparative FEA study between a completed formwork integrated arch, a similar arch that eliminates the steel rod of the integrated formwork whilst retaining a steel joint and a traditional mortar jointed arch

11. Study 11: A comparative analysis between Finite Element Analysis and Heyman's Funicular Polygon

3.5. Study 1: Comparison of the Elastica, Catenary and Circle using Form-finding Software

To understand the difference between the three types of curves, a geometric study based on the use of grasshopper was carried out. Rhinoceros 5 was used in all 3 cases paired with Grasshopper 3D. Two Grasshopper scripts were used; the script developed by (McElwain, 2014) was used to model the Elastica based on the use of elliptical integrals whilst the Catenary script was created for this purpose and makes use of the existing Grasshopper 3D component, catenary which takes into consideration the effects of gravity on a free hanging chain between two fixed points.

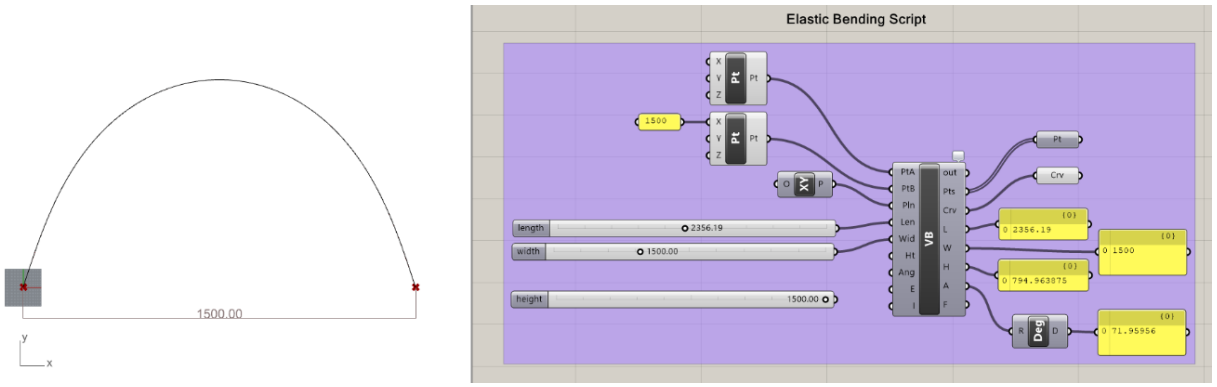

Figure 3.5: Modelling of the Elastica curve through a Grasshopper 3D script devised by (McElwain, 2014)

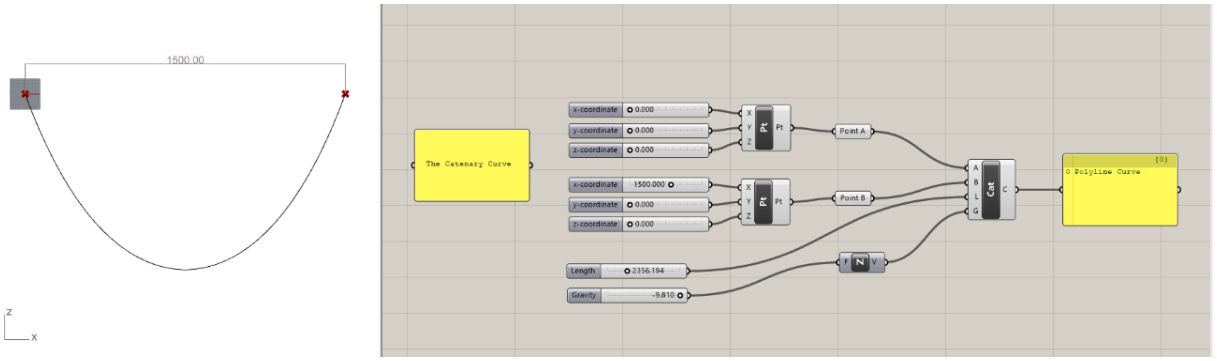

Figure 3.6: Modelling of a Catenary curve through a custom Grasshopper 3D script

For this study, the baseline curve was a semicircle having a radius of 750mm resulting in a clear span of 1500mm. The resulting curvature length of the semicircle was that of 2356.194mm. Using these parameters, the grasshopper scripts were both inputted with these values of curvature length and clear span which generated the Elastica curve found in Figure 3.5 and the catenary found in Figure 3.6. The resulting curves were superimposed on a singular plot. The catenary exhibits the highest rise to span ratio followed by the Elastica and then the semicircle. Such an observation is promising as the aim of the upcoming studies is to load the Elastica. Upon additional load, deflection of the Elastica is expected. The arising question is whether it will turn into a semicircle or not.

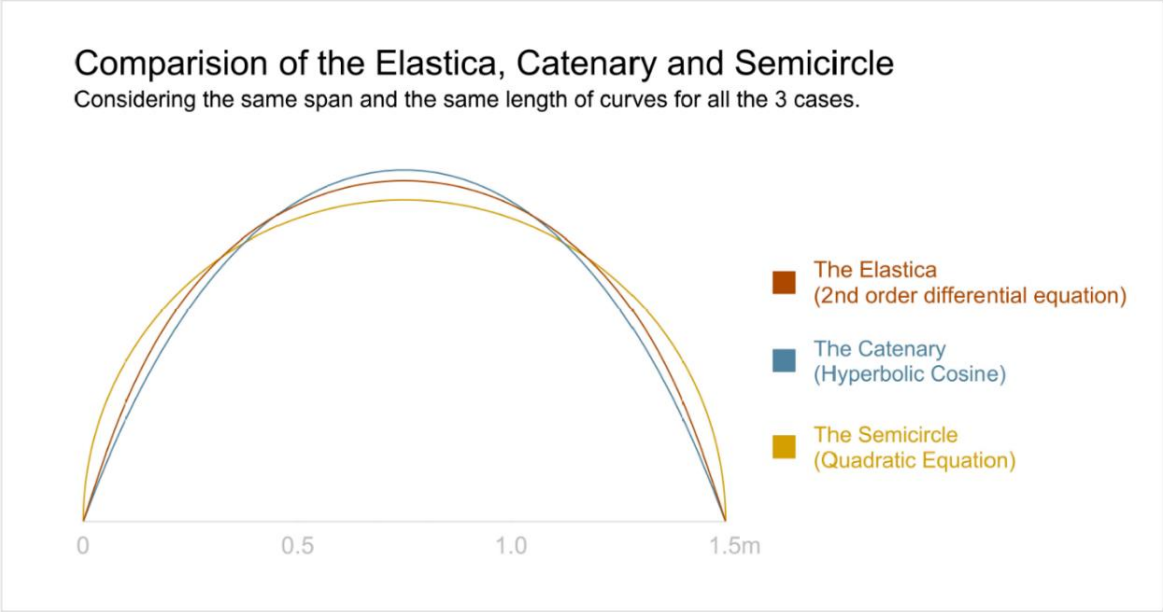

Figure 3.7: Superimposition of the Elastica, Catenary and Semicircular curves having the same span and length

3.6. Study 2: A Comparative Study of the Elastica Curve using the 3 Main Approaches for the Design of Bending-Active Structures.

This study used a physical model, form-finding software and finally, a Finite Element Model. A comparative study was conducted to understand how the Elastica translates in each medium.

Based on the Behaviour Based Approach, a physical study was carried out using a thin steel rod having a diameter of 0.5mm and a length of 300mm. The rod was fixed at one end and elastically bent by applying a horizontal push at the other end in increments of 50mm, each time tracing the formed path.

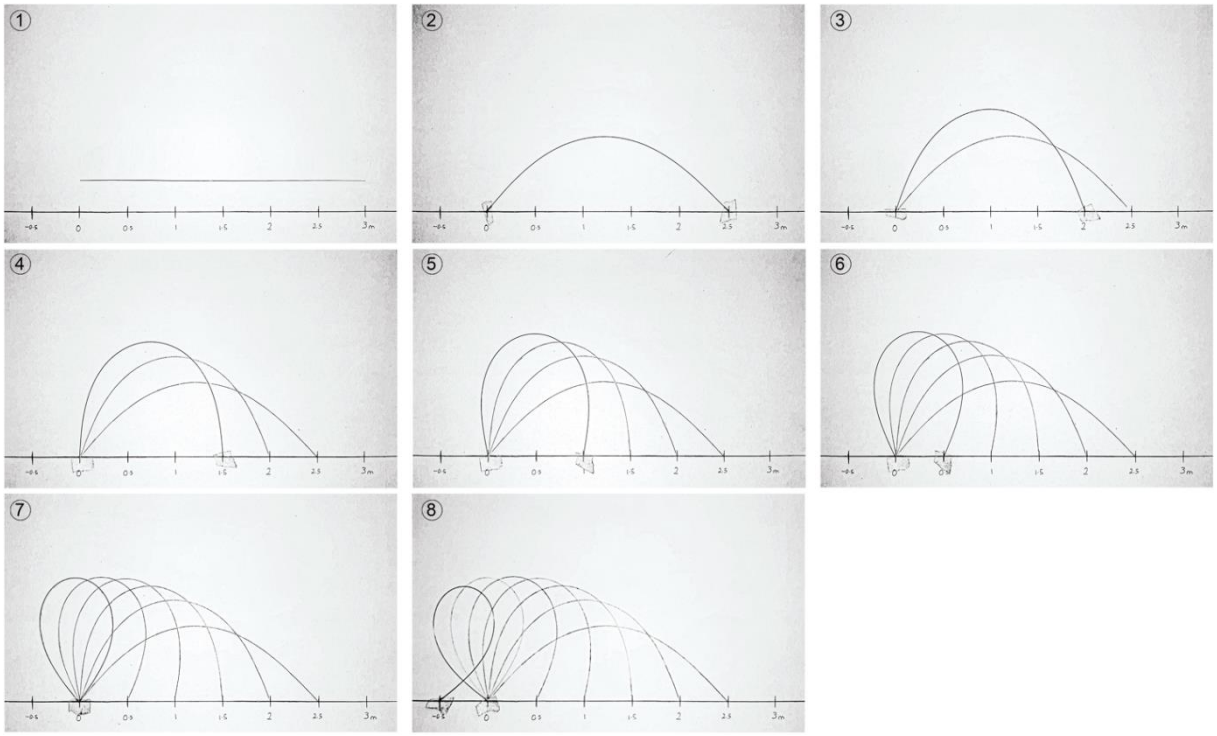

Figure 3.8: Physical Study of the Elastic deformation of a thin steel rod

Based on the Geometry Based Approach, an analytical study was conducted using Grasshopper 3D where for a rod with a length of 3000mm, a Grasshopper 3D script based on mathematical and geometrical equations (McElwain, 2014) was used to elastically deform an initially straight element.

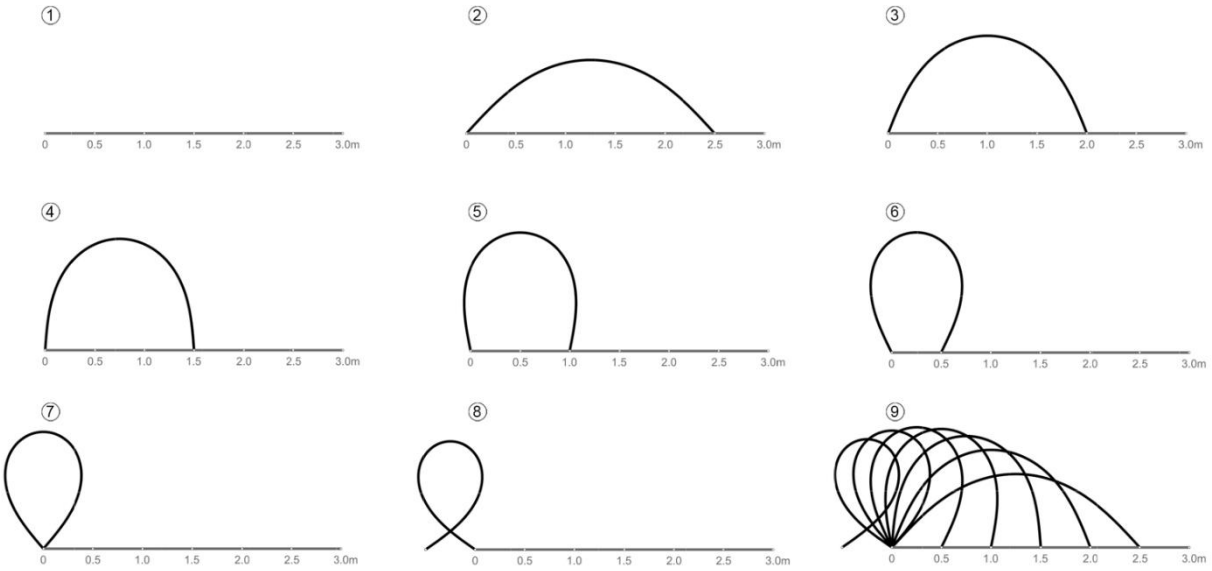

Figure 3.9: Analytical study of the Elastic deformation of a thin steel rod

Lastly, an Integral Approach was used to consider the structure's material, here being elastic steel. The Finite Element software used for this analysis was Lusas Analyst. First an eigenvector analysis was carried out to attain the first mode of vibration (fundamental frequency). The resulting geometry of the deformed element was then used as the initial geometry for the elastic deformation analysis.

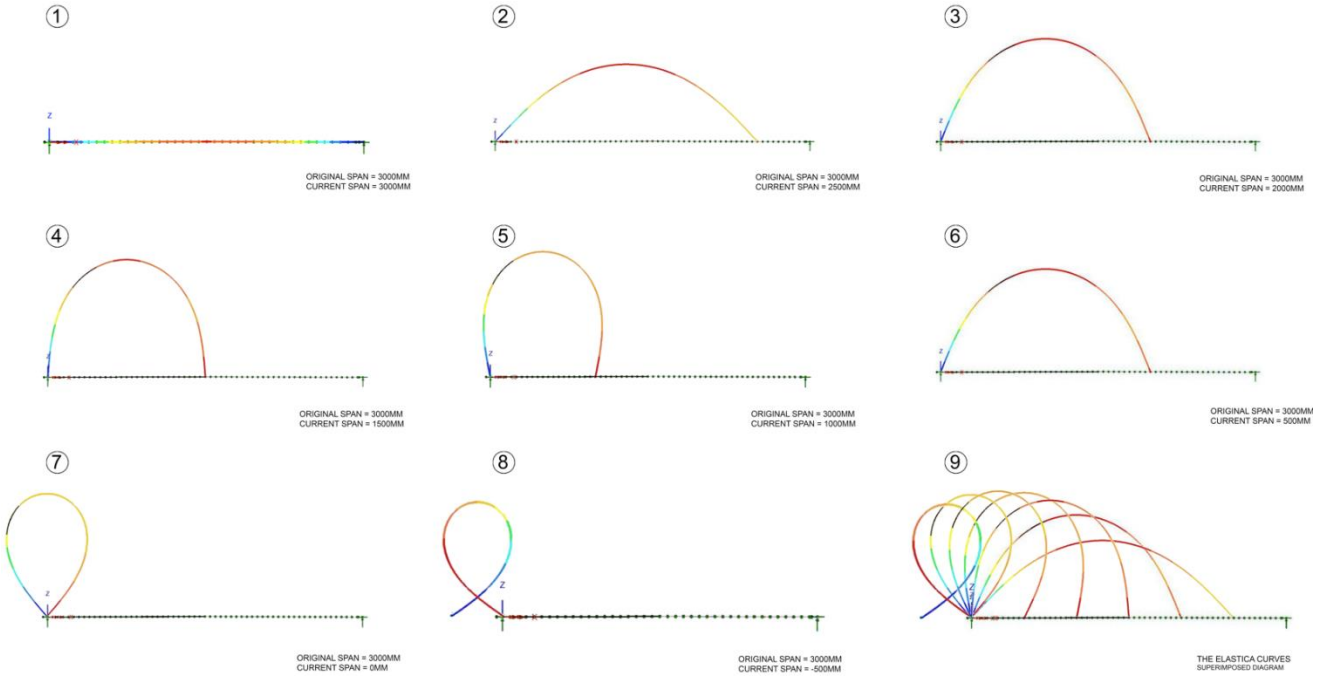

Figure 3.10: Computational Simulation of the Elastica using Finite Element Analysis

The three sets of curves corresponding to each approach were superimposed onto a singular plot to identify the degree of similarity or dissimilarity among the three approaches. It could be noted that through all the 3 approaches, almost identical results were obtained.

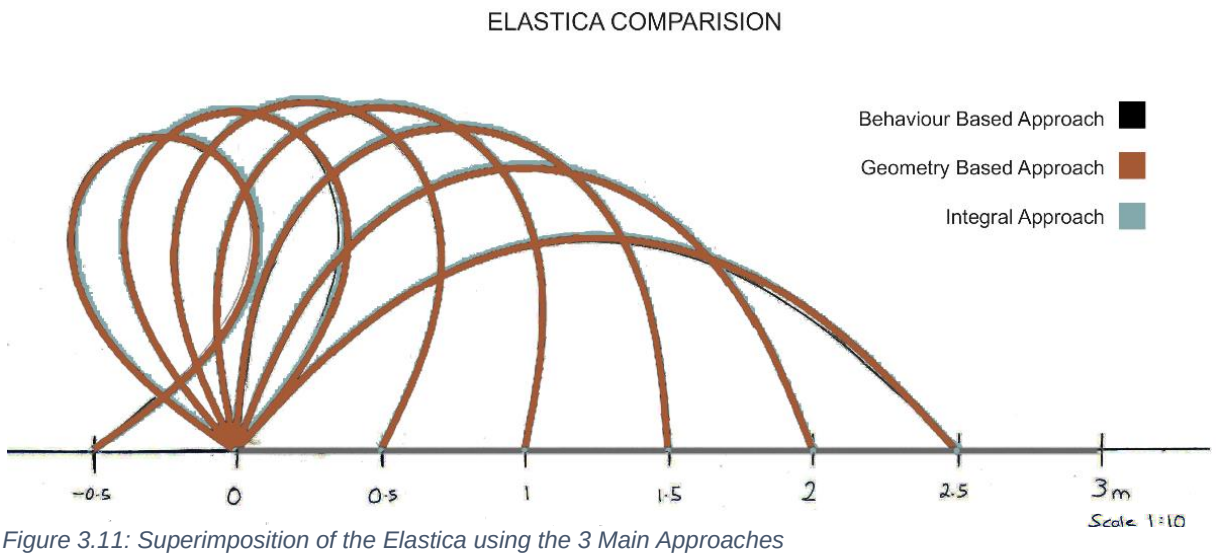

Figure 3.11: Superimposition of the Elastica using the 3 Main Approaches

3.7. Study 3: A 3D Printed Semi-Circular Arch on the Basis of the Geometry Based Approach

As discussed in section 3.3, the geometry of the Elastica and semicircle will not be identical yet similar. Hence a physical study was conducted to test whether an elastically bent integrated formwork can deform into a semicircle if the geometry of the inserted voussoirs is based on a semicircle. The following procedure was used to carry out a geometrical study for the proposed hypothesis.

1. Drawing up of the geometry on Rhinoceros 3D and dividing the arch into an odd amount of voussoirs

2. Creation and preparation of the integrated formwork and voussoirs for 3D printing

3. 3D Printing of the integrated formwork and voussoirs using PLA filament

4. Actively bending the integrated formwork and tying in place to retain the resulting curved shape

5. Filling of the arch with the voussoirs from the ends to the middle until the keystone is locked in

3.7.1. The Formwork and Voussoir Design

A typical masonry arch with mortar joints inspired the design of the formwork. The devised formwork takes the geometry of the mortar in an arch and replaces it with vertical fins. In order to join these vertical elements together as well as to give stiffness to the structure, two shallow continuous elements joining the verticals on each side were added. These elements were kept

to shallow depths in order to allow for enough flexibility during the bending process. Voussoirs would then be fitted within the created voids of the structure. The voussoirs were devised from a semi-circular arch split into an odd number of divisions. This led to the creation of 23 identical voussoirs.

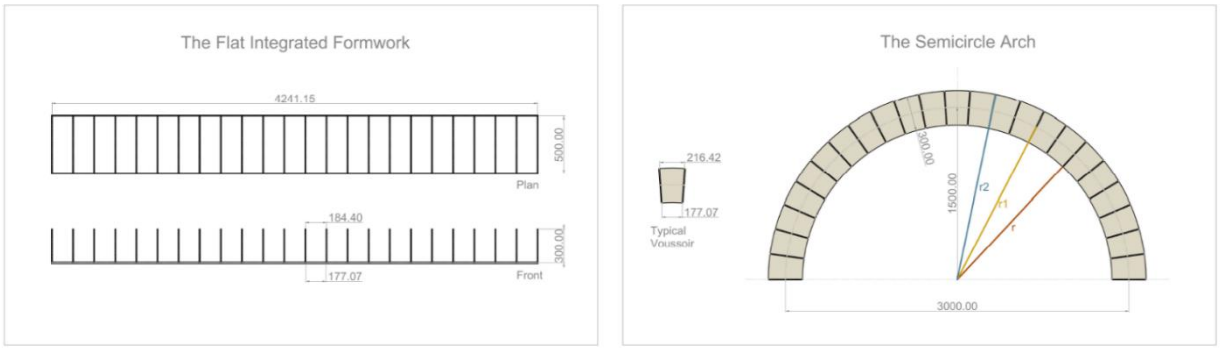

Figure 3.12: Modelling of the Geometry on Rhinoceros 3D of the semicircular arch

3.7.2. Building of the First Prototype

The scale model is 1:10 replica of a an arch which in real life would have a 3m centre-to-centre span with a centre rise (r1) of 1.5m. In reality, the voussoirs would be made out of reconstituted stone, while the integrated formwork would be either steel or timber. However, for the scope of this study, a geometrical approach was undertaken to understand the geometrical behaviour of such a structure.

Figure 3.13: The construction of a 3D printed semicircular arch

The erection process was photographically documented to be able to understand the behaviour of the structure from the initial state when the formwork was elastically deformed and tied as in Figure 3.14 looking at the left image to its transformation into a semi-circular arch with the filling of the 3D printed hollow voussoirs as in Figure 3.14 looking at the image on the right.

Figure 3.14: Left: Elastically bent & tied formwork; Right: Infilled formwork with voussoirs

The Elastica curve could be traced in the initial stage whilst the semi-circular curve is also clearly visible at the final stage. This shows that the initial hypothesis claiming that the formwork will deform into the semicircular curve has been proven to be correct.

3.8. Study 4: Testing of a Joint Formwork in Attempt of Extending the Arch into a Vault

The first attempt at extending the formwork into a 3-dimensional developable surface was to construct a staggered grid pattern with voids. These voids would be later infilled with solid elements once the formwork is erected.

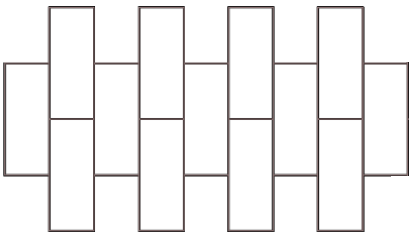

Figure 3.15: The designed joint formwork on Rhinoceros 3D

3.8.1. Why was this configuration chosen?

Such a staggered layout simulates the configuration of typical vaulted structures. The stagger enhances the interlock between each solid member, being a stone voussoir in real life. Moreover, if the printed unit is filled with the solid members, it would form a complete arch which would be able to aid in the load transfer of adjacent stone voussoirs. These would be added on each side of this formwork to extend the structure into a vault.

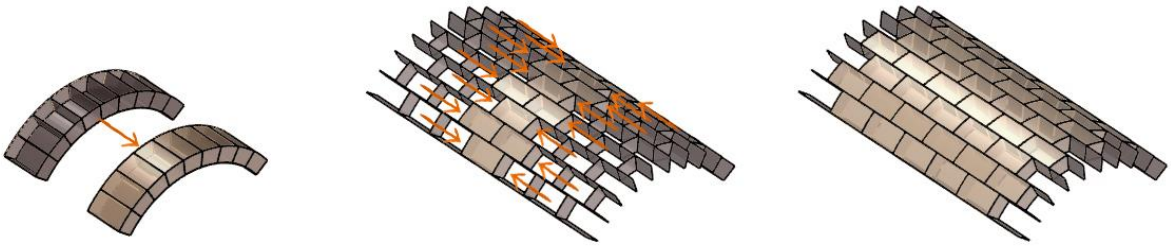

Figure 3.16: Left: Initial concept to develop a 2D arch; Middle: Solving one arch segment to support the adjacent ones; Right: The complete developable surface as a vault

3.8.2. The 3D Printed Form

The joint formwork was 3D printed using PLA and its behaviour under bending was visually analysed. It could be noted that the geometry of the deformed formwork undergoes distortion; the upper end will push outwards whilst the lower end will pull inwards. This creates a re-entrant hexagonal pattern as in Figure 3.17 below. This re-entrant shape is undesirable as it hinders modularity. Hence to overcome such a distortion, study five focuses on a singular strip of the formwork, which can be replicated adjacent to each other as in section 3.11.

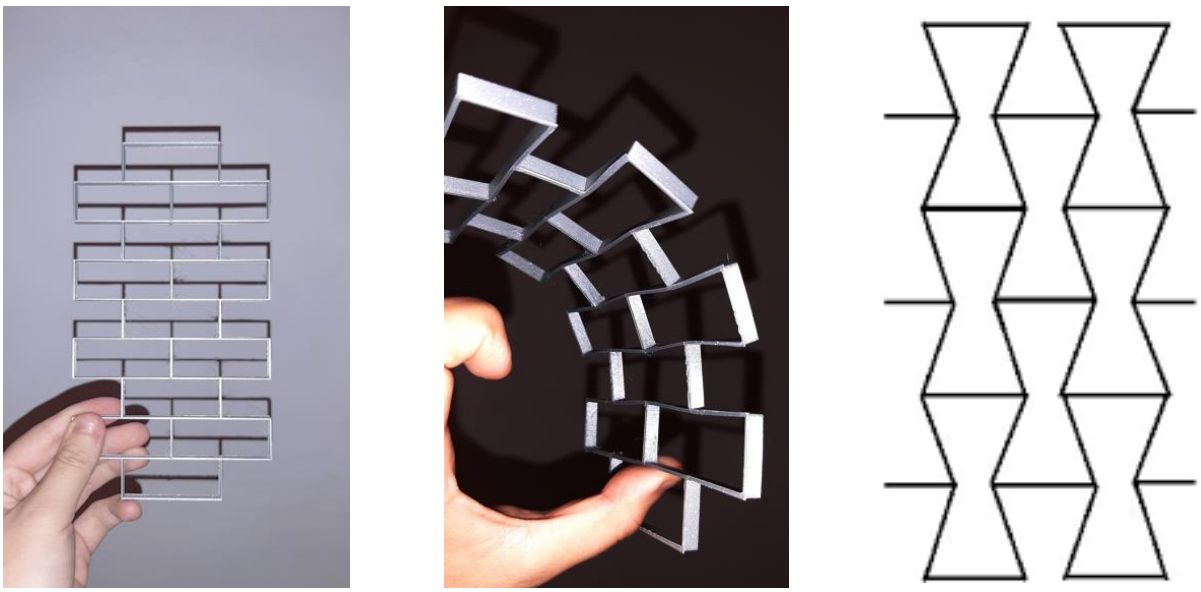

Figure 3.17: Left: Initial state of flat printed joint formwork; Middle: Bent formwork creating the pattern of a re-entrant hexagon; Right: The re-entrant hexagon pattern

3.9. Inspiration from the Curvature of a Catalan Vault

In section 3.7 we have dealt with high span-to-rise ratios resulting in deep arches. These types of arches have been used since the Roman period yet required heavy stones which resulted in bulky and cost inefficient structures (Jagoe, 2021). A more suitable arch for the scope and purpose of this dissertation would be a shallower arch. An inspiring construction system for such a shallow arch is the Catalan Arch/Vault also known as Timbrel Vaulting. This technique was widely used in Spain in the post-medieval period (Gomez-Ferrer, 2009) which led to the production of light, cost and material efficient structures.

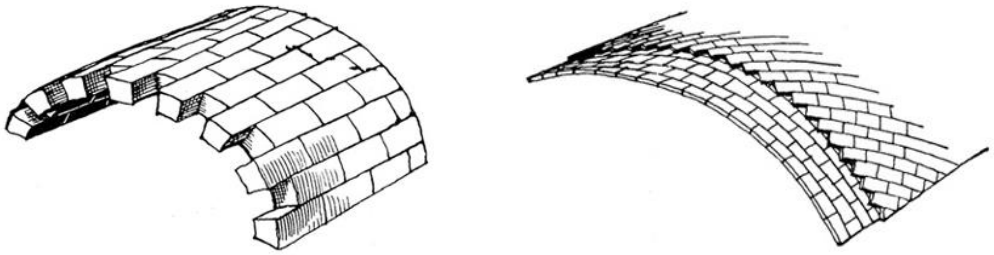

Figure 3.18: Left: A typical stone arch; Right: The Catalan Vault

3.9.1. What is a Catalan Vault?

A Catalan vault can be defined as a vaulted masonry structure typically made up of at least 2 thin layers of bricks which are laid flat and joined together with a rapid setting mortar (at least for the first layer). The following layer is then laid at 45 degrees with respect to the previous layer in order to create a shell effect. The rapid setting mortar eliminates the need of centering throughout the construction process apart from thin strings which are used as a guiding line. This makes the Catalan vault an efficient and cost effective structure (López, 2012).

Figure 3.19: Left: First layer of the Catalan vault using rapid setting mortar; Right: Application of the second layer at a 45 degrees angle

Around the 19th century, architects and engineers like Rafael Gustavino and Antoni Gaudí rekindled the interest in this technique by incorporating modern form-finding techniques and research (Solanki, 2023). Perhaps one of Gaudi's most famous buildings which made use of the Catalan vault technique is the School of the Sagrada Familia which has an iconic wavy roof which is just 0.1m deep. Other impressive shallow roof structures by Gaudi could be viewed at the Coach house in Palau Güell in Barcelona where the rise to span ratios are very low. Looking at Rafael Gustavino, one of his most prominent works is the subway station of New York's City Hall which does not function anymore as a station yet remains as a historical landmark.

Figure 3.20: Left: The roof of the School of the Sagrada Familia; Middle: Coach house in Palau Güell Right: New York's City Hall Subway Station

3.10. Study 5: Moving towards Shallower Segmental Arches

Having been inspired by the works discussed in section 3.9, a process similar to section 3.7 was carried out for a shallower arch version.

3.10.1. Geometrical Script

Prior to the drawing up of the segmental arch, an excel script was created to relate the span and height of a segmental arch to its radius and central coordinates (see Appendix l). The script uses the equation of a circle ((x-a)^2 + (y-b)^2 = r^2) which has 3 unknown parameters being the radius (r) and the central coordinates (a,b). By knowing just 3 coordinates of the circle which correspond to the start, end and rise of the arch segment we can substitute in the general equation of a circle to end up with 3 equations that can be solved simultaneously. The excel solver script was used to find a value for the 3 unknown values.

2. Arriving to the Radius (r) and Circle Centre Coordinates (a,b) from 3 points on a curve

a. 3 Known Points on the Segment of the Circle

	x	y	Units
Point A (start of arch segment	0	0	m
Point B (end of arch segment	3	0	m
Point C (rise of arch segment	1.5	0.1	m

b. Equation of a Circle

$$r^2 = (x-a)^2 + (y-b)^2$$

Where the unknowns are:

r	radius of circle
a	x-coordinate of the centre of a centre
b	y-coordinate of the centre of a centre

c. Writing the 3 Simultaneous Equations from the 3 points on the Circle

	RHS of Equation (x-a)^2 + (y-b)^2		LHS of Equation r^2	
Equation 1	127.6899972	=	127.6896993	*r^2 = (0-a)^2 + (0-b)^2*
Equation 2	127.6899972	=	127.6896993	*r^2 = (3-a)^2 + (0-b)^3*
Equation 3	127.6899972	=	127.6896993	*r^2 = (1.5-a)^2 + (0.1-b)^4*

d. Finding the r, a and b values

r	11.29998669	m
a	1.5	m
b	-11.19999987	m

Figure 3.21: An extract from the segmental arch script (full script found in Appendix (I)

3.10.2. Modifications to the Formwork

In this study, the integrated formwork was simplified to two slender 3D printed rods which fit at the lower end of the vertical fins. These rods shall support the voussoirs which slot into the rods until the arch is closed off by the keystone. The resulting scale model is 1:10 replica of a an arch which in real life would have a 3m centre to centre span with a rise (r) of 0.1m.

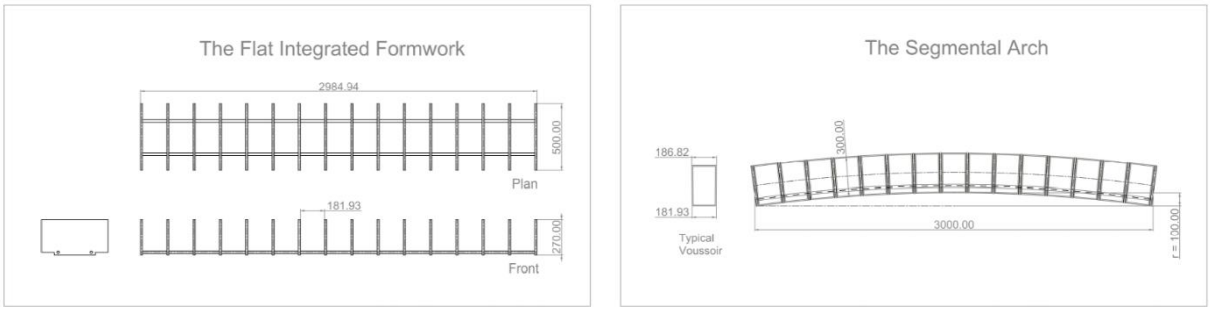

Figure 3.22: Modelling of the Geometry on Rhinoceros 3D of the segmental arch

This study was further explored into the third dimension, from a planar arch to a three-dimensional vault by simply staggering the voussoirs. This creates an interlocking action between the members which can aid in carrying of adjacent stones, as shown in Figure 3.23.

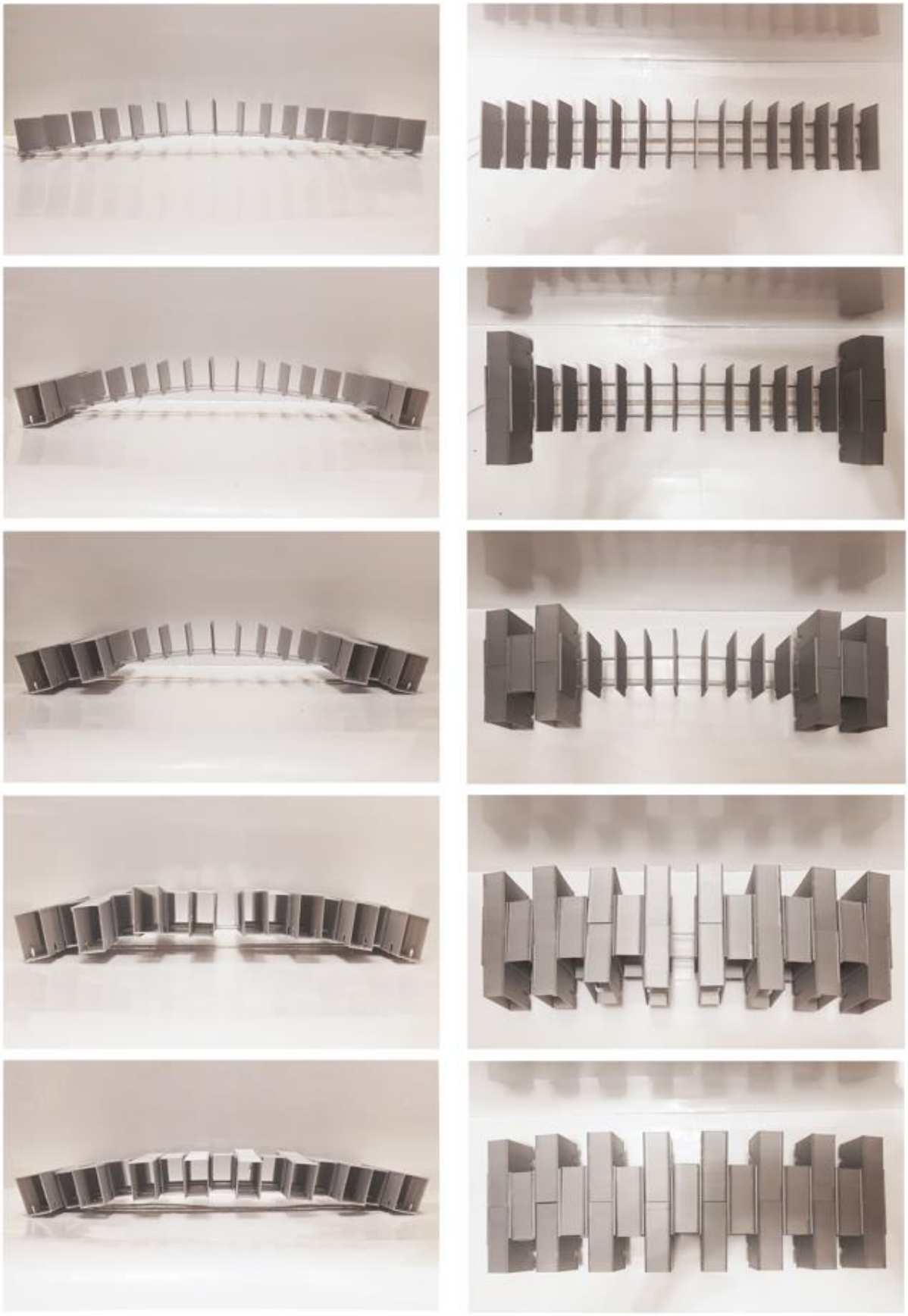

Figure 3.23: The construction of a shallow segmental arch with a rise of 10mm over a span of 300mm
Left: Elevation of the erection process; Right: Plan view of the erection process

Being a very shallow arch, the Elastica and segmental arch curves are very similar unlike in section 3.7, where the rise of the arch was much deeper.

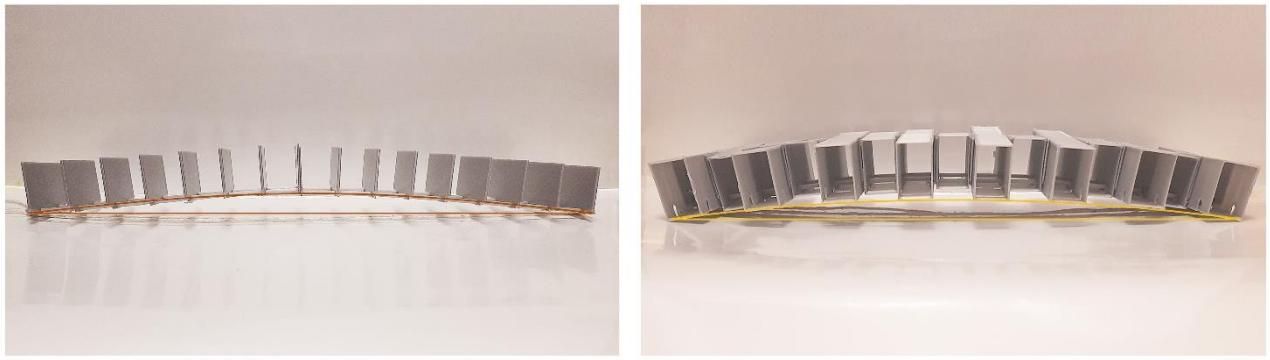

Figure 3.24: Left: Initial state of the deformed empty formwork (Elastica); Right: Filled segmental shallow arch

3.11. Study 6: The Construction of a Shallow Barrel Vault

The testing carried out in sections 3.10 served as a segment prototype of a shallow barrel vault. This led the design to progress into a shallow barrel vaulted roof. A 3x3m room was considered for this study across which the vaulted roof shall span. Again, the physical model was devised at a scale of 1:10.

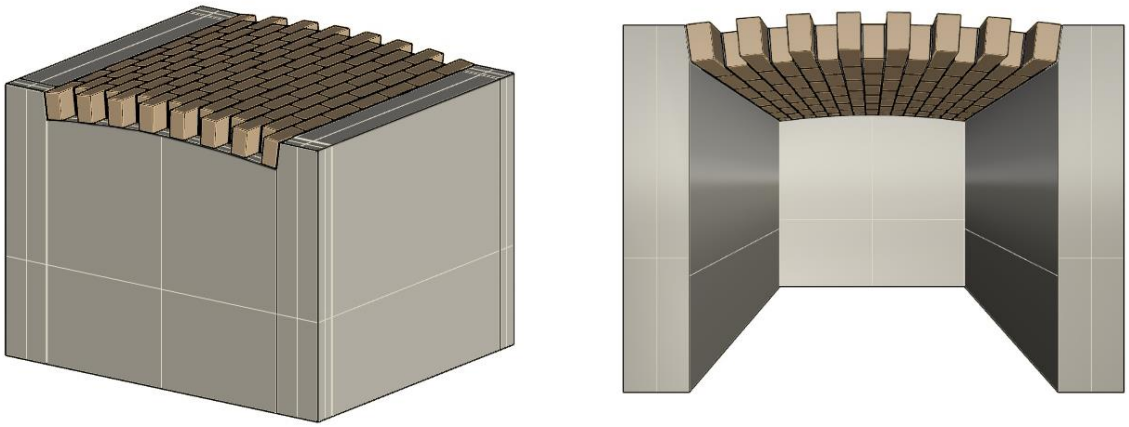

Figure 3.25: 3D Modelling on Rhinoceros 3D of the shallow barrel vault

3.11.1. Modifications to the Design in section 3.10

The same parameters for the rise (10mm) and span (300mm) were used as in section 3.10 yet small modifications in the formwork materials and voussoir design were made as follows;

a. The rods of the integrated formwork were changed to 1.5mm diameter steel rods. This was done in effort to replicate the real life scenario where the anticipated material is elastic steel.

b. The 3D printed PLA voussoirs were printed as hollow structures similar to a hollow concrete block. This would allow for the filling of the voids with a heavier material such as lead or sand in order to replicate the weight effect of the stone voussoir which would be present in the real life scenario.

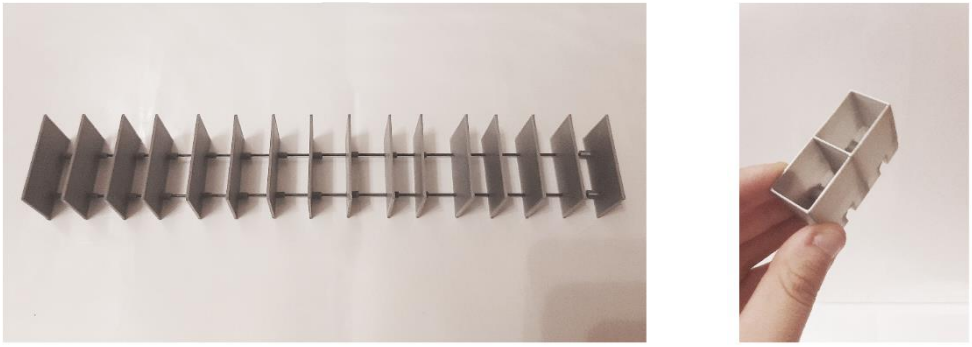

Figure 3.26: Left: Steel rods incorporated in the formwork; Right: A typical hollow voussoir

Being a shallow arch, a thick structure was needed to cater for the high lateral thrust at the abutments. In the scale model, a timber structure was built with chamfered walls at the point of intersection of the vault structure with the walls. In real life, the thick structure would translate into thick masonry walls. The formwork was actively bent using the ease-down method in between the walls of the structure. Starting from the ends, voussoirs were placed in a staggered manner until the central keystones were fitted.

Figure 3.27: The construction of a shallow segmental vault with a rise to span ratio of 0.033
Left: Elevation of the erection process; Right: Planar view of the erection process

When comparing the stiffness of the empty formwork to the completed arch version, a significant increase in stiffness could be noted. The formwork's stiffness was sufficient in supporting the 3D printed voussoirs yet such an observation requires further analysis since the voussoirs used were relatively light in comparison to the real life ones which will exert a larger force on the formwork due to their weight. This was analysed in study 8 through the use of Finite Element software.

In this study only part of the vault was constructed. The same methodology could be adopted for its completion yet for the scope of the study this was not necessary.

3.12. Study 7: Fifth Prototype of a Flat Arch

Study 7 was carried out to understand the effect of curvature ,even if shallow, on the behaviour of the structure. Hence a flat arch with rectangular voussoirs was devised making use of the same span of 300mm as in the previous studies. The construction process has been photographically documented in Figure 3.28.

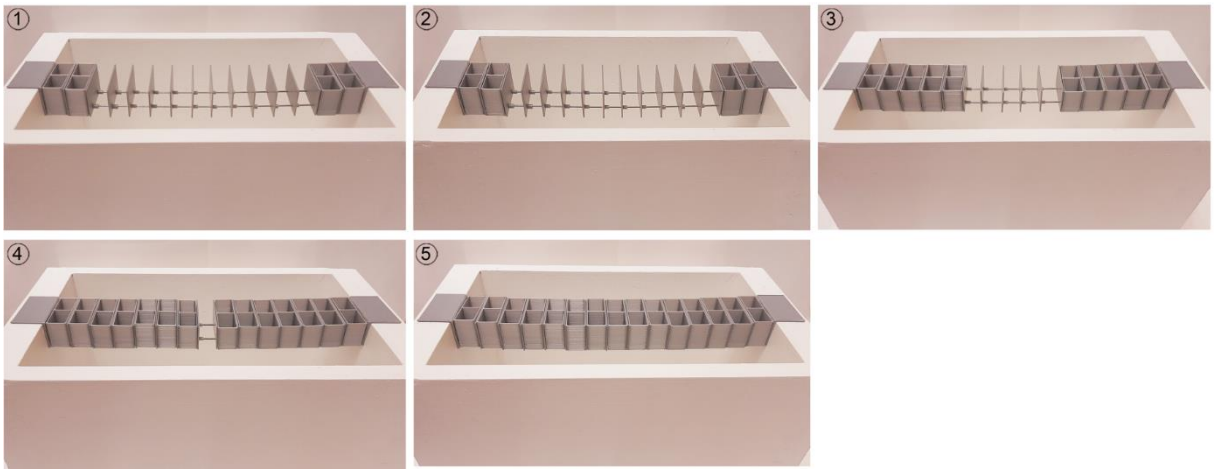

Figure 3.28: Physical model of a flat arch – construction process

The structure displayed a low level of stiffness when compared to the other arched physical models. Upon loading, the structure started to deflect downwards even though the voussoirs were relatively light. Moreover, once the structure was complete, no additional stiffness was gained and beam behaviour was predominant. This observation verifies the significant improvement in structural behaviour resulting from curvature, even if the value of such a curvature is low.

3.13. Finite Element Analysis

3.13.1. An introduction to the Finite Element Method and Analysis

Finite Element is a powerful computational tool by which engineers can simulate complex physical problems that traditional structural software cannot solve. Essentially, the Method of Finite Element is a numerical approach similar to methods like the finite difference yet is more capable at analysing complex geometries and structures which have a high degree of sophistication (Reddy, 2009). So how does it work?

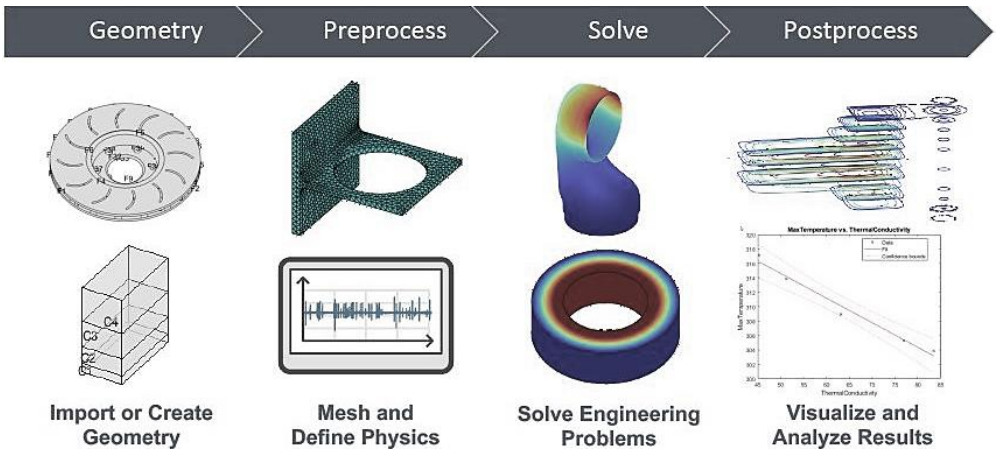

Figure 3.29: Steps of Finite Element Analysis (Mathworks, 2023)

3.13.2. How does the Finite Element Method work?

The Method of Finite Element works by taking the structure under analysis referred to as the *domain* and breaks it down into a number of geometrically smaller units which are referred to as *finite elements.* The process of breaking down the domain into smaller finite elements is known as discretization. Each finite element is made up of a number of edge points which are referred to as *nodes* joined together by a *mesh.* Each finite element can have its unique properties such as size and material. The software then generates algebraic equations for each local element and combines them together to obtain a solution for the global structure (Grasp, 2023).

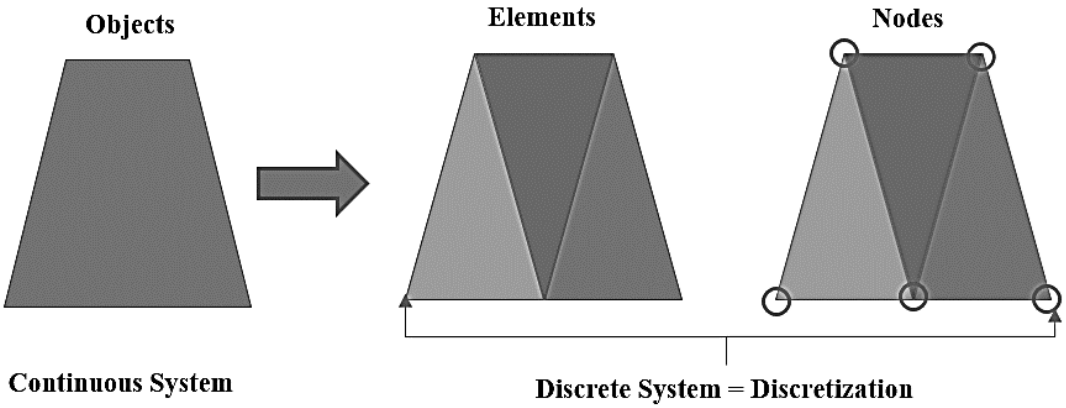

Figure 3.30: The discretization process (Grasp, 2023)

3.13.3. Modes of Analysis

Finite Element Analysis can be carried out either linearly or nonlinearly. The system can be considered as linear if the equation of equilibrium can be expressed on the undistorted member and if a multiplication of Force F by n will also increase the displacement of the deformed member denoted by the letter u by a factor n. This results in a constant stiffness matrix denoted by the letter K. This linear system can be expressed mathematically as per equation 3.2:

$$\begin{aligned} &\textit{Linear:} \\ &\underline{\underline{K}} \cdot \underline{u} = \underline{F} \\ &\underline{F} \cdot n = \underline{\underline{K}} \cdot \underline{u} \cdot n \end{aligned} \tag{3.2}$$

On the other hand, in a nonlinear system equilibrium can only be achieved when the member has undergone deformation leading to an inconstant stiffness matrix made up of the final deflections of the member. Similarly here a multiplication of Force F by n will also increase the displacement of the deformed member by a factor m yet n and m will not be equal. This nonlinear system can be expressed mathematically as per equation 3.3 and is known as nonlinearity in geometry:

$$\begin{aligned} &\textit{Nonlinear:} \\ &\underline{\underline{K}}(\underline{u}) \cdot \underline{u} = \underline{F} \\ &\underline{F} \cdot n = \underline{\underline{K}}(\underline{u}) \cdot \underline{u} \cdot m \\ &\textit{with } n \neq m \end{aligned} \tag{3.3}$$

For the scope of this dissertation study, a nonlinear approach was adopted due to the expected large stresses and deformations. All Finite Element Analysis was carried out with the software LUSAS Analyst Plus version 19 (Lusas, 2023).

3.14. Study 8: Finite Element Analysis of Stage 1: The Erection Process and Filling of the Formwork

The following study was devised as a Finite Element Analysis of physical study 6 found in section 3.11.

The proposed structural system can be divided into **two** main stages;

a. The *first stage* corresponds to the filling of the voussoirs into the formwork. At this stage, beam action is the primary action where the steel rods will predominantly undergo bending.

b. The second stage corresponds to completed arch stage where arch action is predominant. One of the main concerns regarding the filling of the formwork with the stone voussoirs is its behaviour under the loading progression and hence this was studied in this section.

3.14.1. Modelling the Geometry

The model in study 6 is a three dimensional vaulted structure. For the purpose of this analysis and the understanding of the structural behaviour, a 250mm typical segment of the arch was

taken as indicated in Figure 3.31 below. This segment consists of a tension rod, vertical fins and voussoirs of 250mm width.

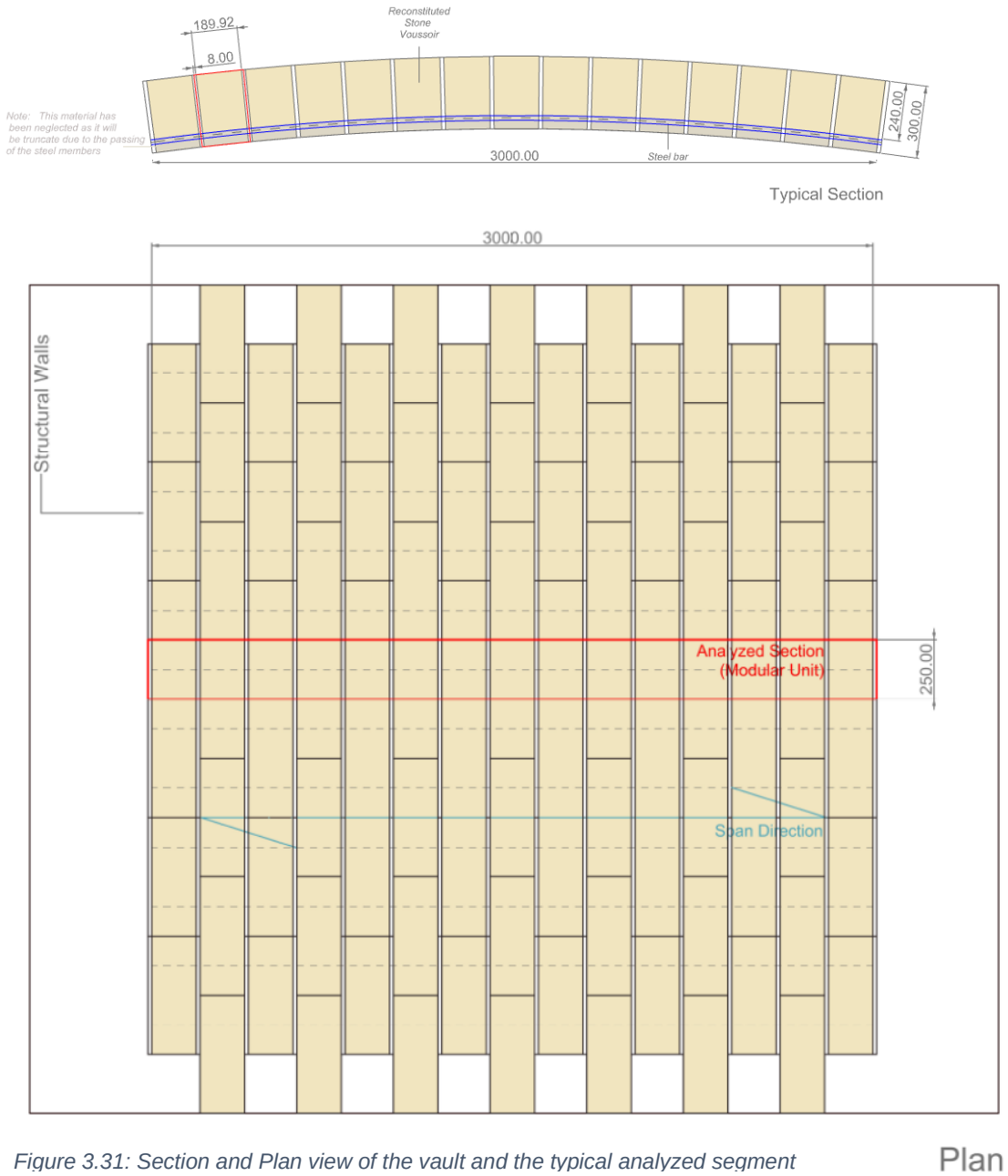

Figure 3.31: Section and Plan view of the vault and the typical analyzed segment

The analysis of this typical segment was carried out using 3 approaches:

Approach 1: The Simplified Approach

Approach 2: The Middle Approach

Approach 3: The True Formwork

The aim behind these 3 approaches is to understand whether the vertical fins offer any additional stiffness to the formwork. In both approaches, the considered materials were steel for the rod and vertical fins whilst the voussoirs were modelled as a nonlinear concrete to replicate the behaviour of reconstituted stone.

3.14.1.1. The Simplified Approach

In this Approach, the formwork was simplified by ignoring the vertical fins and modelling only the rod part. This was modelled as a flat line element to which the geometrical properties of a rod element were assigned along with the material here being steel. The member supports were assigned as a roller and pin. Using these parameters, an eigenvector analysis to attain the first mode of vibration (fundamental frequency) was carried out. This was followed by a linear buckling analysis which was carried out through the application of a prescribed displacement applied to one side of the structure. From this analysis, the geometry corresponding to a span of 3000mm and rise of 100mm was used as the base geometry for the loading stage.

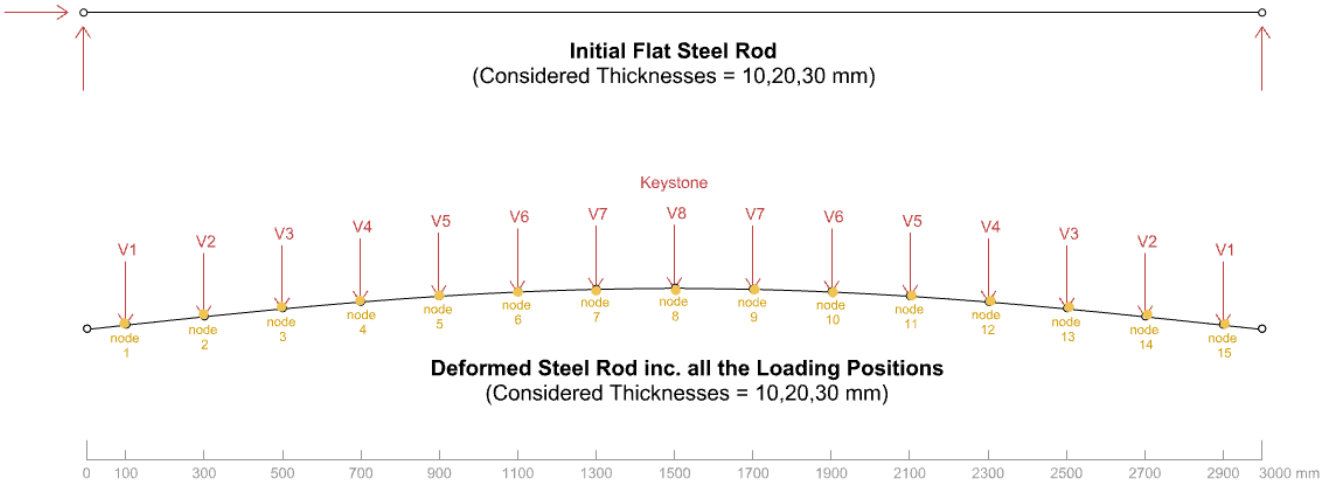

Figure 3.32: Approach 1: Simplified model
Top: Initial Flat Steel Rod; Bottom: Elastically bent steel rod with applied point loads

The second stage corresponded to the loading of the formwork with the voussoirs. In this analysis, the supports were altered as being both pinned whilst a concentrated load having the equivalent load of the voussoir and half of the steel vertical fin on each side was created. The analysis was carried out by applying the concentrated loads along the formwork in progressive steps at the denoted locations in Figure 3.32, each time noting the corresponding stresses and displacements. Three rod thicknesses were used being 10, 20 and 30mm in diameter.

3.14.1.2. The Middle Approach

Moving closer to the true behaviour of the formwork, the actual formwork was modelled yet loading was applied in the same manner as in section 3.14.1.1, in the form of concentrated point loads. This would simulate the true formwork's behaviour while eliminates any second order effects from the voussoirs. This was also repeated for the 10, 20 and 30mm diameter rods.

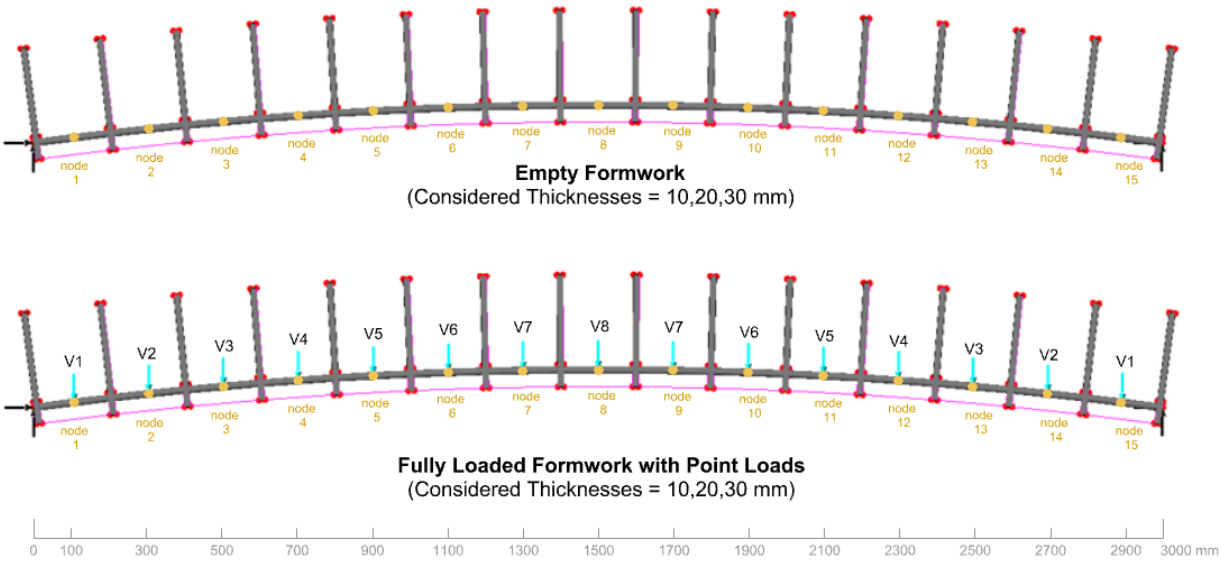

Figure 3.33: Approach 2: The Middle Approach
Top: Model of the Empty Formwork; Bottom: Model of the Formwork with applied point loads

3.14.1.3. The True Formwork

Lastly, the true formwork was then modelled including the vertical fins and stone voussoirs. Since the rise to span ratio is so low, the Elastica and semicircle curves are almost identical. Due to the increased complexity of the model, the formwork forming part of an arch segment was modelled on Rhinoceros 3D and imported in Lusas Analyst. To model the true interaction between the formwork and voussoirs, the actual voussoir was now modelled and a slide line was used to model the interaction between the formwork and voussoirs. The vertical steel fin was fixed at a thickness of 16mm. Again, the thickness of the steel rod was varied between 10-30mm in order to be able to compare with the simplified approach in section 3.14.1.1.

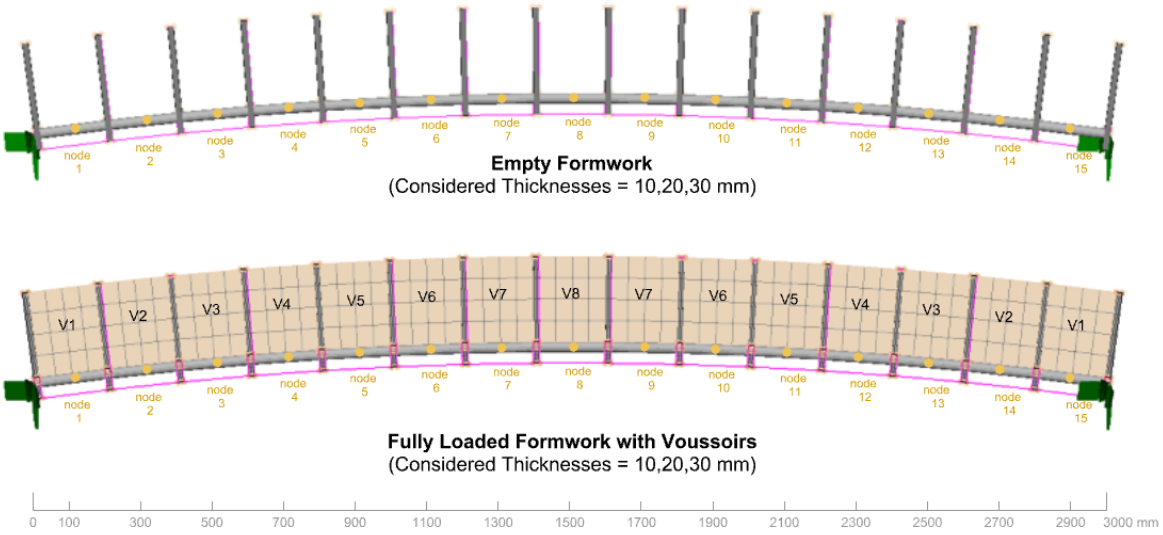

Figure 3.34: Approach 3: The True Formwork
Top: Model of the Empty Formwork; Bottom: Model of the filled Formwork with Voussoirs

3.15. Study 9: Finite Element Analysis of the 2 Phases of the Structure continuing with Stage 2: Understanding the Behaviour of the Completed arch

In study 8, the filling of the formwork with the voussoirs corresponding to stage 1 was outlined. Study 9 here focusses on the behaviour of the arch with the integrated formwork. Taking the model described by Figure 3.35, the arch was analysed under a uniformly distributed load. In order to understand how the rod thickness affects the final behaviour of the arch, the model was analysed for the 10, 20 and 30mm rod diameters respectively. A load of 1N/mm was applied to the structure and incrementally increased up until the collapse load was reached. The recorded parameters for every load increment were;

a. The central displacements

b. The compressive stresses within the middle reconstituted stone voussoir at the top node

c. The corresponding horizontal reaction

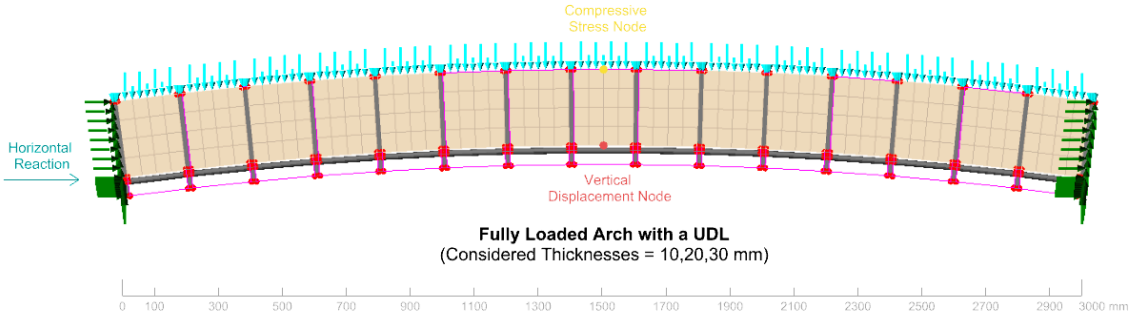

Figure 3.35: Model and analyzed parameters for study 9

3.16. Study 10: A Comparative FEA study between a Completed Formwork Integrated Arch, a similar Arch that eliminates the Steel Rod of the Integrated Formwork whilst retaining a Steel Joint and a Traditional Mortar Jointed Arch

The aim of study 10 was to understand whether the integrated formwork offers any structural behavioural enhancements over a traditional masonry arch constructed from stone voussoirs and mortar joints. To manifest the difference in structural behaviour, 3 models were used being:

Model 1: The full integrated filled formwork as displayed in Figure 3.35 considering a 20mm rod. This rod thickness was selected to ensure that on site, the integrated formwork could be elastically bent into position. This was deemed as reasonable for a 3000mm span.

Model 2: Model 1 was altered by removing the lower end of the integrated formwork, ending up with an arch having the mortar joint replaced by steel plates as in Figure 3.36.

Model 3: Model 3 took the geometry of model 2 yet the joint between the voussoirs was altered to mortar, turning model 3 into a traditional arch as in Figure 3.37.

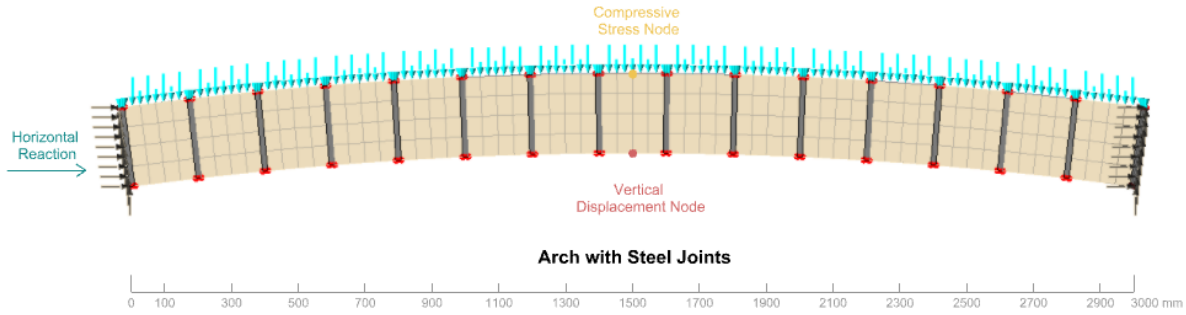

Figure 3.36: Arch with steel joints

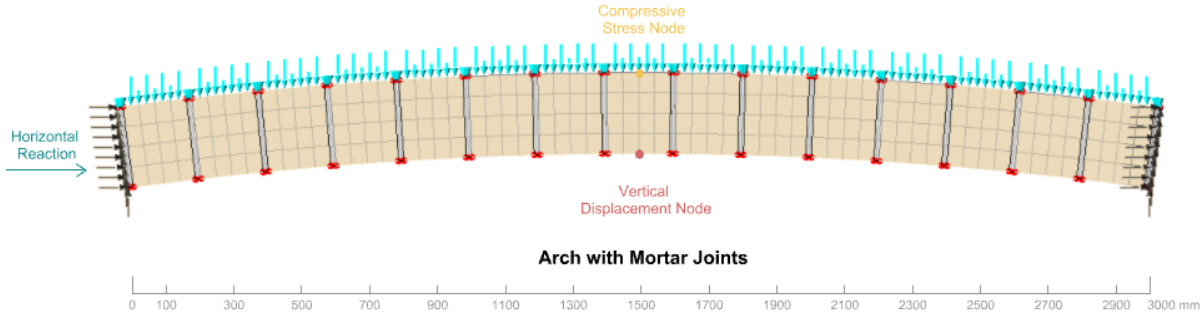

Figure 3.37: Arch with mortar joints

The structures were assessed under a 1N/mm uniformly distributed load which was incrementally increased up to the collapse load. Similar to study 9, the three models were compared by noting the central displacements at the lower node, the compressive stresses within the middle reconstituted stone voussoir at the top node and the corresponding horizontal reaction.

3.17. Study 11: A Comparative Analysis between Finite Element Analysis and Heyman's Funicular Polygon

The final study deals with the comparison of the Method of Finite Element with the traditional elastic method brought forward by Heyman, the Funicular polygon.

The Method of Finite Element makes use of discretization whilst taking into consideration the material of the structure along with its support conditions. Using these conditions, the software is able to converge to a solution. On the other hand, the Funicular polygon adopts a simplified approach where via a graphical study based on the attainment of equilibrium, a value for the horizontal reaction and corresponding line of thrust can be attained.

Whereas Finite Element Analysis can offer a detailed result consisting of displacements, stresses, support reactions, etc., the Funicular Polygon method simply assumes a direct compressive path which is the line of thrust. This method does not factor in the material properties nor any nonlinearities which might arise within the structure.

The aim of this study was to analyse a mortar jointed arch having equivalent stone thickness as the formwork integrated arch both with the Method of Finite Element as well as using the method of the Funicular Polygon for a live load of 5KN/m^2. Hence the study was split into 2 parts:

Part 1: Analysis in Finite Element

The study started off with the analysis of a traditional mortar jointed arch under the prescribed loading in Figure 3.38. A full outline of the applied loading can be found in Appendix V. The horizontal reactions and central vertical displacements were noted. This procedure was repeated on a formwork integrated arch having a 20mm bar as in Figure 3.35.

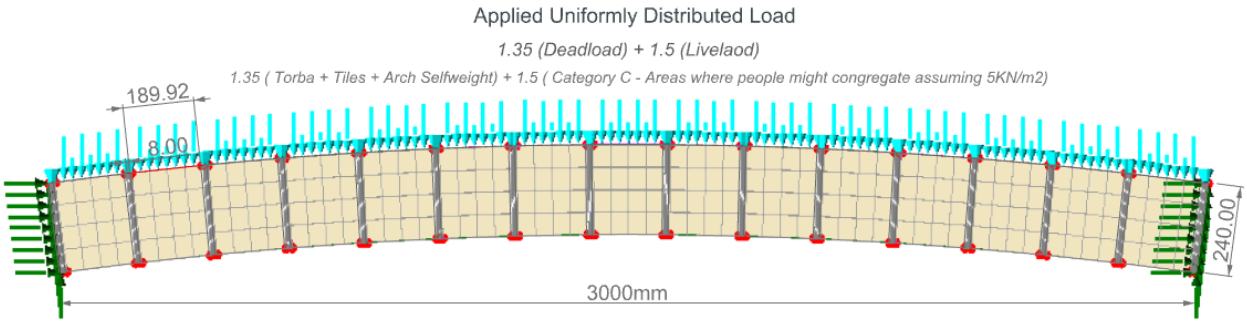

Figure 3.38: Traditional Arch under analysis by FEM and the Method of Funicular Polygon

Part 2: Heyman's Funicular Polygon

The investigation proceeded by the geometrical study of the Funicular Polygon Method. For this study, the uniformly distributed load was converted into 15 equivalent point loads as seen in Figure 3.39 in order to attain a smooth line of thrust. This resulting shape from this approach of analysis is the catenary which when inverted will result into the line of thrust of the arch.

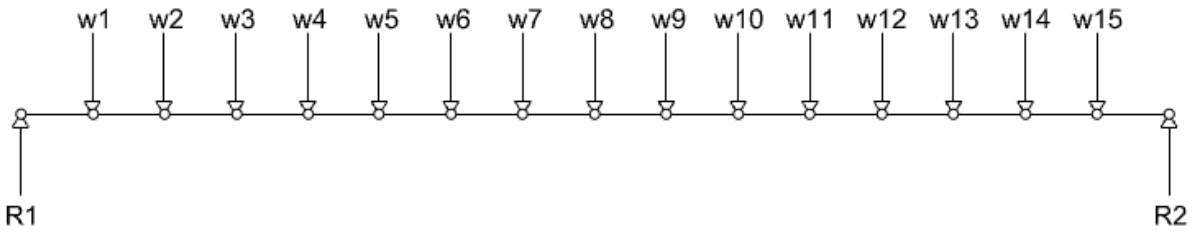

Figure 3.39: Simplified Diagram for the geometrical setup of the Funicular Polygon

By assuming 5 values of horizontal reactions being 10, 15, 20, 25 & 30KN, the corresponding lines of thrust could be derived. The derived lines of thrust were fitted within the arch geometry to get an estimate of the factor of safety of the arch for each horizontal force.

By analysing a traditional arch in Finite Element and by the Method of Funicular Polygon, the attained results could be compared with the possibility of offering an insight on which of the methods is the more conservative. The results from the Finite Element Analysis on the devised integrated formwork arch and traditional arch could then be compared to those attained by the Method of Funicular Polygon.

3.18. Conclusion

The chapter started off with a reminder of the fundamental questions of this study which guided the content of this section. Gaussian Curvature was introduced to describe the resulting geometry of the devised structures in terms of positive, negative and zero curvature. Zero curvature corresponding to developable surfaces was the geometry of interest for the rest of the studies.

Having already introduced the Elastica and its geometry, this section delved further into the relationship between the radius of curvature along the Elastica which was concluded to be variable. Tensile restraining systems were a possible solution for the modification of the Elastica into a semicircle yet this was not the desirable approach for this carried out studies.
In order to understand whether it is possible for a bending-active formwork having the geometry of the Elastica to geometrically deform into a segment of a circle along with the resulting arch behaviour from the filling of the formwork, **eleven** short studies were conducted as follows;

1. Study 1 aimed to understand the geometrical differences in the formwork between the erection (the Elastica) and completion stages (the arch) from which it could be concluded that the Elastica curve is deeper and narrower for the same parameters of span and length.

2. Study 2 aimed to understand whether any differences arise in the Elastica geometry when considering the 3 main design approaches for bending-active structures which resulted in almost identical results for the three approaches.

3. The third study prototyped the first 3D printed deep arch which exhibited the transformation of the Elastica corresponding to the formwork stage into the semicircle which corresponds to the completed arch stage.

4. An attempt at a joined formwork in Study 4 offered undesirable results due to the formation of a re-entrant shape.

5. A shallow 3D printed arch prototype was done in Study 5 in effort of replication of the shallow roof structures created by Gaudi.

6. Study 6 prototyped a vaulted structure on the basis of the results from Study 5.

7. Having a flat form, study 7 resulted in beam action over the arch action found in study 6.

Studies 8-11 were also briefly outlined in this section. The following chapter shall outline the results attained through Finite Element Analysis for the named studies.

4. Results

4.1. Introduction

In the previous chapter, the various physical models done to visualise and test the geometrical feasibility of the devised formwork have been outlined and demonstrated. These physical models have led to the development of Finite Element studies 8,9,10, and 11, which have also been outlined in Chapter 3. In this chapter, the aim is to analyse the results obtained through Finite Element Analysis and understand how the behaviour of the formwork changes between the loading stage and the final stage when considering different material thicknesses. One of the objectives is to understand whether the formwork enhances the arch's behaviour and ultimately understand the structure's load-bearing capacity. Finally, Finite Element Analysis results were compared to Heyman's Funicular Polygon Method as a way to relate older and more traditional methods of analyses to contemporary and new software based methods like the Finite Element Method.

4.2. Study 8: The Behaviour of the Formwork under Loading

4.2.1. The Simplified Approach

In section 3.14.1.1, the modelling of the simplified formwork on Lusas was explained. The obtained results were the resulting outcomes from the application of progressive loading in the form of point loads V1 to V8 on each side of the formwork, equivalent to the load of each voussoir and corresponding vertical fins on each side of the voussoir for the three different rod thicknesses. Below are the attained displacements results for the 10, 20 and 30mm rods respectively. The resulting deformations were scaled by a factor of 10 in Figures 4.1- 4.3.

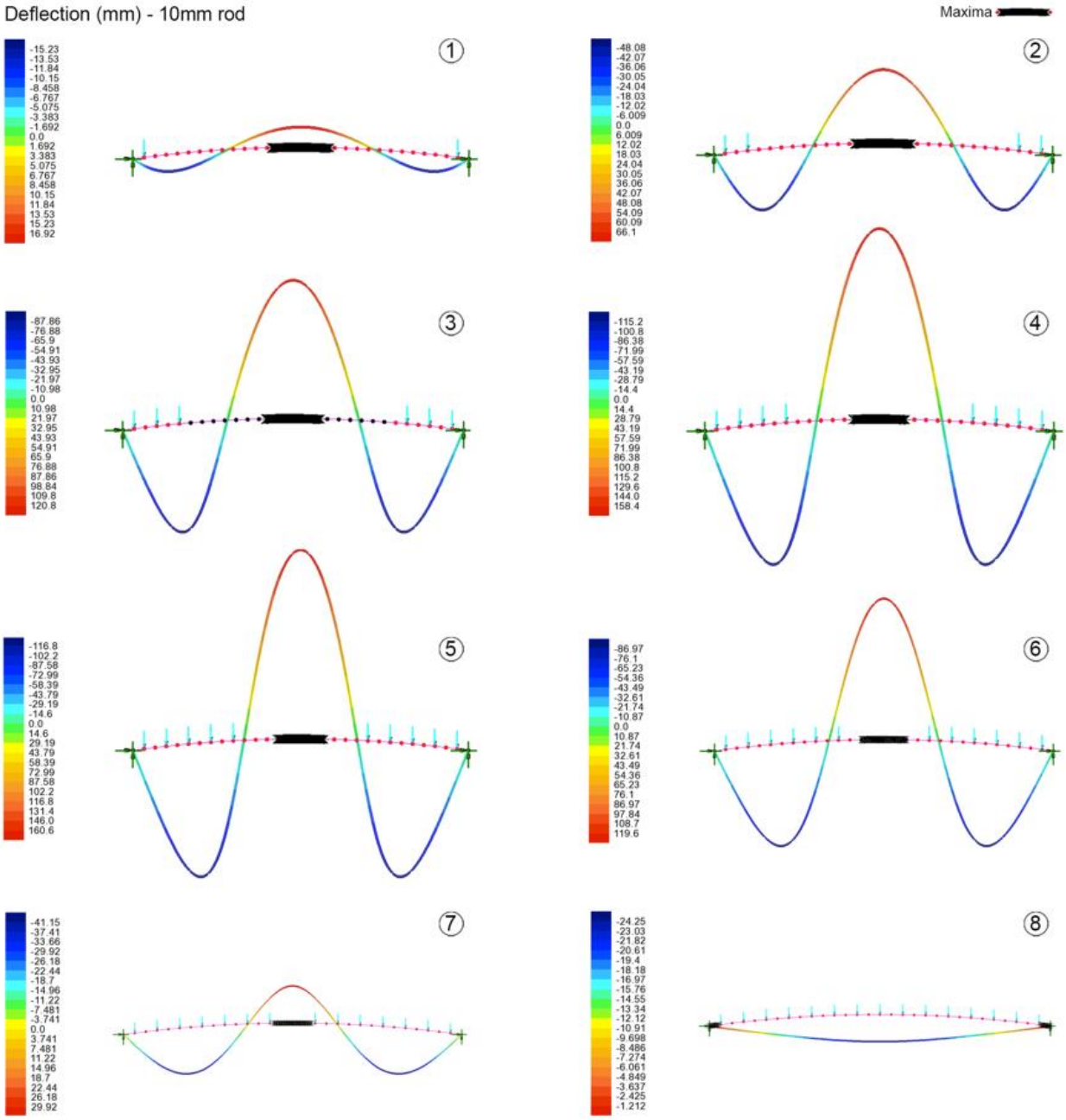

Figure 4.1: Deformations for the Simplified approach using a 10mm rod

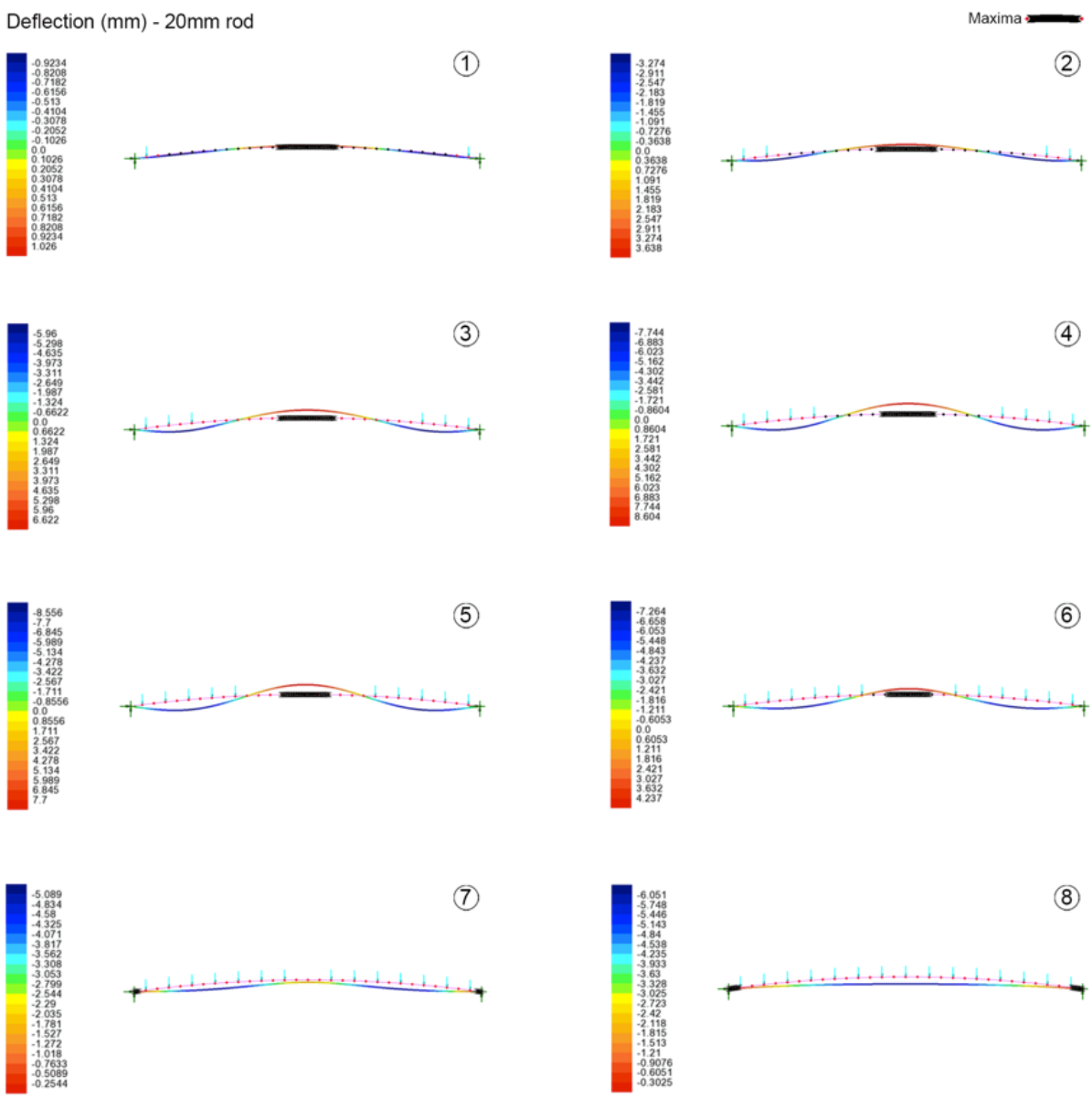

Figure 4.2: Deformations for the Simplified approach using a 20mm rod

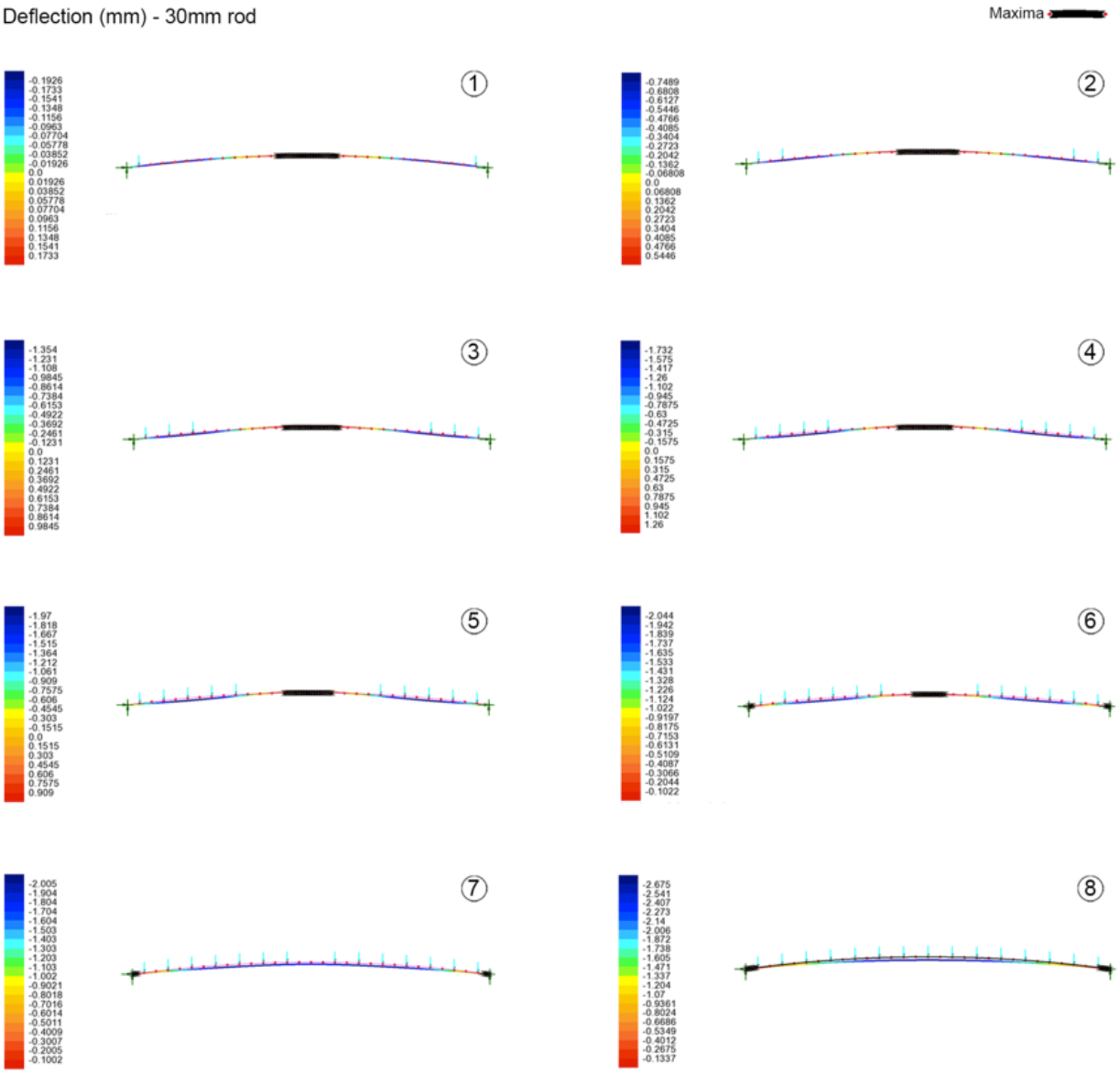

Figure 4.3: Deformations for the Simplified approach using a 30mm rod

Firstly, the central displacements corresponding to each loading case starting from the ends and progressively moving towards the centre were plotted on a singular graph and displayed in Figure 4.4. Each curve represents a rod thickness, with every point on the graph corresponding to a loading position which is marked on Figure 3.32. The plotted data was extracted from the analysis results represented in Figures 4.1,4.2 and 4.3 from which the central displacements were noted and plotted against the loading position. In Appendix (II) result tables can be found.

Two main observations could be drawn from the resulting graph in Figure 4.4;

(i) Firstly, the effect of thickness on deflection where it was observed that the 10mm rod had the worst central deflection of +171.7mm, whilst for a rod with double the diameter (20mm) deflections fell to +8.9mm. In comparison, deflections were more than 20 times greater for the 10mm rod. The 30mm rod exhibited superior behaviour, with the worst central deflection corresponding to -2.7mm.

(ii) The second observation corresponds to the loading locations which lead to the worst global deformations in Figures 4.5-4.7. A pattern could be noted that deformations peaked when progressive loading reached point loads V4 & V5 for the 10 and 20mm rods. These loads fall at a distance of around 750mm from the end supports.

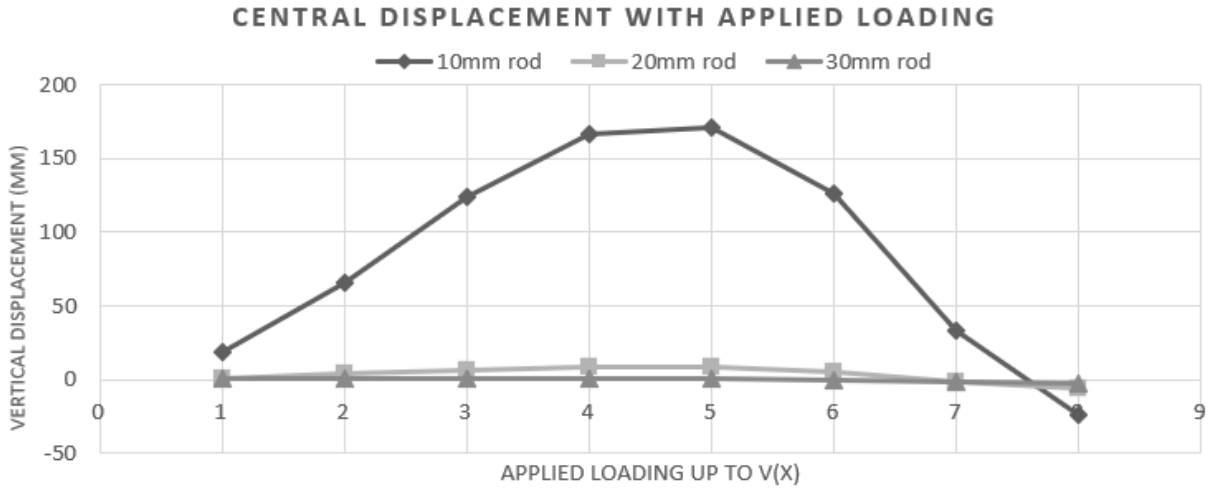

Figure 4.4: Central Displacement vs applied loads for the simplified approach

For every loading combination starting with loads V1, loads V1-V2 up to loads V1-V8, the corresponding displacements at nodes 1-15 as indicated in Figure 3.32 were documented and plotted on a graph. This resulted in the graphs found in Figures 4.5-4.7 corresponding to the 3 different types of rods.

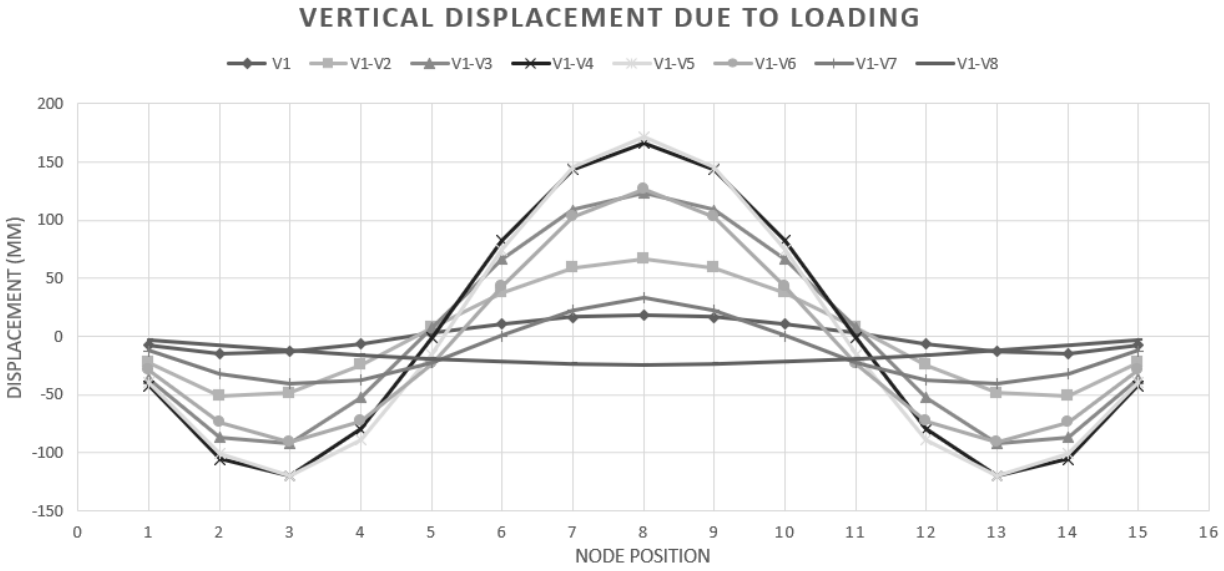

Figure 4.5: Vertical displacements for a 10mm rod at nodes 1-15 for progressive loading starting from V1 up to V8

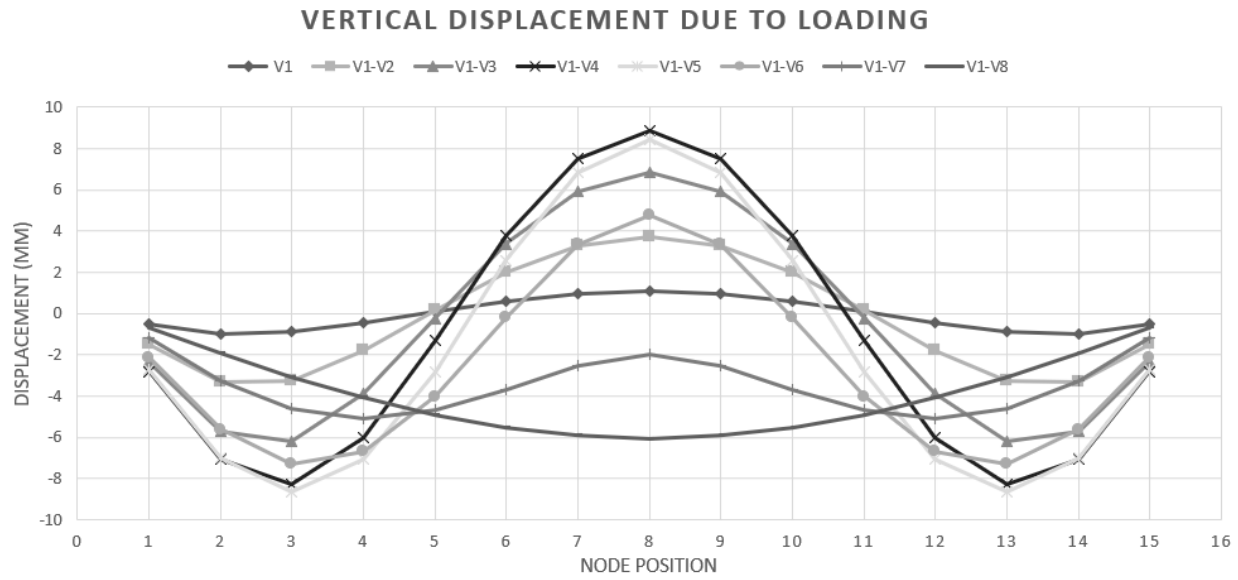

Figure 4.6: Vertical displacements for a 20mm rod at nodes 1-15 for progressive loading starting from V1 up to V8

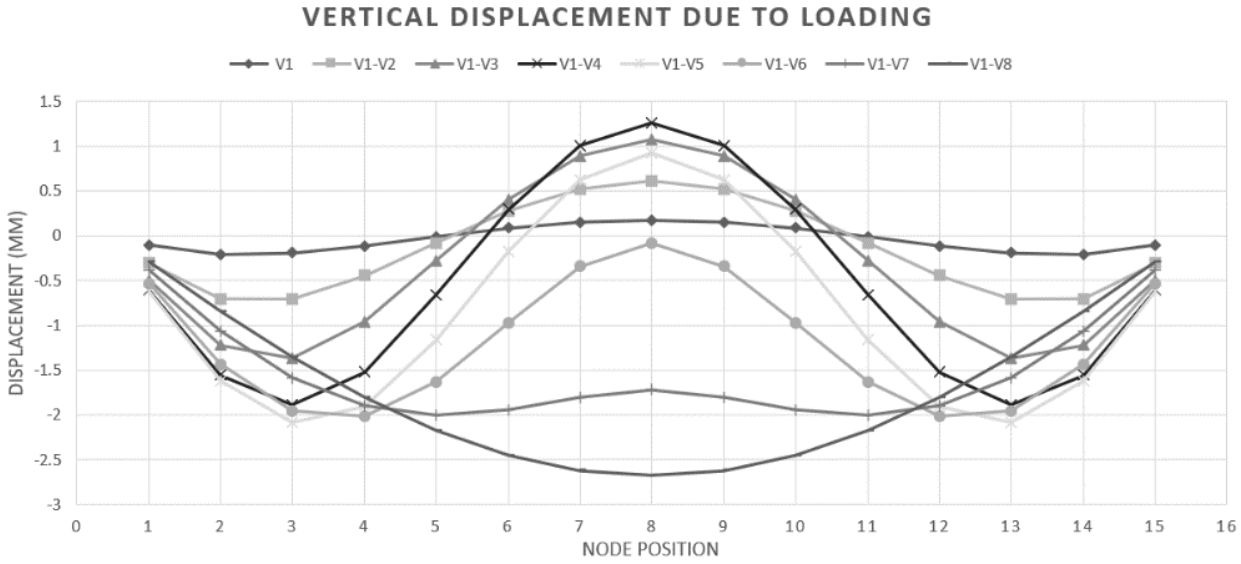

Figure 4.7: Vertical displacements for a 30mm rod at nodes 1-15 for progressive loading starting from V1 up to V8

A pattern could be drawn from the three different plots. Until loading reaches the middle of the formwork, the deformed shape follows a sine curve geometry with the ends deflecting vertically downwards while the central part deflects upwards. This behaviour changes when the central load V8 is applied, resulting in a sagging curve for all three rods.

4.2.2. The Middle Approach

Similar to the analysis in 4.2.1, the middle approach was adopted where the true formwork was loaded with point loads equivalent to the voussoirs loads. The attained displacements results for the 10, 20 and 30mm rods can be found in Figures 4.8, 4.9 & 4.10 respectively. The shown deformations were scaled by a factor of 10.

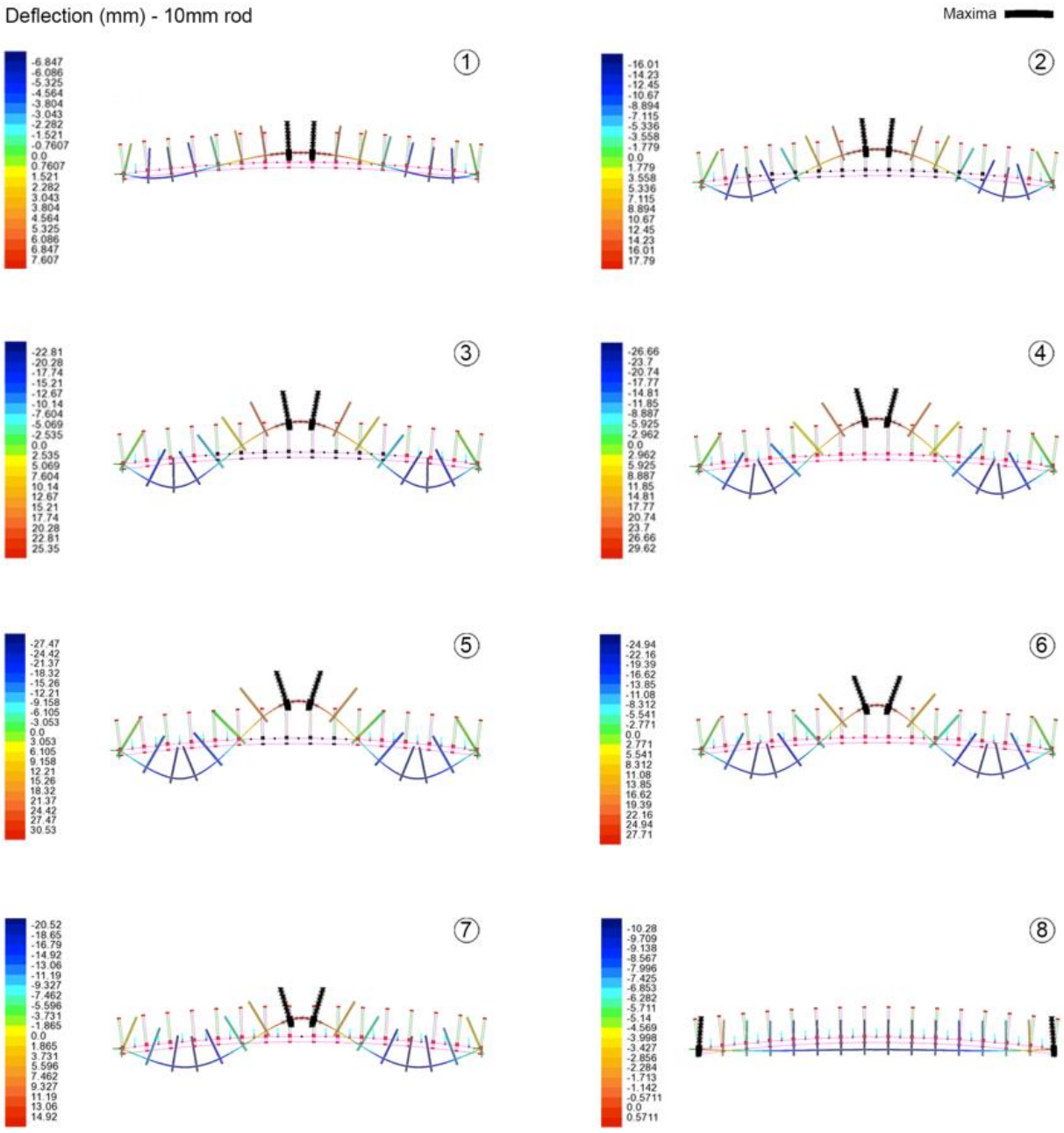

Figure 4.8: Deformations for the Middle approach using a 10mm rod

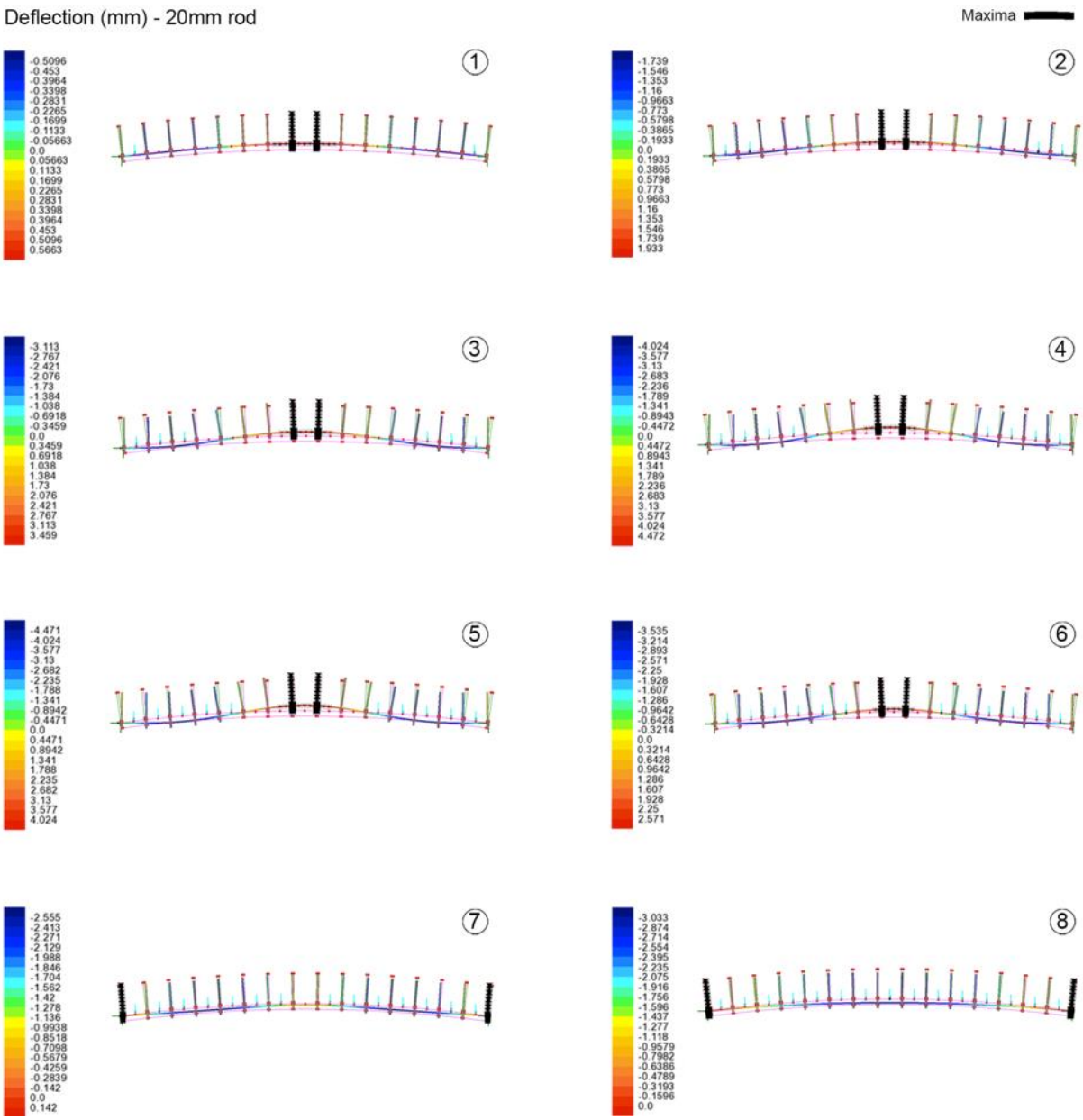

Figure 4.9: Deformations for the Middle approach using a 20mm rod

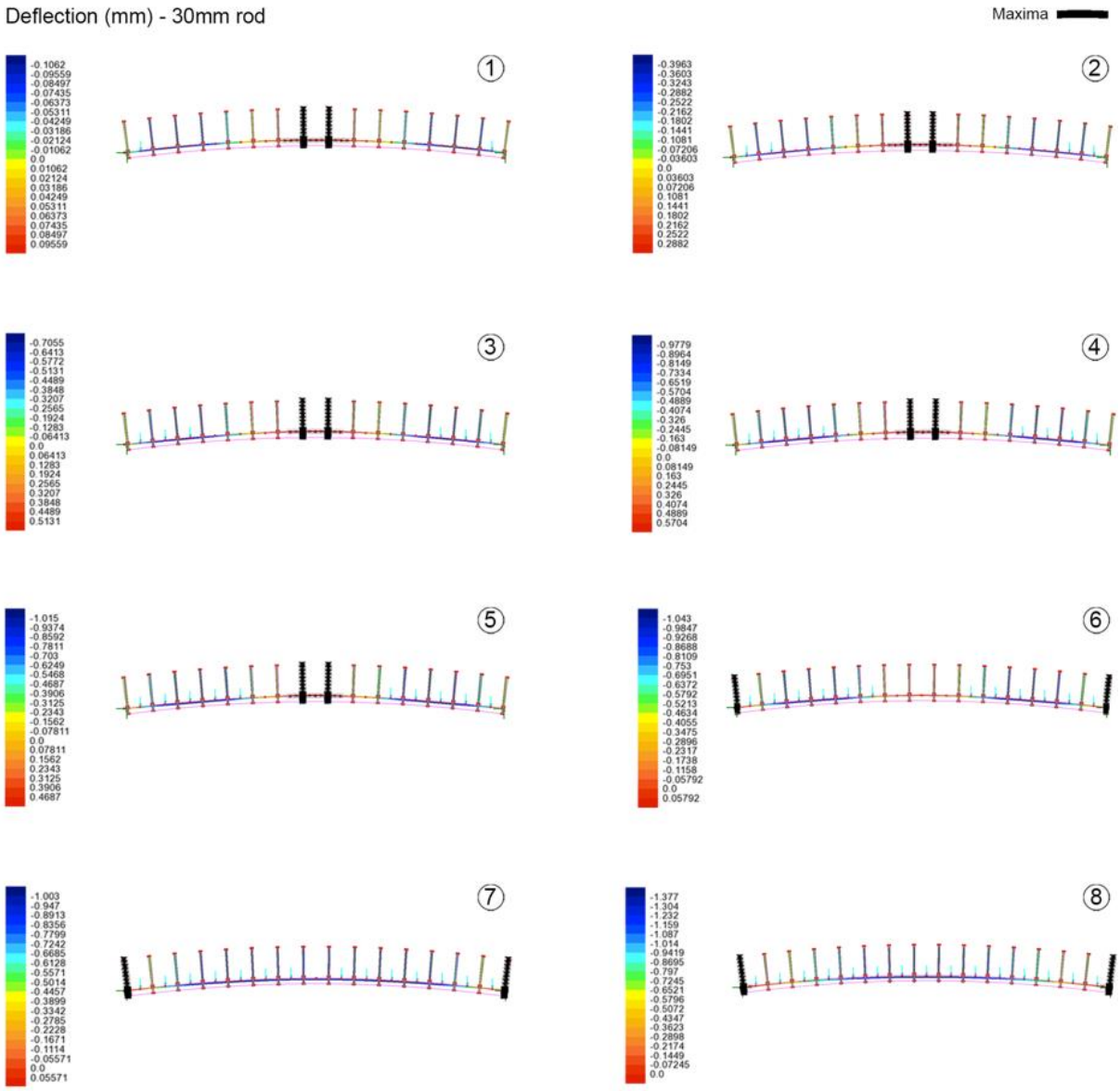

Figure 4.10: Deformations for the Middle approach using a 30mm rod

Again, the central displacements corresponding to each loading case starting from the ends and progressively moving towards the centre were plotted on a singular graph and displayed in Figure 4.11.

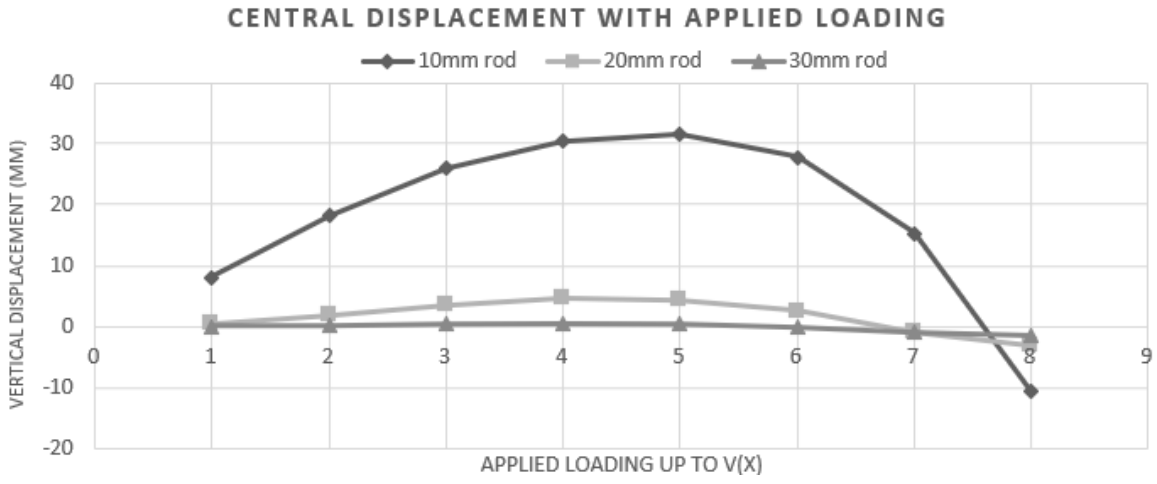

Figure 4.11: Central Displacement vs applied loads for the middle approach

A similar pattern as in Figure 4.4 could be observed where maximum displacements were noted for the 10mm bar. Displacements are still relatively high yet have undergone a reduction following the introduction of the vertical steel fins. The maximum central displacement for a 10mm rod was noted as 31.45mm followed by 4.59mm for a 20mm rod and just -1.4mm for a 30mm rod. Again central peak deflections correspond to the locations where progressive loading reached point loads V4 & V5 for the 10 and 20mm rods.

The nodal displacement under each progressive loading combination was recorded and plotted for the 10,20 and 30mm rods in Figures 4.12,4.13 and 4.14 to understand how the whole formwork deforms.

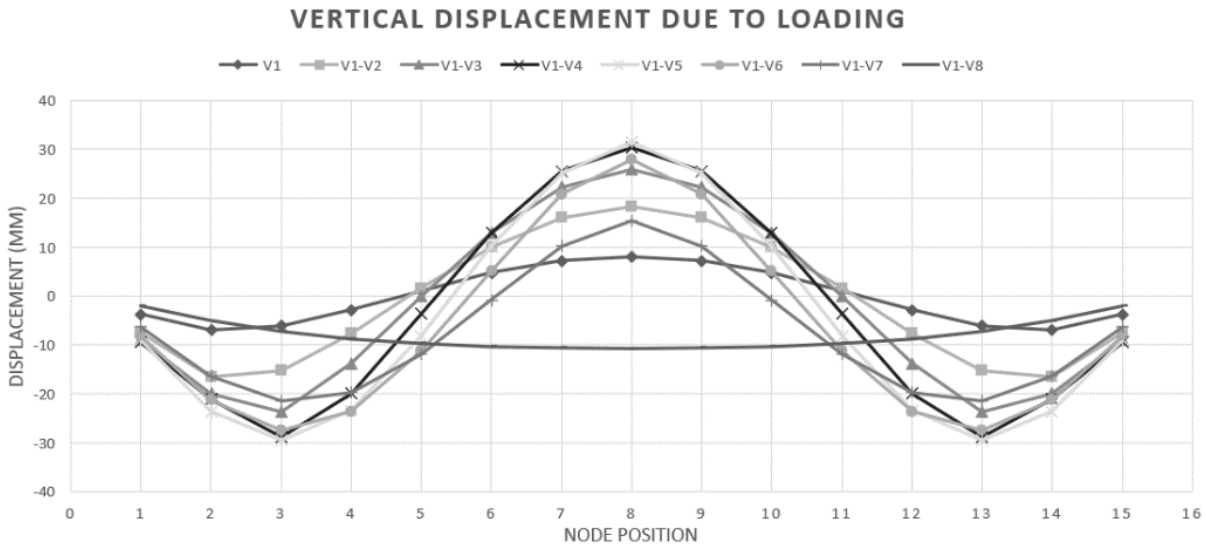

Figure 4.12: Vertical displacements for a 10mm rod at nodes 1-15 for progressive loading starting from V1 up to V8

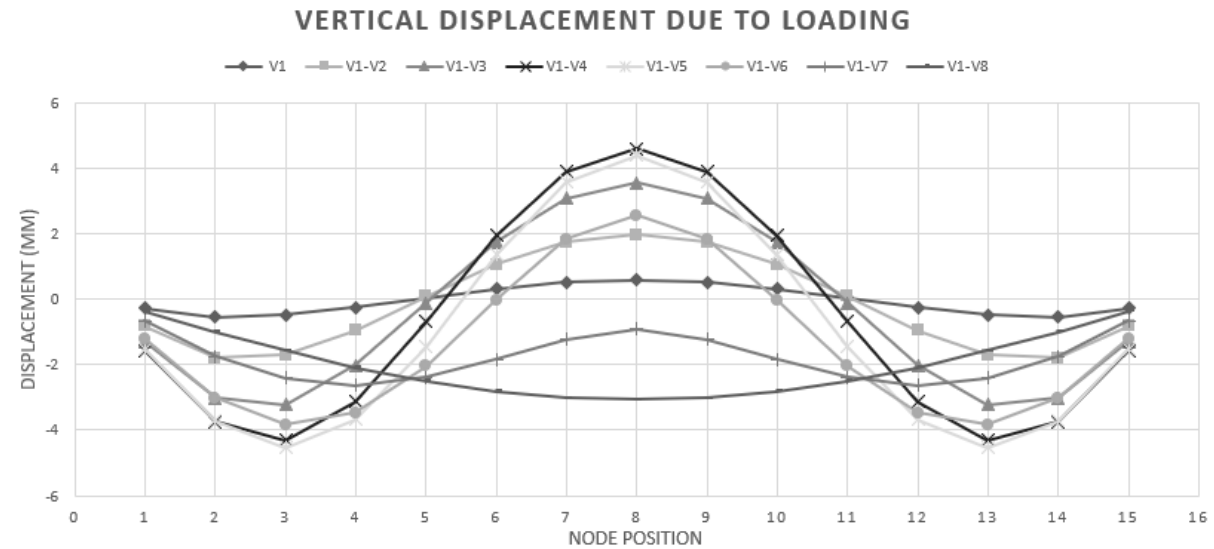

Figure 4.13: Vertical displacements for a 20mm rod at nodes 1-15 for progressive loading starting from V1 up to V8

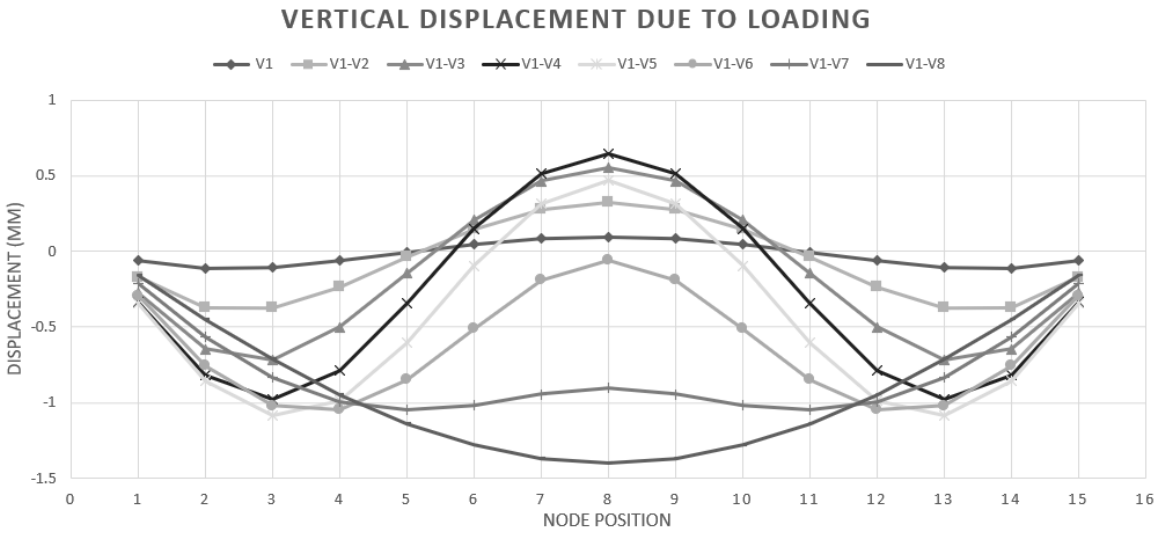

Figure 4.14: Vertical displacements for a 30mm rod at nodes 1-15 for progressive loading starting from V1 up to V8

These results, although closer to the real case fail to take into consideration how the voussoirs would hinder certain rotations and movements of the vertical fins. Hence in the upcoming section, the true formwork was modelled including the voussoirs.

4.2.3. The True Approach

To conclude the testing of the formwork behaviour under loading with the voussoirs, the true formwork was analysed by the progressive filling of the voussoirs. Figures 4.15, 4.16 and 4.17 display the resulting displacements which have been scaled by a factor of 20.

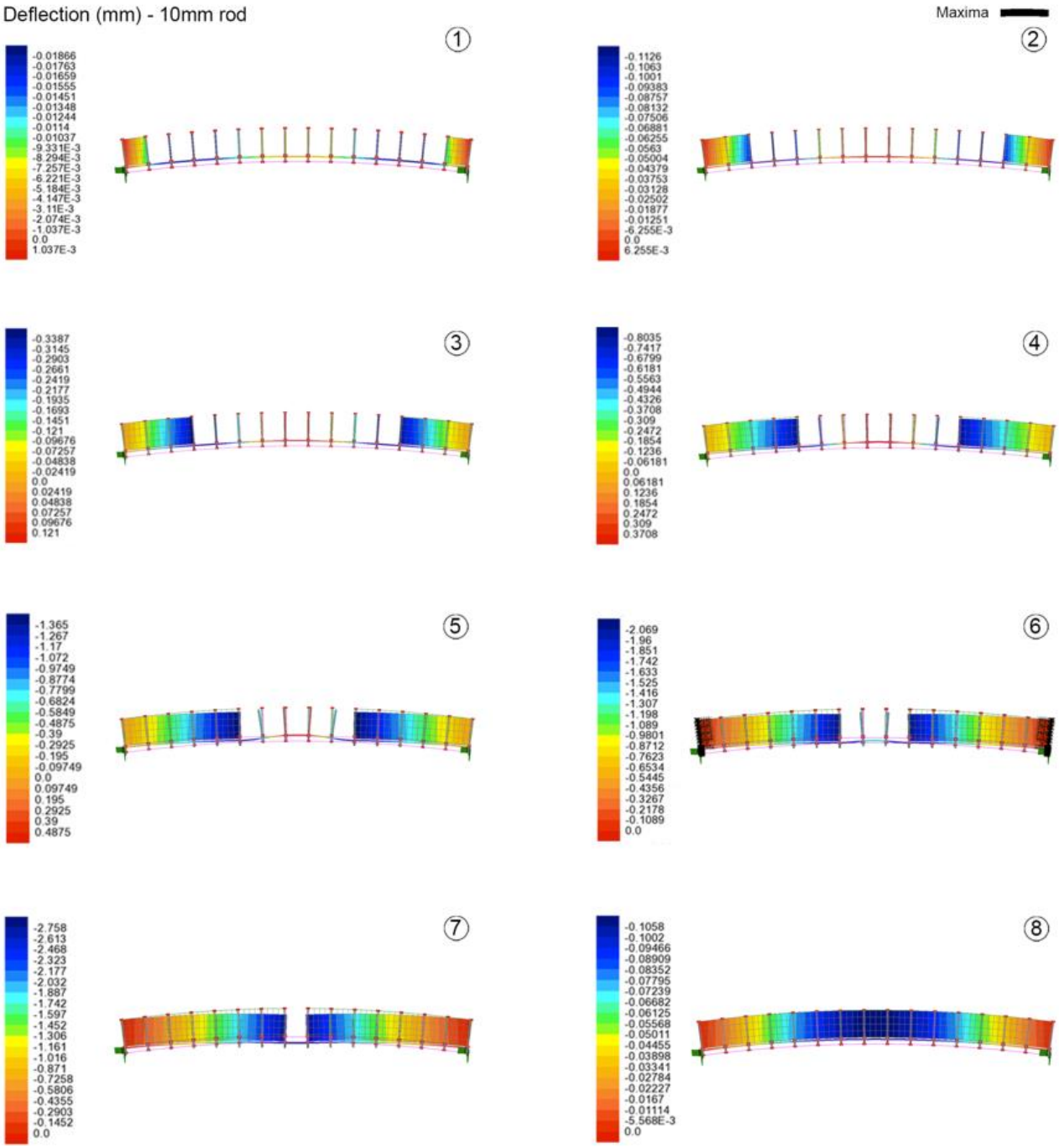

Figure 4.15: Deformations for the true approach using a 10mm rod

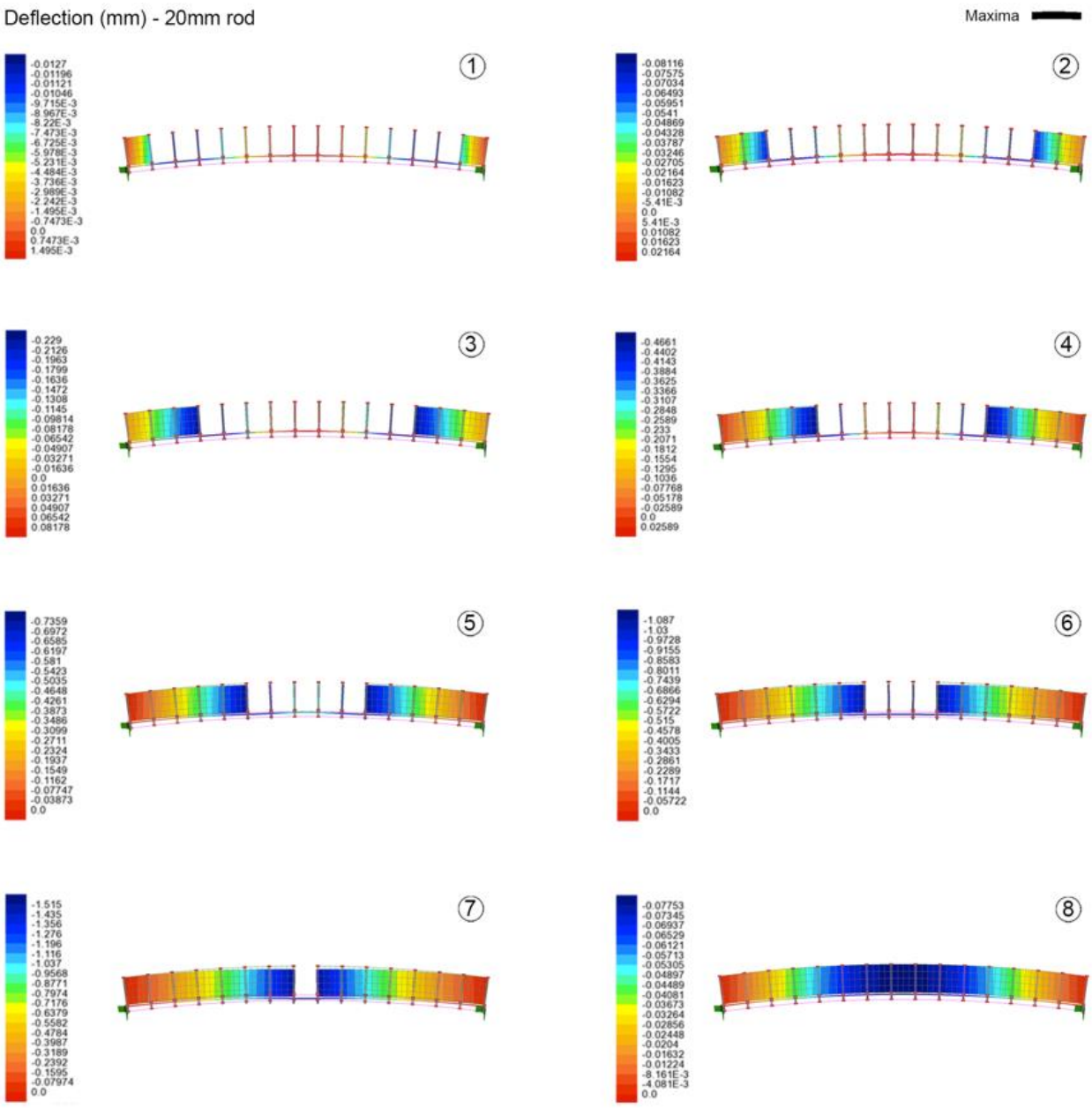

Figure 4.16: Deformations for the true approach using a 20mm rod

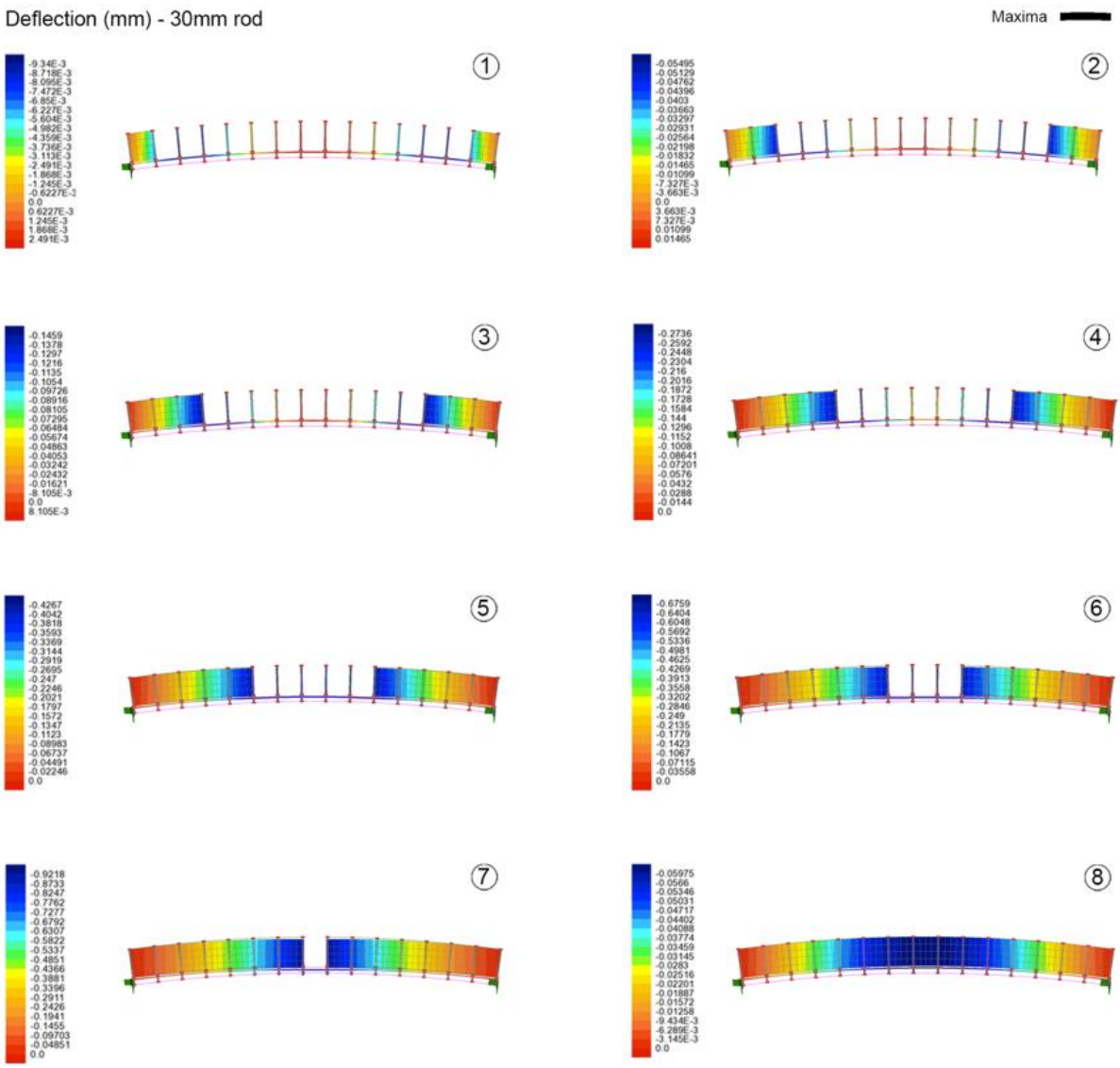

Figure 4.17: Deformations for the true approach using a 30mm rod

As in sections 4.2.1 and 4.2.2, the central displacements were plotted for the three different rod thicknesses as Figure 4.18.

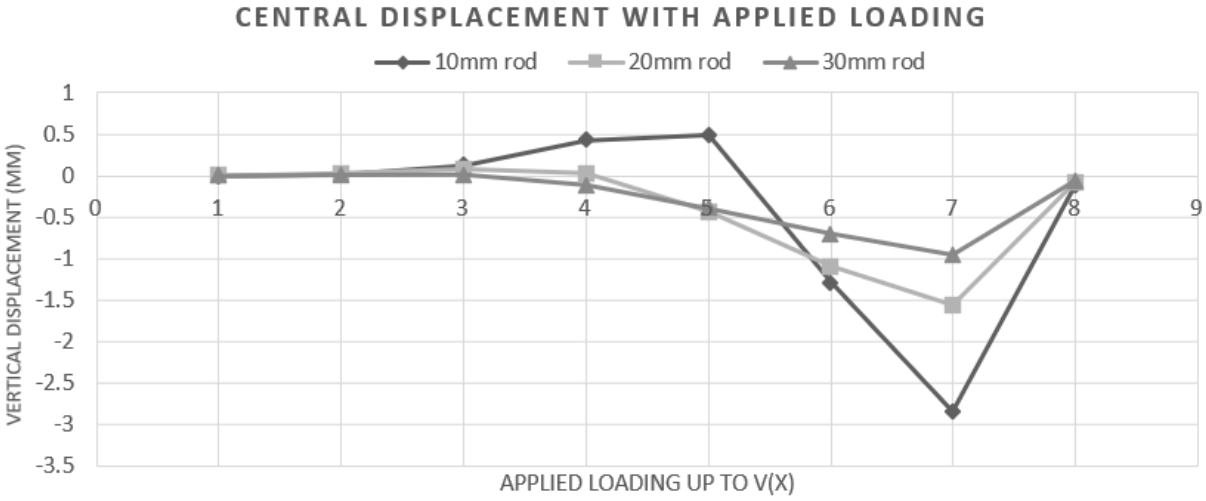

Figure 4.18: Central Displacement vs applied loads for the true approach

Filling of the formwork with the voussoirs led to a considerable reduction in deformations. The worst central displacement could be noted for the 10mm rod formwork corresponding to a value of -2.84mm followed by the 20mm rod with a vertical displacement of -1.56mm and lastly the 30mm rod gave the lowest central displacement at -0.95mm. Whereas in the previous studies 4.2.1 & 4.2.2 the worst central deformations were generally noted when the formwork was loaded up with loads V1 to V4 and V1 to V5, a different behaviour could be observed in the true approach.

The worst central displacements occurred when the formwork was loaded up to V7, hence just prior to completing the arch. Although these displacements are relatively low, when it comes to manually fitting the keystone by hand, even such small deflections will complicate such a task. Moreover, whereas the central node was generally displacing vertically up in the previous 2 studies, in the real approach the central node was displacing vertically down apart from the 10mm rod which up until loading reached V5, the formwork was displacing upwards.

The behaviour of the whole formwork under progressive loading was also recorded by taking nodal displacement for the 10,20 and 30mm rods which have been plotted in Figures 4.19, 4.20 and 4.21.

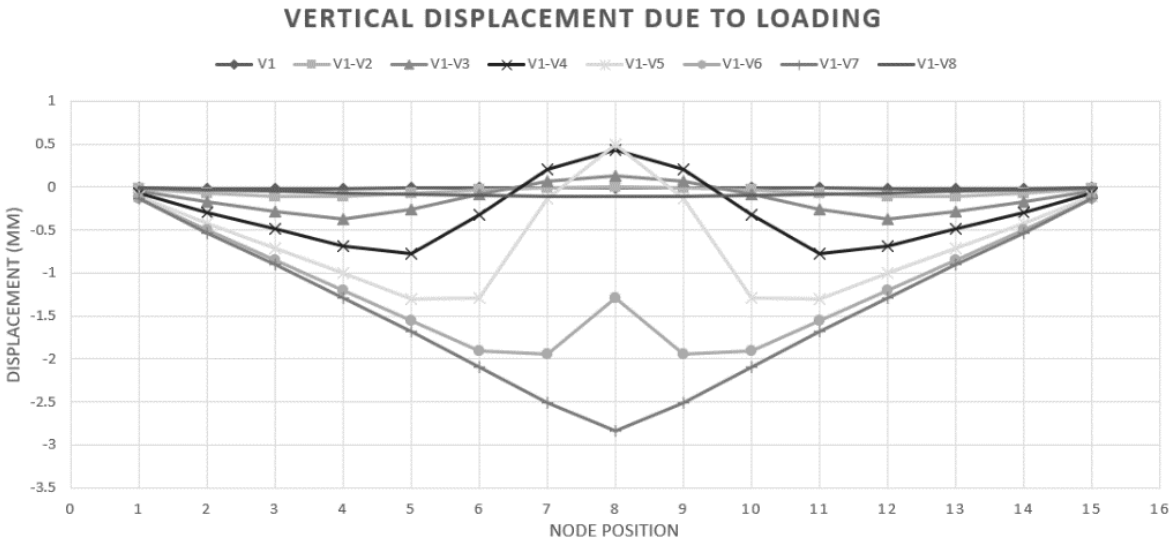

Figure 4.19: Vertical displacements for a 10mm rod at nodes 1-15 for progressive loading starting from V1 up to V8

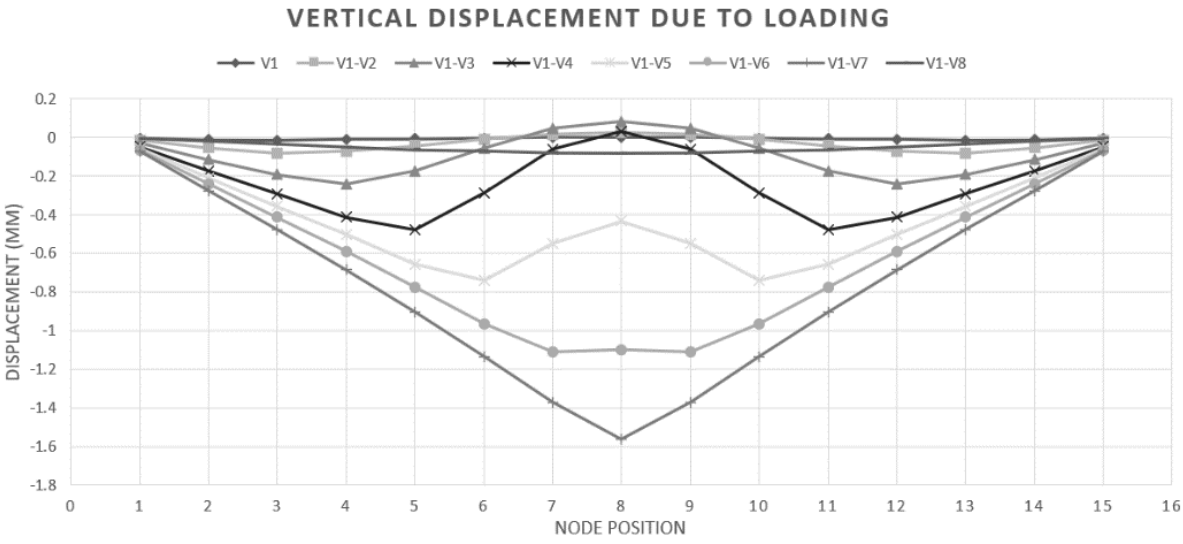

Figure 4.20: Vertical displacements for a 20mm rod at nodes 1-15 for progressive loading starting from V1 up to V8

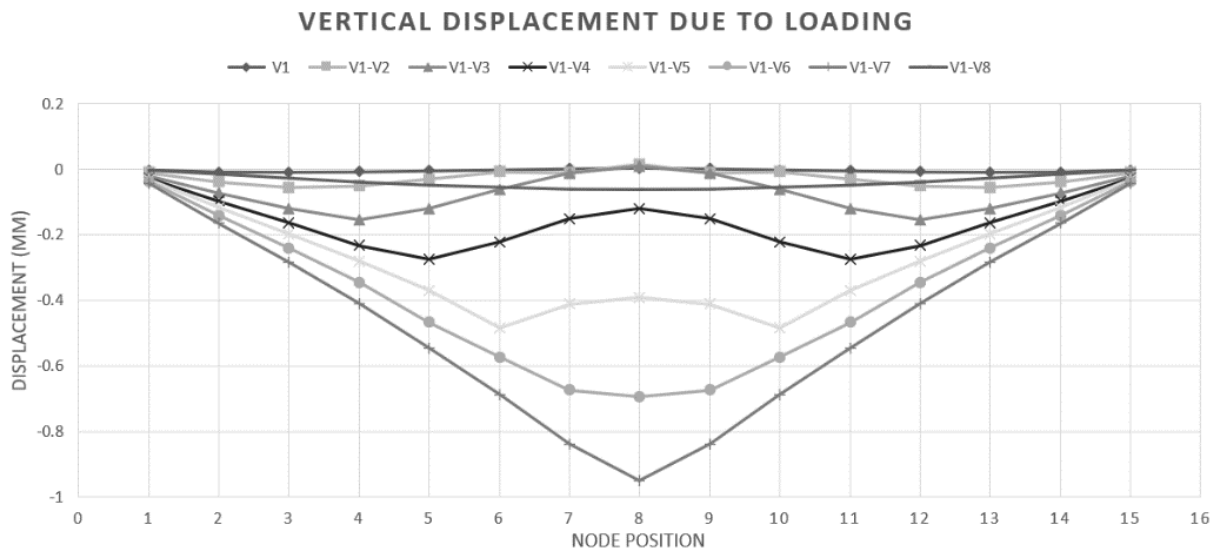

Figure 4.21: Vertical displacements for a 30mm rod at nodes 1-15 for progressive loading starting from V1 up to V8

4.3. Study 9: Understanding the Behaviour of the Completed Arch

The completed arch was analysed in Lusas Analyst under a uniformly distributed load to understand how stresses, deformations and horizontal thrust vary with vertical loading. The compressive strengths for the stone and mortar were set as 18N/mm^2 and 2.5N/mm^2 respectively. Through studies on masonry and mortar tensile strengths by (Mortar in Tension, 2004) and (Jigme et al., 2021) respectively, the tensile strength of the stone and mortar was averaged as 1.5N/mm^2. This is a conservative assumption as the lowest values of tensile strength were averaged out.

The *first* parameter which was investigated was vertical displacement. A lower central node was selected as indicated in Figure 3.35 for which the vertical displacement was noted for every load factor. The final load increment results before failure for the three different rod thicknesses were plotted superimposed on the graph in Figure 4.22. The data of plotted results can be found in Appendix (III).

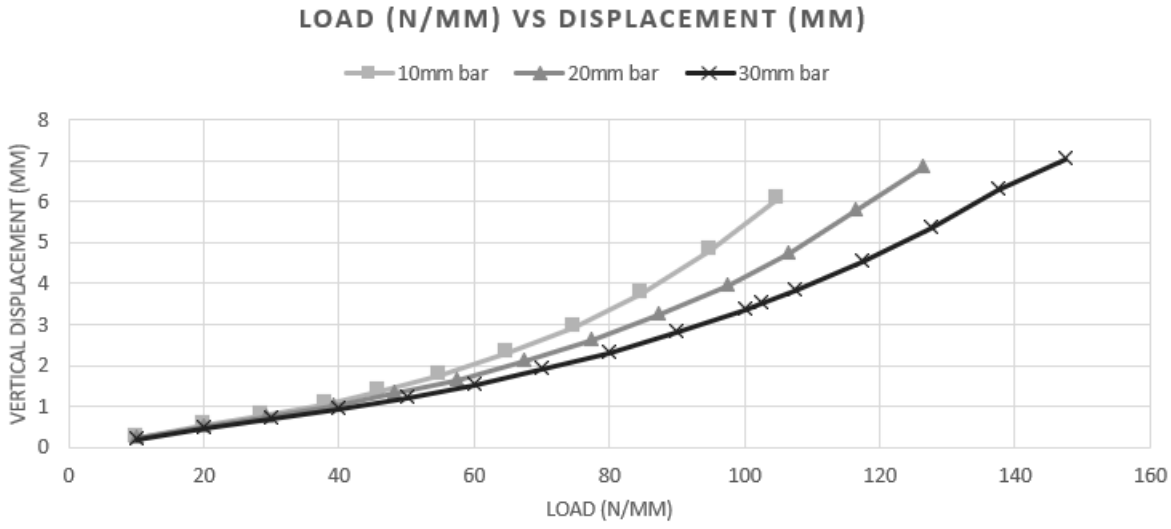

Figure 4.22: Central displacement variation with loading for the lower central node

The deformed structures at the final loading increment prior to collapse have been shown in Figures 4.23 at a scale factor of 10. From the deformed shape it can be concluded that the central part of the arch is deflecting downwards with a reduction in deformations as you reach the supports.

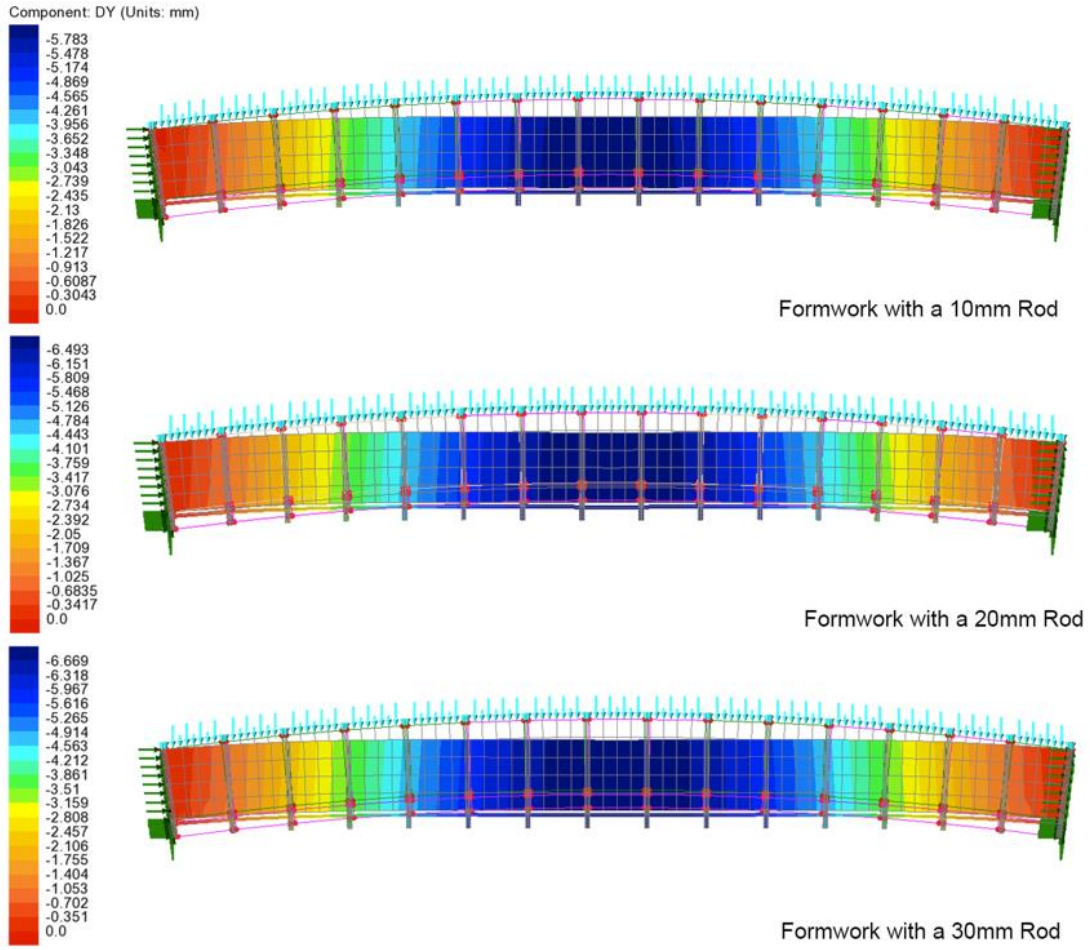

Figure 4.23: Deformed structure at the final load increment prior to collapse

The *second* investigated parameter was compressive stress. An upper central node was selected as indicated in Figure 3.35 for which the compressive stress variation was recorded with increased loading increments. Similarly to the first parameter, the results for the 3 rod thicknesses were plotted as in Figure 4.24 below.

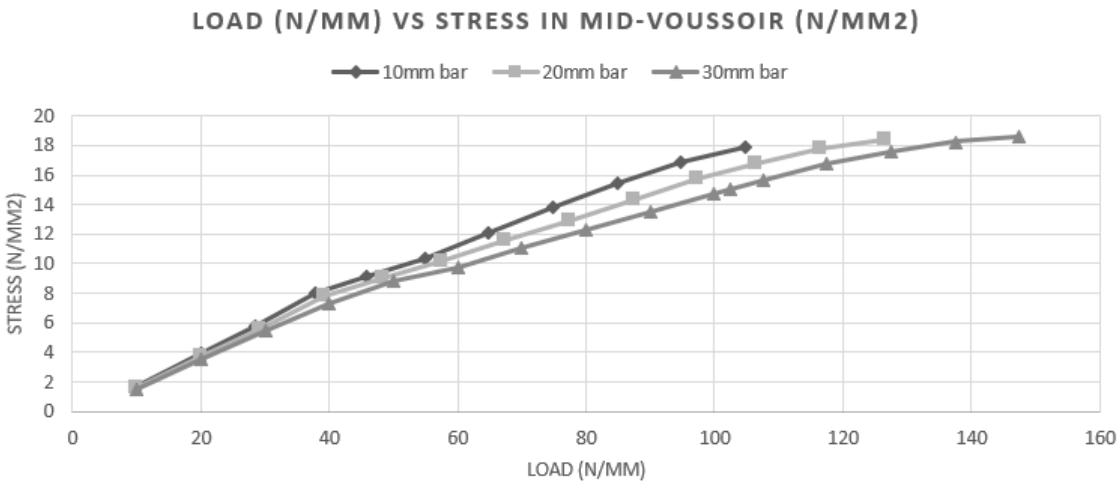

Figure 4.24: Compressive stress variation with loading for the upper central node

The planar stresses within the stone voussoirs and steel formwork have been documented in Figure 4.25 at a scale factor of 10. At the left of Figure 4.25, maximum compressive stresses can be noted to form at the middle top of the part of the arches as well as at the lower ends of the support. Very low levels of tensile stress below the value of 1.5N/mm^2 were noted to develop in the lower central part of the arch along with the top parts near the supports. Looking at the right of Figure 4.25, the same pattern followed where high compressive forces developed near the support within the steel rod whilst at the central part of the steel high tensile forces have been noted.

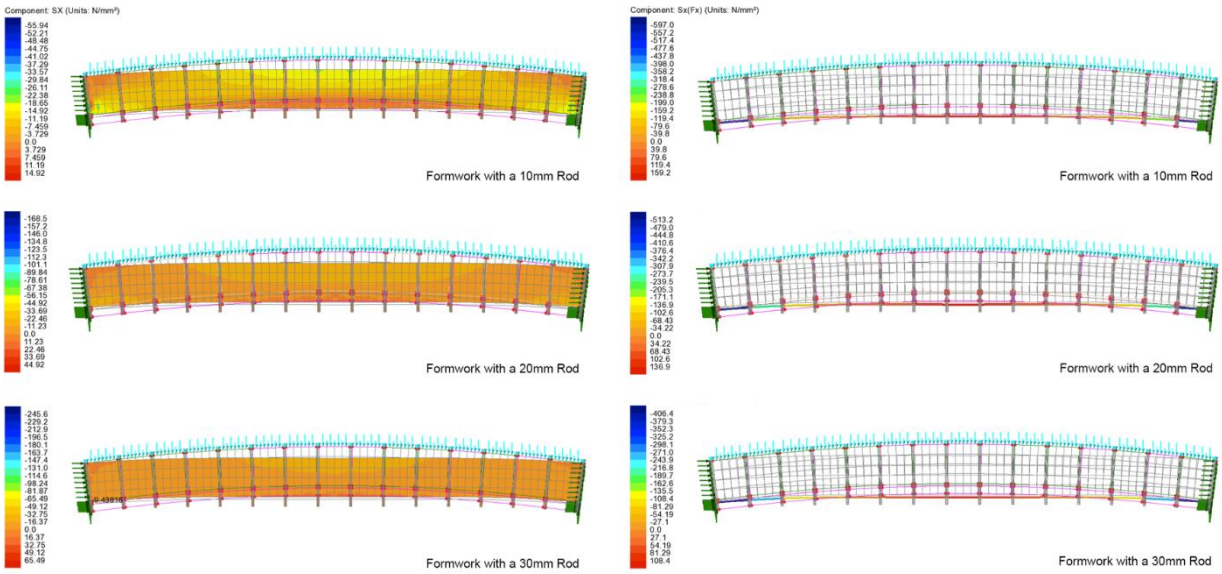

Figure 4.25: Left: Stresses within the stone voussoirs at the final load increment prior to collapse
Right: Stresses within the steel formwork at the final load increment prior to collapse
Note: -ve = compression, +ve = tension

The last parameter under investigation was the horizontal reaction. Again the variation in horizontal reaction was plotted against the loading increments for the 10, 20 and 30mm rods, resulting in the graph found in Figure 4.26.

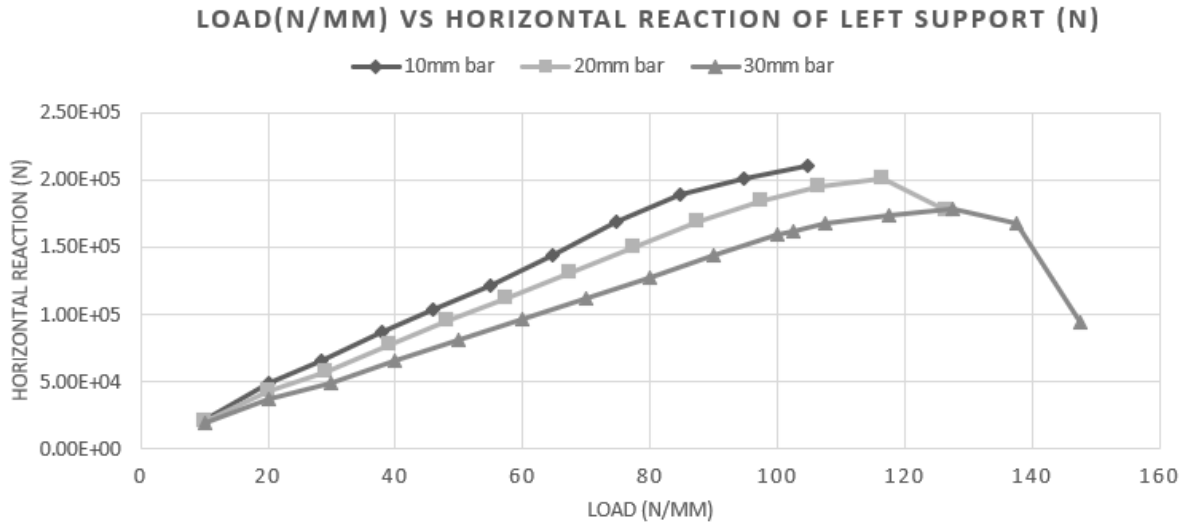

Figure 4.26: Horizontal reaction variation with loading

The arches were deemed to have failed when displacements were unreasonably high, exceeding the limit of l/200, corresponding to a value of 15mm. Hence all plotted results show the behaviour of the structures up until the considered point of failure. Starting with the graph in Figure 4.22, the analysed three arches structurally failed at similar deformations values being 6mm for the 10mm bar, 6.82mm for the 20mm bar and 7.01mm for the 30mm bar. Beyond these values, deformations became unreasonably high signifying that failure had occurred. As expected, the arch making use of an integrated formwork with a rod thickness of 30mm withstood the highest load being 147.5N/mm, followed by the 20mm bar formwork integrated arch at a load of 126.5 N/mm and lastly, the 10mm bar withstood the ultimate load of 104.8N/mm.

These failure loads correspond to the stone's ultimate crushing strength, which was set as 18N/mm^2. Figure 4.24 shows that for the three arches, failure occurred at similar compressive stress values in the central upper node of the arch, being that of 18N/mm2 yet for each case, this value was reached at different loading values. It must be noted that at this point, high stresses were developing at the ends of the arch within the joint between the steel vertical fins and the steel rod running through as displayed in Figure 4.27. As the voussoirs in the middle were experiencing maximum compressive stress, these joints were under maximum compressive stresses of 57.45N/mm2, 133.04N/mm2, 250.71N/mm2 respectively corresponding to the 10,20 and 30mm formwork integrated rods.

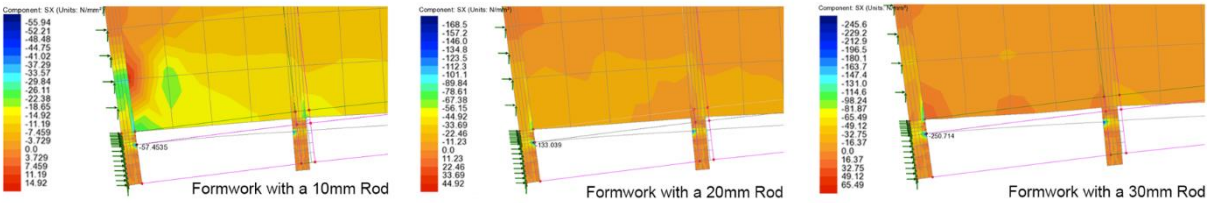

Figure 4.27: Maximum stresses in the joint between the steel vertical fins and steel rods for the 10, 20 and 30mm integrated formworks

Figure 4.26 shows a clear relationship between vertical loading and horizontal thrust. As the loading on the arch progressively increased, so did the values of the horizontal reaction up to a maximum until the values started to reduce until failure was reached. The arch with a 10mm integrated rod exhibited no loss in horizontal reaction yet as it started to reach failure, a lower increase rate in the horizontal thrust could be noted. The 20mm integrated rod arch started to experience a reduction in the horizontal thrust at a load of 116.515N/mm and lastly the 30mm rod arch started to experience a loss in the support at a load of 127.5N/mm.

As loss in support was being experienced, stress in the steel integrated formwork rod was increasing. Such a loss in the horizontal support could be attributed to the fact that loading in the arch is being partly carrying as an axial force by the abutments and partly by the steel formwork in bending. In this manner, the arch can be thought of as being a composite arch which carries loading through a combination of bending and axial compression.

4.4. Study 10: How does a Formwork Integrated Arch compare to a Traditional Arch with Steel and Mortar Jointing?

The following analysis was carried out in effort of understanding how the displacement, stresses and horizontal reactions vary with loading for a steel reinforced arch due to the integrated formwork against 2 typical arches with steel and mortar jointing, each having the same depth of 240mm as outlined in section 3.16 .

Starting with vertical displacement and similar to study 9, a lower central node was selected as indicated in Figures 3.35, 3.36 & 3.37 for which the vertical displacement was noted for every load increment. For the three different arches, different loading increments were used due to the difference in their ultimate load bearing capacity. The displacements were tabulated and plotted on a singular graph which can be found in Figure 4.28. The whole set of results could be found in Appendix (IV).

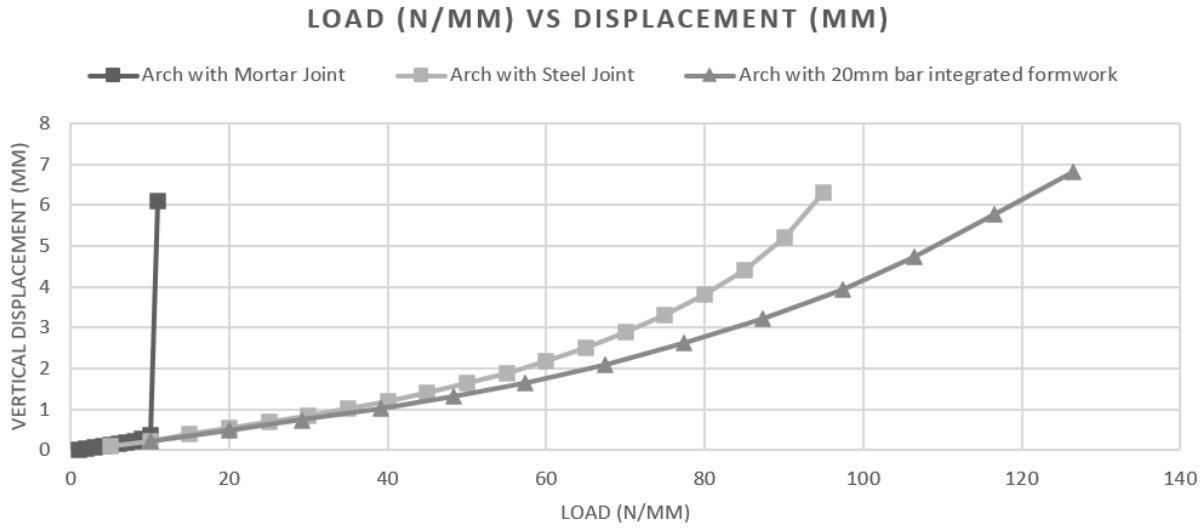

Figure 4.28: Central displacement variation with loading for the lower central node

Similar to the previous section, the deformed structure just before the point of structural collapse have been visually documented in Figure 4.29. The deformed pattern is similar for the 3 arches yet it could be noted that the traditional arch with the mortar joint experienced a wider stretch of flattening in the central part when compared to the other 3 cases.

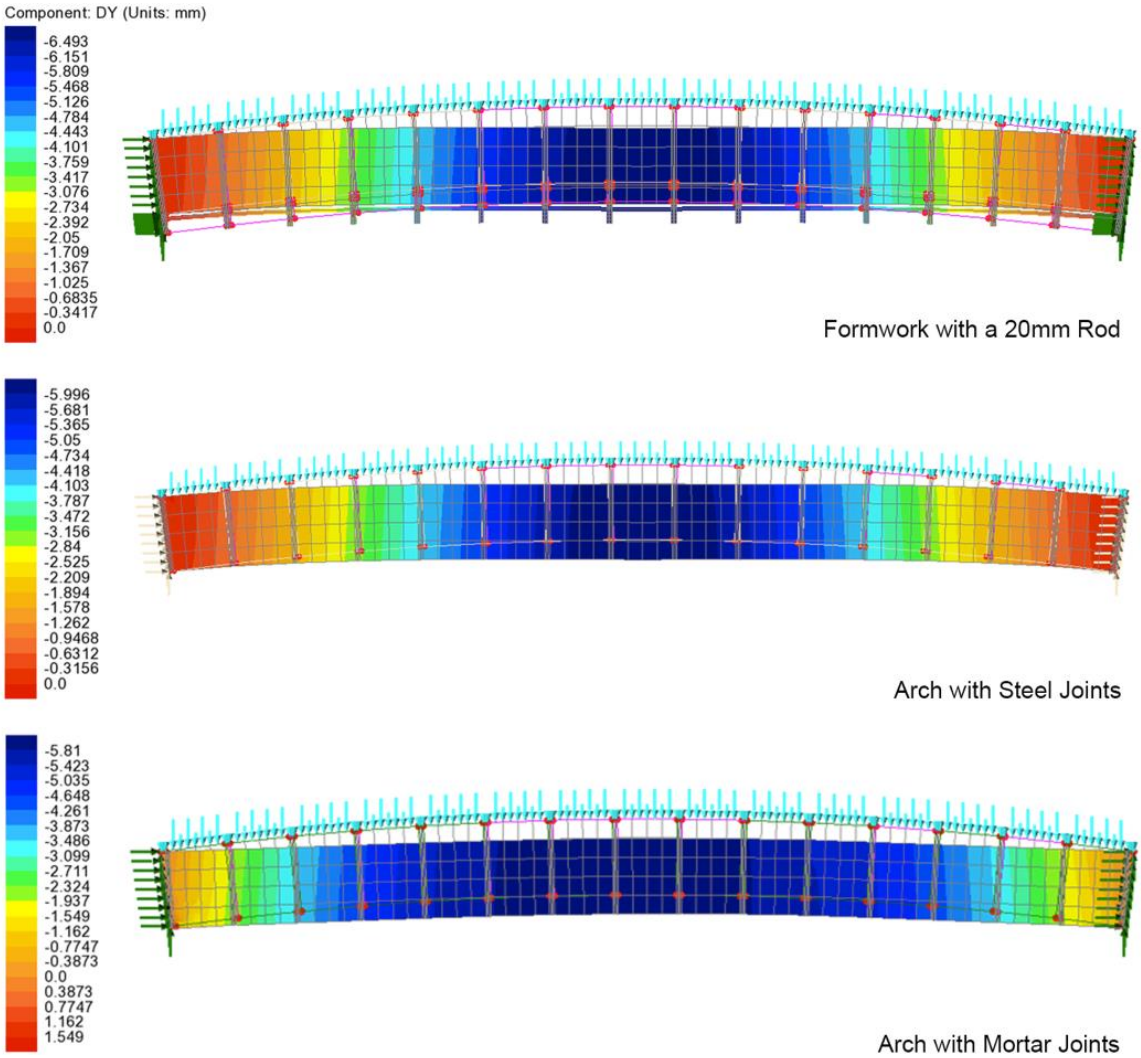

Figure 4.29: Deformed Structures at the final load increment prior to collapse

When it comes to compressive stresses, an upper central node was selected as indicated in Figures 3.35, 3.36 & 3.37 and the corresponding compressive stresses at this node were recorded as loading progressed. Figure 4.30 shows the resulting compressive stresses at the indicated node.

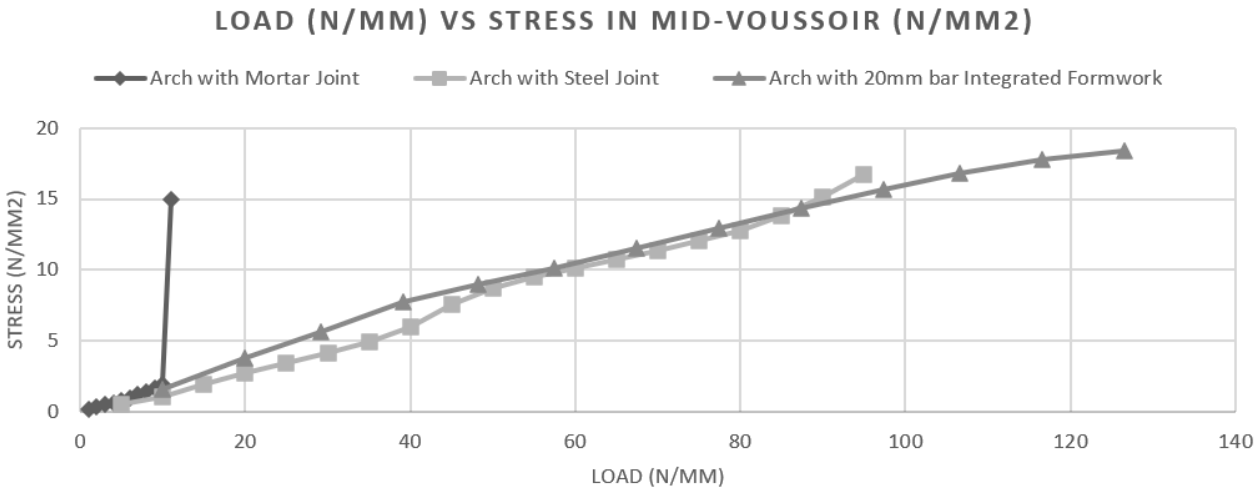

Figure 4.30: Compressive stress variation with loading for the upper central node

Apart from documenting the nodal stress at the top node, the stress distribution within the three arches for the final loading increment prior to failure was captured by Figure 4.31. When looking at the arch with the 20mm rod formwork, stresses within the voussoirs remained below the value of 18N/mm2, with the steel rod aiding in the compressive stresses at the supports whilst taking the tensile forces in the middle. A failure occurred when the middle and end support voussoirs reached their ultimate compressive strength. Moving onto the Arch with steel joints, the behaviour was similar to the previously discussed arch with stresses maxima forming at the same locations. Yet in this case, the eliminated rod led the arch to reach its maximum compressive stresses at a lower load of 95N/mm.

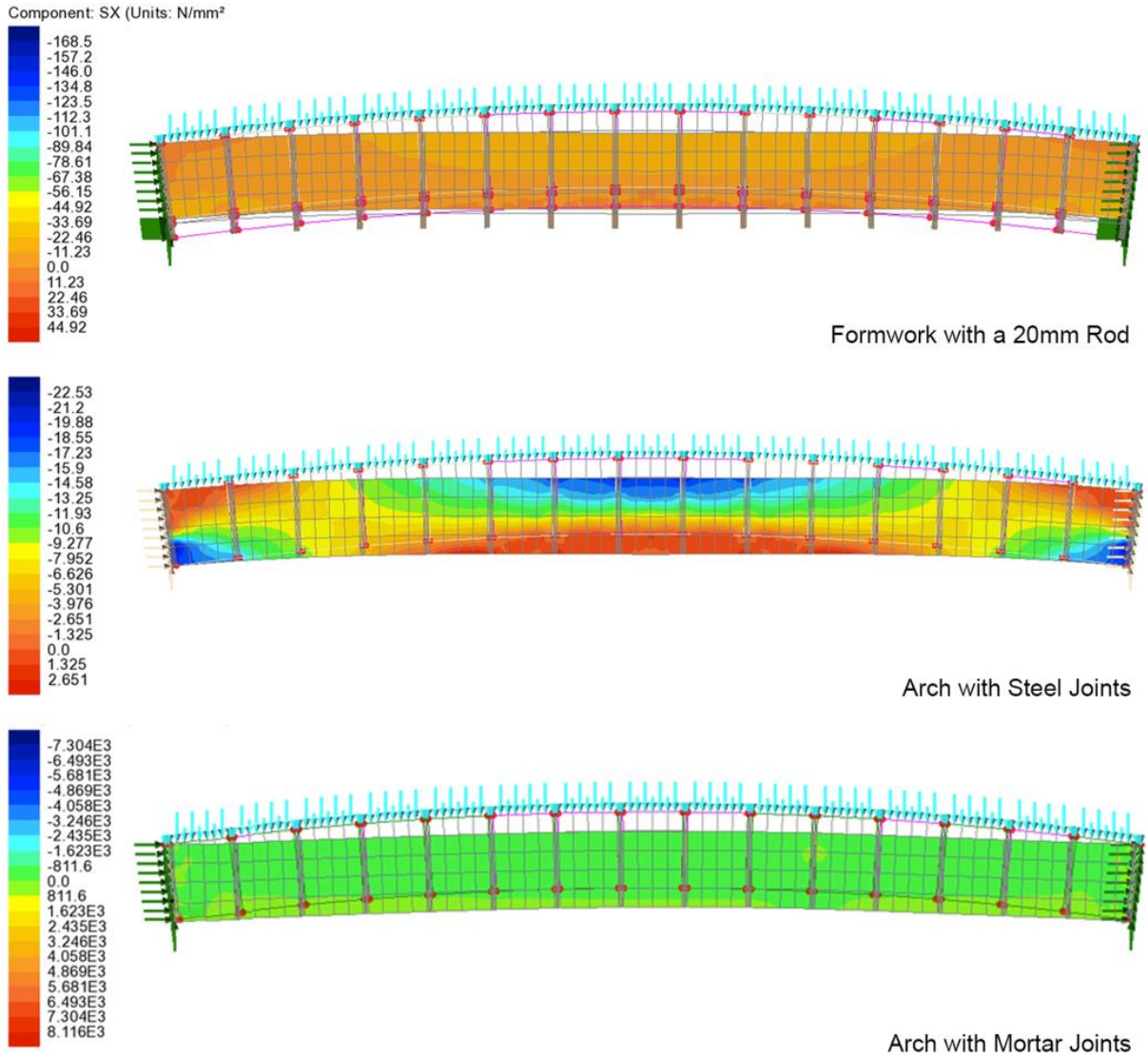

Figure 4.31: Stresses within the stone voussoirs at the final load increment prior to collapse
Note: -ve = compression, +ve = tension

The traditional arch with mortar joints exhibited relatively low compressive stresses throughout the incremental loading. Up to a load of 10N/mm, the monitored central upper node corresponded to a compressive stress of 1.92N/mm^2. Just an increase by 1N/mm led to a sudden increase in stresses, with the same node experiencing a stress of 14.93N/mm^2. This was coupled with a very high stress concentration at the abutments as displayed in Figure 4.32. Although the stress at the abutments was way beyond the allowable compressive stress, it can be noted that failure had not yet occurred at this point.

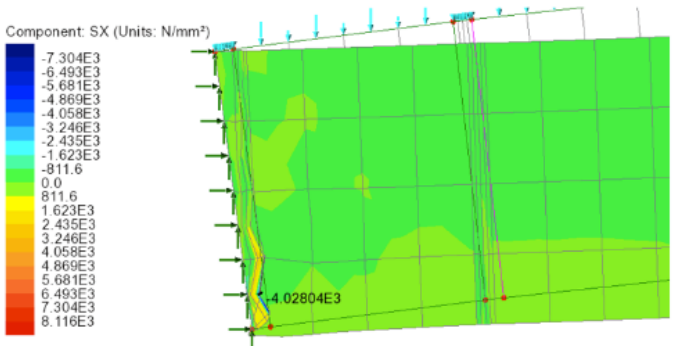

Figure 4.32: Stresses near the abutments of the traditional arch with mortar joints at the final loading increment prior to failure
Note: -ve = compression, +ve = tension

To conclude the analysis for this section, the maximum horizontal reactions were noted for the three different arches and again plotted on the same axis as in Figure 4.33

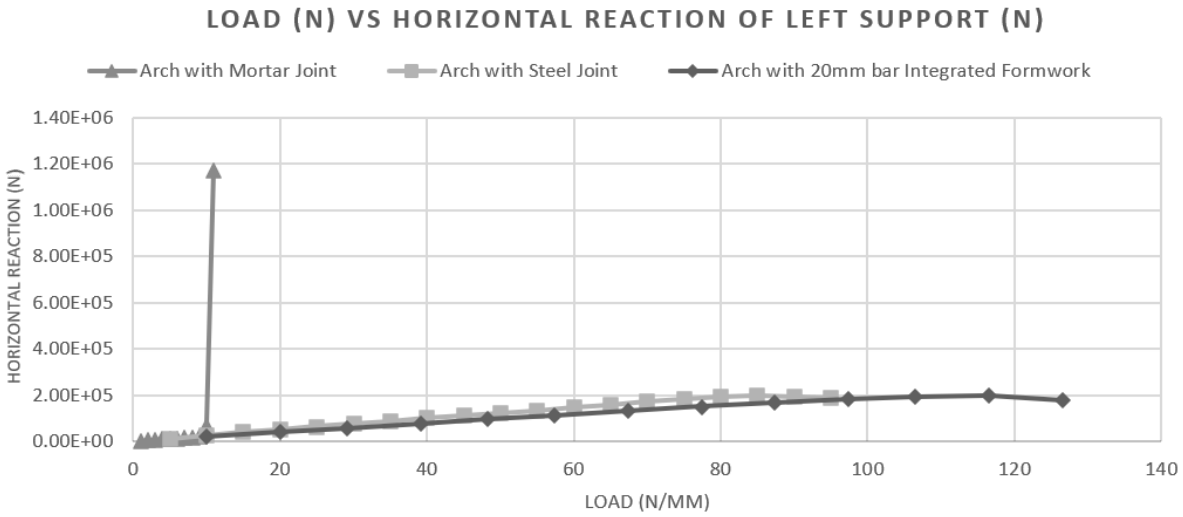

Figure 4.33: Horizontal reaction variation with loading for the 3 Arches

Considering vertical displacements, similar results could be noted for the three arches prior to undergoing unreasonable deformations yet the load at which such a failure occurred was vastly different. The mortar jointed arch having a mortar compressive strength of 2.5N/mm^2 was able to withstand a load of 11N/mm with a central displacement of 6.1mm. This was followed by the arch with steel joints at a load of 95N/mm and a central displacement of 6.3mm. The arch which withstood the highest load was the formwork integrated arch with a 20mm bar whose ultimate load capacity was that of 126.5N/mm resulting in a central displacement of 6.8mm. The formwork integrated arch managed to withstand a 10 times greater than the traditional arch. An important observation is the sudden increase in displacement in the mortar jointed arch where just an increase in loading by 1N/mm increased displacements from 0.36mm to 6.1mm, leading to instant collapse. This observation corresponds to brittle behaviour and is a typical property of unreinforced masonry.

For the masonry arch jointed with mortar, central compressive stresses were relatively low up until a load of 10N/mm. However a sudden rise in stress occurs at a load of 11N/mm where from a low stress of 1.91N/mm^2, the compressive stress suddenly increases to 14.93N/mm2. A further increase in loading by just 1N/mm led to the structural collapse of the arch. As discussed in the previous paragraph, this behaviour follows from the brittle nature of such an

arch. The steel jointed arch along with the formwork integrated arch having a steel rod of 20mm behaved showed similar behaviour with their ultimate load bearing capacity being 95N/mm & 126.5N/mm respectively. In both cases, the applied load led both arches to reach the limit compressive strength of the stone and hence failed by crushing.

Lastly, the horizontal reactions shall be discussed. A direct link could be drawn between load bearing capacity and the corresponding lateral thrust of the arch. The arch with the lowest loading capability was the traditional arch which at its ultimate capacity corresponding to an applied load of 11N/mm, was pushing on the abutments at a force of 1172.9KN. This is a very high force when compared to the steel jointed and formwork integrated arch with a steel rod of 20mm which withstood much higher loads that led to horizontal reactions of 188.2KN and 177.5KN respectively. This observation relates to the explained behaviour in the previous study found in section 4.3. A traditional arch is only capable of carrying load primarily through axial compressive forces. When steel was introduced, the tensile capacity of the arch improved. This allowed the arch to carry part of the loading through compression by the stone voussoirs and tension by the steel, resulting in bending. Hence the horizontal resultant thrust for a traditional arch with mortar joints is expected to be higher when taking into consideration the outlined explanation.

4.5. Study 11: A Comparative Analysis between Finite Element Analysis and Heyman's Funicular Polygon

For structural engineers, it is more interesting to understand how a structure behaves under a typical load rather than taking the structure to its utmost and finding its collapse load. For this section, it was decided that the structural behaviour of the formwork integrated arch and a traditional arch with mortar joints would be analysed for a live load corresponding to category C. This category is dedicated for structures in which people might congregate. This category offers a range of loads varying between 2-7.5KN/m^2. For this study it was decided that the live load of 5KN/m^2 would be adopted.

4.5.1. Part 1: Analysis in Finite Element

As outlined in section 3.17, the traditional mortar arch and a similar integrated steel formwork arch having a 20mm bar were analysed under the prescribed load. For the factored load of 5KN/m2 and assuming that the arch is loaded by a layer of 'torba' and tiles, the traditional mortar arch exhibited a lateral thrust of 8.67KN and a central displacement of 0.09mm. On the other hand, for the same loading conditions the integrated steel formwork arch had a central displacement of 0.07mm with a lower lateral thrust of 6.98KN. Figure 4.34 displays the outlined resultants and deformations.

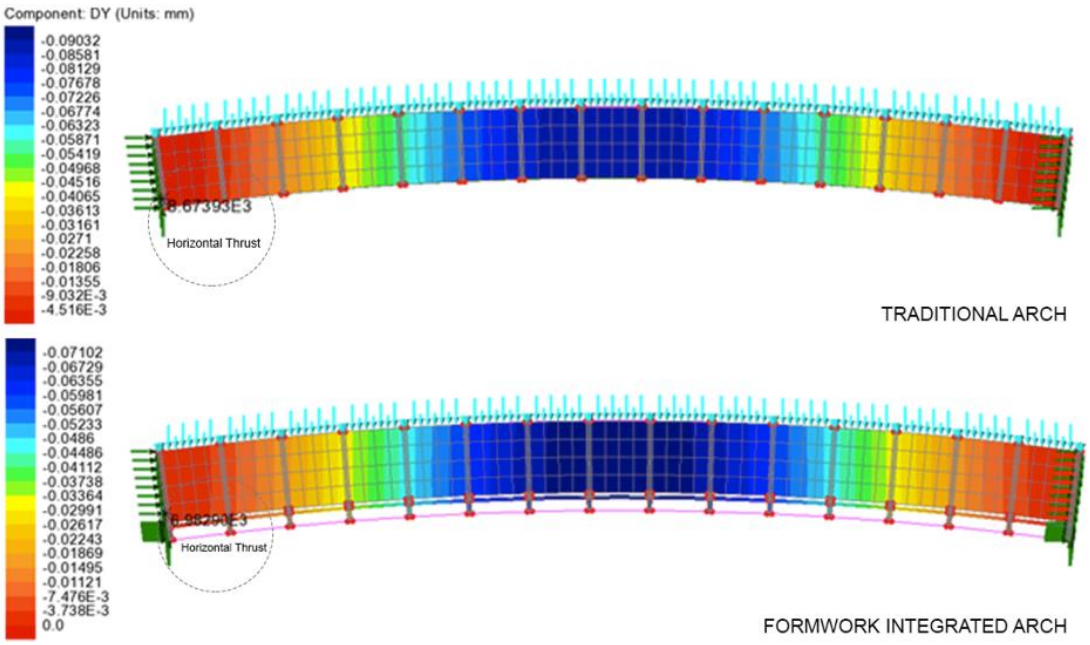

Figure 4.34: FEA of the traditional and formwork integrated arches showing the displacements and horizontal reaction

The internal stresses were also noted as displayed in Figure 4.35. Similar stress patterns could be observed yet if we were to compare the maximum compressive stresses near the abutments, in the traditional arch these occur in the lower part of the voussoir whilst in the formwork integrated arch these occur within the vertical fin as pointed out in section 4.3 by Figure 4.27. In both cases, the magnitude of the stresses is very low.

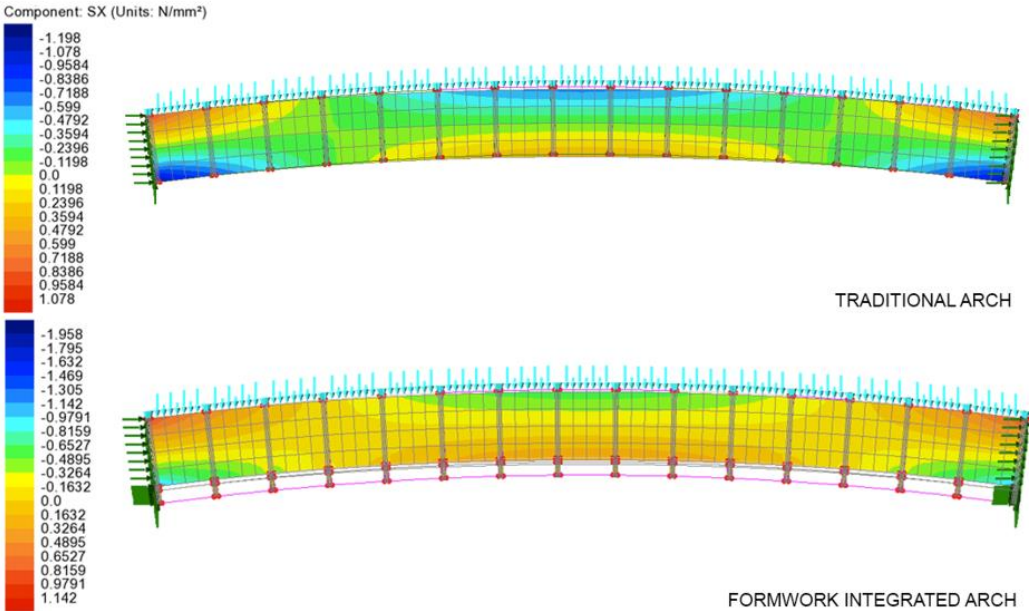

Figure 4.35: FEA of the traditional and formwork integrated arches showing the planar stresses
Note: -ve = compression, +ve = tension

4.5.2. Part 2: Heyman's Funicular Polygon

By using Figure 3.39 and considering vertical equilibrium, the magnitude of the support reactions could be attained. The loading values (W1-W15) were graphically drawn along with the reactions R1 and R2 as in Figure 4.36. The horizontal reaction value was assumed, starting with a value of 10KN. A line was drawn between each point load and the end of the horizontal reaction. The length of each of these diagonals corresponds to the internal compressive stress at the drawn location. Since loading was symmetrical, the reactions were identical; hence, the resulting Funicular Polygon was also symmetrical. This procedure was repeated for the horizontal reactions of 15,20,25 and 30KN. The full set of the drawn funicular polygons can be found in Appendix V.

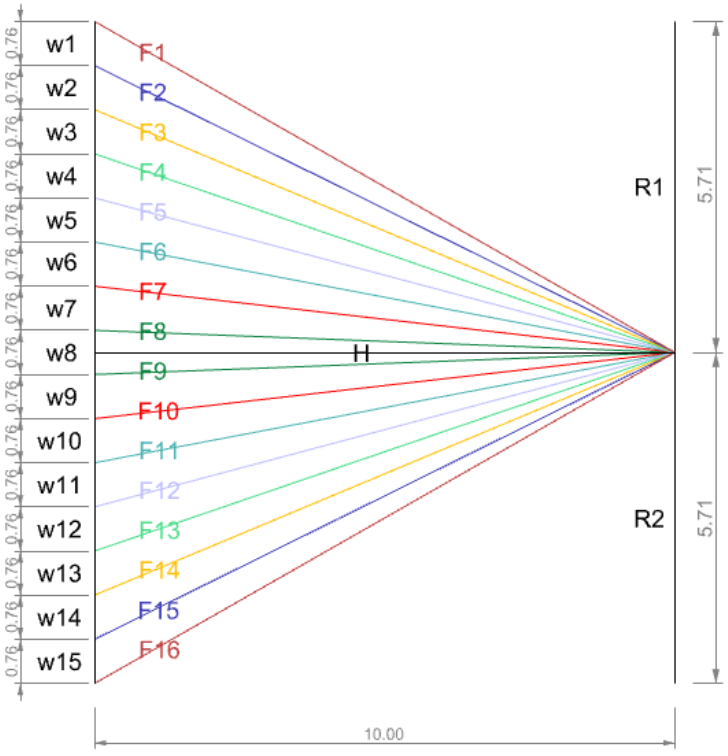

Figure 4.36: Funicular polygon for a horizontal reaction of 10KN

By taking the inclination of each of the joined lines, the resulting lines of thrust could be drawn out for every horizontal reaction and fitted within the arch geometry as in Figure 4.37.

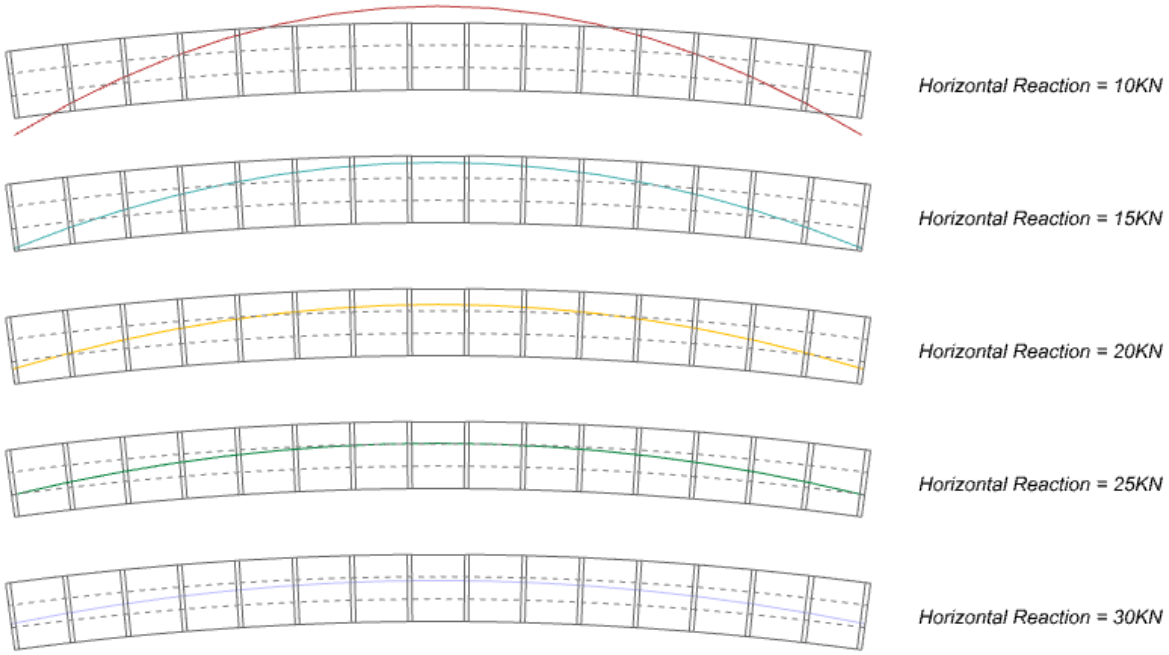

Figure 4.37: Fitting the lines of thrust for varying horizontal reactions within a 240mm deep arch

When the line of thrust was just about to touch the extrados and intrados, this could be classified as having a factor of safety of 1 whilst when the line of thrust fell within the middle third, the factor of safety could be deemed as 3. Looking at Figure 4.37, a factor of safety of 1 was attained for a horizontal reaction of 15KN whilst a factor of safety of 3 could be deducted for a horizontal reaction of 25KN.

Furthermore, the resulting lines of thrust were superimposed on the same plot as in Figure 4.38. It could be noted that both curves are identical yet they vary in the vertical scale.

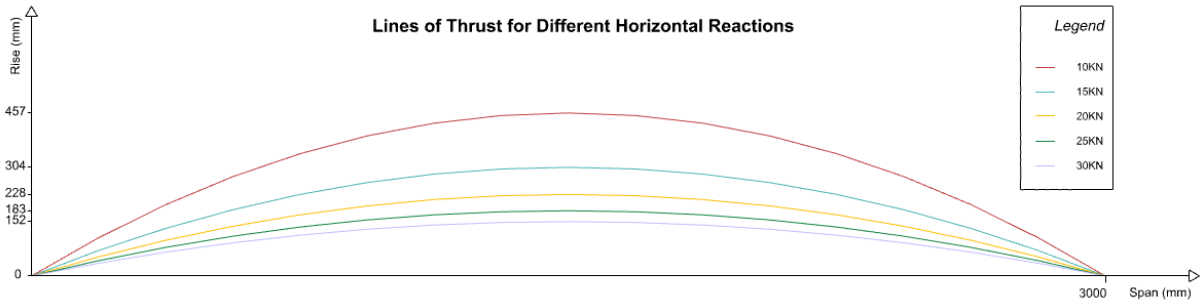

Figure 4.38: Superimposed lines of thrust for varying horizontal reactions

4.5.3. Comparing Finite Element Results with the Funicular Polygon Results

The above results have been summarized in Figure 4.39. The required horizontal thrust results attained through the Funicular Polygon were relatively high compared to those in Finite Element. Moreover, Finite Element results varied for the different arch construction configurations. Under identical loading conditions, the integrated formwork arch exhibited slightly lower values in the horizontal thrust.

	Horizontal Reaction	
Analysed Arch	Finite Element Analysis	The Funicular Polygon
Traditional Mortar jointed Arch	8.67KN	FOS 1 = 15KN FOS 3 = 25KN
Integrated steel formwork arch	6.98KN	

Figure 4.39: Summary of the horizontal reactions using the two methods of analysis

Although the Method of the Funicular Polygon is a straightforward approach through which a quick estimate of the forces within an arch can be calculated, it fails to consider several aspects. The Funicular Polygon Method assumes that the structure can only carry pure axial forces: compression in an arch and tension in a hanging string. This assumption fails to take into consideration the material of the structure which has its own strength and stiffness. These will directly impact the deformations of the structure upon loading. Moreover, the Method of the Funicular Polygon fails to give any data regarding the internal stresses and structural behaviour under loading such as the resulting deformations. The method only offers an estimate of the horizontal reactions and internal forces.

In comparison, the method of Finite Element factors in the properties of the considered material such as the strength and plasticity, to arrive at a more complete overview of the behaviour of the considered structure.

4.6. Conclusion

The primary tool of analysis for this section was the method of Finite Element which makes use of a process called discretization in which a number of equivalent smaller elements are used to analyse structures. The behaviour of the devised formwork in Chapter 3 was analysed using three main approaches; the simplified approach, the middle approach and the true approach. The primary aim was to monitor deformations as these impact the formwork's filling stage with voussoirs.

(i) In the simplified approach, deformations for the 10 and 20mm rods were too high yet for a 30mm rod, worst central deformations were as low as -2.7mm.

(ii) In the middle approach, deflections reduced where for a 20mm rod (being of most interest), the highest central deflections fell from +8.9mm to +4.59mm. Up to this point, worst deflections were in the upward direction for the 10 and 20mm rods.

(iii) In true approach, the voussoirs lowered the deflections by hindering the rotation of the vertical fins, leading to deformation reductions for a 20mm rod formwork to just -1.56mm, now all corresponding to the downward direction.

The completed arch was analysed under three rod thicknesses. The formwork having a 30mm rod performed best under loading, failing at the highest load. Maximum deformations were similar in all three cases yet at different load increments. Failure loads could be linked to the reach in maximum compressive stresses, corresponding to the reconstituted stone's crushing strength of 18N/mm^2. Maximum compressive forces formed at the arch's top central part and lower ends while very high compressive stresses formed at the ends of the arch, between the steel fins and steel rods. As the load carrying capacity of the arch kept increasing, the lateral thrust was reducing for the 20 and 30mm rods due to the activation of the steel formwork which aided the arch in carrying forces through bending.

The study proceeded with the comparison of a 20mm rod formwork integrated arch with an arch that eliminates the steel rods whilst retaining a steel joint and a traditional arch with mortar joints. Although the three arches failed at completely different loads and their ultimate displacements were relatively similar, the following main points could be deduced;

(i) In the case of the arch with mortar joints, there was a sudden increase in the displacement, stresses and lateral thrust followed by complete collapse. Such a sudden increase reflects the brittle nature of this type of construction.

(ii) In the arches with the steel joints and integrated formwork, ductile behaviour could be deduced since a smooth curved plot which corresponds to the yielding of the structure could be observed.

To compare the Method of Finite Element with the Funicular Polygon Method, two arches, being the 20mm integrated formwork arch and the mortar jointed arch were analysed in Finite Element under a live load of 5KN/m^2. Considering an arch of the same thickness, the method of the funicular polygon was used to arrive to a value for the horizontal reactions. Two values were obtained, 15KN for a factor of safety of 1 and 25KN for a factor of safety of 3. These were relatively greater than the 8.67 and 6.98KN attained for the traditional and integrated steel formwork arch respectively through Finite Element Analysis. This discrepancy results from the shortcomings of the Method of Funicular Polygons which fails to consider the influence of the structure's material . On the other hand, the Method of Finite Element factors in the effects of material, giving a more complete picture of the structural behaviour of the arch.

5. Conclusion

5.1. Discussion

Maltese architecture has its roots in masonry construction. The popularity in this building material mainly resulted from its abundance and excellent workability properties. Maltese craftsmen were very knowledgeable of the material, understanding well its strengths and weaknesses; weak in tension and strong in compression. These fundamental properties guided the development of roofing systems on the Maltese islands, resulting in an architecture founded on the use of funicular structures such as arches, vaults and domes.

Only in recent years has there been a shift from these traditional forms towards the more modern forms of construction, which primarily rely on bending actions of beams and slabs. With the emergence of new materials such as steel and concrete, this construction method has been favoured primarily due to the straight-forward design and construction associated with beam elements over arched elements, leading to savings in costs and time.

The primary drawback of constructing curved elements using masonry is the extensive formwork required until the structure's completion. This dissertation aimed to eliminate the need for a temporary formwork and instead integrate it within the final form. The objective was to design an integrated formwork which would ultimately aid in the structural performance of the final structure.

The formwork integrated curved structure can be divided in two stages. Active-bending was the solution for the primary stage of formwork erection. This stage was followed by the filled state which would form the funicular structure. The anticipated forms within this study’s scope were arches and vaults; hence, in-depth research on these typologies followed. The catenary chain analogy demonstrated the effect of rise on the lateral force, with shallower forms leading to larger lateral forces and vice versa. The importance of geometry on the overall structural stability of masonry arches was emphasised, being the most crucial factor for reasonably sized structures. Apart from serving as a link between the stone voussoirs, mortar serves as a smooth contact element between the voussoirs. This eliminates the risk of the formation of high concertation stress areas.

To attain a tangible understanding of the researched data, computational and physical models were the choice of preference for the initial stages of the testing which eventually led to the division of the final arch integrated formwork structure. 3D printing was the chosen method for the production of physical models. Gaussian curvature was used to define the geometry of the devised structure being a developable surface with a Gaussian curvature of zero. This property agrees with the reversibility of bending-active structures that can be erected or flattened without undergoing any permanent deformations. This facilitates transportation by enabling elements to be transported in their flattened state.

The initial studies brought out an important characteristic of the Elastica. The radius of curvature along its path is not uniform, which was not ideal primarily because the voussoirs would not be modular, leading to a significant increase in costs and production time. This observation initiated the first study of the Elastica. To understand whether it would be possible for the Elastica to deform into a semicircle, the geometries of the Elastica and semicircle were superimposed on a singular plot. The Elastica curve proved to have a higher rise for the same span and length. This observation was favourable as the formwork would be expected to deflect downwards upon loading. The remaining question was whether the Elastica would deform into a semicircle.

Before answering this question, it was essential to understand whether the Elastica's geometry changed depending on the approach used for its derivation. A physical study was carried out where the Elastica was manually devised followed by a geometrical study using Grasshopper 3D. Lastly, a Finite Element model was used to attain the deformed shape. Comparing all three results, it could be observed that regardless of which approach was chosen, the geometry of the Elastica was almost identical in all three cases.

To answer the pending question, a physical model of a semicircular arch was constructed where the initial formwork was elastically deformed. The voussoirs were shaped as segments of a semicircle and inserted within the deformed formwork. Upon completion it was confirmed that indeed the formwork would adapt to accommodate the semicircular arch geometry.

Having attained a holistic understanding of the problem, a vaulted structure with the same parameters as in study five was constructed. Whereas in previous studies , the horizontal thrust of the arch was resisted by a tie element, study six used a timber structure that provided the required lateral support. The effects of curvature on structural behaviour were proven by study seven where curvature was reduced to 0. The model's behaviour was completely different, behaving purely as a beam . This shows that even at low curvature values, the predominant action will be arch action with significant improvements in the load bearing capacity and a reduction in the vertical deformations of a structure.

An important note on scale must be made here. Although a linear relationship in the scalability of the parameters of bending-active structures has been proven, the effect of weight must not be neglected. Having a cubic relationship with scale, the mass of the formwork will impact the linearity in scaling up. The behaviour of the formwork in the 1:10 models might not accurately represent the true behaviour in the real life scenario. To minimise this error, the formwork was designed in a slender manner to reduce its weight and have a lower impact on the behaviour of the real-life structure.

Although the outlined studies proved to be crucial in understanding the geometrical behaviour of the formwork and its filling with voussoirs, these fail to consider the true scale of the structure along with the true material properties. Hence Finite Element Analysis was adopted to test the geometries resulting from physical models and attain a holistic understanding of the formwork behaviour and its incorporation within the arching form.

5.2. Critical Reflection

The main objective of this research was to understand whether it is possible to integrate the formwork of a roof under single curvature as part of the final structure and its potential benefits concerning structural performance and on-site construction.

The first research question (i), "What is the ideal geometric pattern for the integrated bending-active formwork for a roof in single curvature as part of the final structure and what is its structural feasibility?" was tackled by studies (1-7) in chapter 3. The formwork in study 5 was deemed to be the most adequate integrated formwork from the studied configurations as;

i. The formwork could be actively bent into the required geometry without undergoing and undesirable deformations as witnessed in study (4).
ii. Under the insertion of the voussoirs, the formwork was flexible enough to deform from the Elastica curve to a segment of a circle. This allowed for the possibility of modularity in the production of the voussoirs.

iii. The selected formwork allows for its extension from a 2D arch to a 3D vault by its repetitive use which allows for the staggering of the voussoirs. This results in a stiffer and more efficient structure.

Looking at research question (iii), " Which material can undergo bending to create the desired curved geometry whilst being stiff enough once fixed in place to accommodate the loading of the stone?", it could be seen that bending-active structures should use materials which are flexible enough to undergo active bending whilst still being stiff enough under loading. From the considered materials and the local context, it could be concluded that steel would be the preferred material mainly due to its high strength to weight ratio.

Regarding on-site construction, study 8 indicates that for a span of 3000mm, a 20mm rod integrated formwork would be able to withstand the resulting loading from the reconstituted stone voussoirs at a minimal downward deflection value of 1.56mm. Based on engineering judgement, this rod thickness was deemed to be flexible enough to deform in the required form yet withstand the applied load. Keeping the deflection value as low as possible was critical as the deflection of the formwork leads to the inward rotation of the central vertical fins, reducing the gap dedicated for the final voussoir. This makes it challenging to fit the keystone. Hence it could be concluded that on site, theoretically this system would be feasible.

For the structural behaviour of the roofing structure, the following research question was imposed; "What is the load-bearing capacity of such a curved reconstituted stone roof with the integrated formwork and how does it compare to a traditional masonry curved roof ?". Study 9 tackles the first part of the research question by analysing the proposed integrated formwork with 3 different rod thicknesses being the 10,20 and 30mm rods. The formwork with the 30mm rod failed at the highest applied uniformly distributed load of 147.5N/mm followed by the 20mm rod which failed at a load of 125.5N/mm and lastly the 10mm rod failed at 104.8N/mm. Hence it could be concluded that the load bearing capacity increased with the diameter of the rods within the formwork. Such failure could be directly linked to the reach in maximum compressive stresses, corresponding to the reconstituted stone's crushing strength of 18N/mm^2. The main observation resulting from determining the structure's load bearing capacity was the link with the lateral thrust. As the load carrying capacity of the arch kept increasing, the lateral thrust was reducing for the 20 and 30mm rods due to the activation of the steel formwork which aided the arch in carrying forces through bending.

Studies (10-11) answer the second part of research question (iii), so the structural performance could be determined. Having established that the 20mm diameter rod integrated formwork is one of interest for real life applications, the structure was compared to an arch with steel joints and another with mortar joints, corresponding to a traditional masonry arch. Interesting observations could be drawn out between the integrated formwork and traditional arch. Although both underwent structural failure at similar deflection values, the loading value at which they failed was drastically different. Whereas the masonry arch could withstand an ultimate load of 11N/mm, applied along the length of the arch, the formwork integrated arch could withstand loads up to 126.5N/mm. Hence it could be concluded that the load bearing capacity of a formwork integrated arch with a 20mm rod is approximately eleven times more than that of a traditional masonry arch.

The mode by which they failed was of the most interest. The masonry arch exhibited brittle failure, undergoing sudden and instant collapse. The documentation of such a collapse could have been improved by reducing the loading increment value. This would allow for a smoother transition and a more in-depth understanding of the behaviour between the 10-

11N/mm loading increments. What was of most interest was that although at the final loading increment extremely high compressive stresses developed near the abutments of the structure which would lead to crushing, yet structural collapse did not occur from such an action. Structural collapse occurred only when the following loading increment was applied. This load led to a sudden increase in stresses and displacements within all adjacent voussoirs. On the other hand, as outlined in the previous study, the formwork integrated arch underwent ductile behaviour with failure of the structure associated with high values of deformation.

The performance of the arch was significantly improved with the introduction of the formwork as:

i. The ultimate load bearing capacity of the arch was improved by a factor of approximately eleven.

ii. Arch failure follows ductile behaviour when integrated with the formwork, which is the preferred mode of failure when compared to brittle behaviour in arches.

iii. The formwork integrated arch is able to accommodate for bending due to composite action between the reconstituted stone voussoirs and steel integrated formwork.

The Method of Finite Element is quite a recent tool of analysis. In the past, simplified methods like the method of the Funicular Polygon were the only available means for the structural analysis of arches and vaults. Hence it was of interest to see how these two methods compare with each other. The analysed arches in Finite Element were both subjected to the same loading conditions, that being of a typical live load of 5KN/m2. Comparing the results attained from the Method of the Funicular Polygon being 15 and 25KN for a safety factor of 1 and 3 respectively, with the results from Finite Element being 8.67KN, a significant discrepancy could be noted. Several reasons could account for such an outcome.

The Method of the Funicular Polygon adopts an elastic approach which is based on a number of simplified assumptions. Firstly, it assumes that the arch can only carry compressive forces. Hence, the results attained from the funicular polygon cannot represent the formwork integrated arch since such an arch has the increased capacity of carrying tension resulting from the steel. Moreover, this method fails to consider the material properties and their effect on the overall structural behaviour. The Funicular Polygon assumes a statically determinate system. This conflicts with the assumed end conditions throughout the Finite Element Analysis where pinned supports were modelled, resulting in a statically indeterminate system by a degree of 1. This assumption could explain for the conservative results attained by the Method of the Funicular Polygon over the Method of Finite Element.

5.3. Future Work

This study offers an insight into how active-bending can be used to elastically deform formwork which can be integrated within a shallow reconstituted/natural stone curved roof. The attained results are promising, proving the concept utilizing small scale physical models and structural analysis. Further research is still required when it comes to its physical application in a real-life scaled structure.

The simulation of the formwork erection in a real life scenario has yet to be tested. Although preliminary values regarding the required thicknesses for the formwork have been established through Finite Element Analysis, whether such thicknesses will allow for sufficient flexibility in the formwork to be manually deformed and erected by the working personnel has yet to be

verified. This would be the preferred scenario, eliminating the need for heavy machinery which would increase costs. A possible solution could be the use of the ease-down method as explained in Chapter 2 yet this would require the use of a crane which is undesirable.

Within this study, the formwork was infilled in a sequential order by starting from the ends and progressively moving inwards until the keystone was placed within the arch. Such an order resulted in an inward rotation of the middle fins which hindered the insertion of the keystone. Further research could test different chronological orders for the insertion of the voussoirs to determine the ideal sequential order that would result in an outward rotation, facilitating the insertion of the final voussoir.

Staggering within the final structure was presented as the correct approach in ensuring voussoir interlock and load transmission. It has been shown that by the completion of a singular segment of an arch, the added adjacent voussoirs would be entirely supported by the completed arch. Although this property was not relied on within this study and the formwork was introduced throughout the vault structure, an attempt at using the integrated formwork just to complete a singular arch could be tested. To activate contact between the completed arch and additional voussoirs added on each side, a contact element would need to be inserted to ensure a tight fitting voussoir that can transfer its load to the main arch as shown in Figure 3.16.

A fundamental principle for arches to work is lateral confinement. The possible options to contain such high lateral forces could be further investigated, with possible options being tying action and strong abutments as briefly mentioned within this study. It would be interesting to explore typical masonry wall construction behaviour when subjected to the lateral forces exerted by shallow arch construction. Using a ring beam to contain the lateral thrust could also be explored further.

Throughout the study, the considered type of loading was always a uniformly distributed load which varies in magnitude. This type of loading is ideal for funicular forms, as the resulting lines of thrust are relatively uniform and easier to fit within the thickness of the arch. The effects of uneven loading with respect to loading position and value could be further investigated. This would result in a further understanding of how such a variation in loading impacts the overall behaviour of the structure.

In effort to replicate a traditional arch which makes use of trimmed stone voussoirs whilst pertaining to the advantage of the use of dry trades, the devised formwork was designed with the concept of infilling the voids with precast solid elements. A different approach could be tested where casting could occur directly within the formwork. A preliminary attempt has already been undertaken in study six where the voussoirs were 3D printed as hollow. Further studies could use a similar design and attempt the direct casting of reconstituted stone within the negative spaces. Moreover, the positive space of the 3D printed voussoir could be translated in reality as a hollow reconstituted stone voussoir. The impacts of voids within the voussoirs on the overall structural behaviour could be further studied.

This research was focused on structures having singular curvature. A possible development of this research could be the study of roofs in double curvature, such as domes. Although double curvature complicates the formwork and voussoir design since double curvature will impose constraints on modularity, just by the completion of a singular compression ring within the dome, the stiffness and load bearing capacity of the formwork is expected to increase significantly.

Technological advancement have led to a rapid progress in the fields of architecture and structural engineering. These advancements gave rise to new building typologies with ever increasing complexities. Amongst all this progress, it is fundamental not to lose sight of the foundational roots upon which traditional architecture evolved and flourished. Traditional architecture's adopted principles and typologies are timeless and will retain their relevancy indefinitely. The integration of these principles and typologies with new principles and structural understanding can pave the path towards the architecture of the future. In this manner, the core roots and character defining a place's architecture will retain legibility through the expression of form and structure.

"Originality consists of returning to the origin. Thus, originality means returning, through one's resources, to the simplicity of the early solutions."

Antoni Gaudí

6. Bibliography

Alpermann, H. i Gengnagel, C. (2012). *Shaping actively-bent elements by restraining systems.* Department of Architecture, University of the Arts, Berlin, Germany: Research Gate.

Brancart, S., De Laet, L., Vergauwen, A. i De Temmerman, N. (2014). *Transformable active bending: A kinematical concept.* Brussels,Belgium: Department of Architectural Engineering, Vrije Universiteit.

Brutting, J., Korner, A., Sonntag, D. i Knippers, J. (2017). *Bending-Active Segmented Shells.* Hamburg, Germany: Proceedings of the IASS Annual Symposium.

(2023). *Building a Mudhif.* Ottawa: Iraqi Embassy .

C.Truesdell. (1970). *The Rational Mechanics Of Flexible Or Elastic Bodies 1638 - 1788: Introduction to Leonhardi Euleri Opera Omnia. Vol. X et XI.* Baltimore, USA: Orell Fussli.

Calleja, L. (2018). *Auxetics in Architecture: A Study on Geometry and Topology.* Malta: University of Malta.

Different types of Nomadic Tents in Turkey. (2023, May 21). Pobrano z lokalizacji theblacktentproject: https://www.theblacktentproject.com/different-types-of-nomadic-tents-in-turkey/

Dixit, U. S. (n.d.). *FINITE ELEMENT METHOD: AN INTRODUCTION.* Guwahati, India: Department of Mechanical Engineering, Indian Institute of Technology.

DOUTHE, C., BAVEREL, O. i CARON, J.-F. (2006). *Form-finding of a grid shell in composite materials.* Marne-la-Vallée, France: Journal of the International Association for Shell and Spatial Structures.

Dragoș , N., Harris, R. i Williams, C. (2014). *TIMBER GRIDSHELLS: DESIGN METHODS AND THEIR.* Quebec, Canada: World Conference of Timber Engineering.

Engel, H. (1997). *Tragsysteme Structure Systems.* Germany: Hatje Cantz Verlag.

G.Fertis, D. (2006). Nonlinear Structural Engineering: With Unique Theories and Methods to Solve Effectively Complex Nonlinear Problems. W D. G.Fertis, *Nonlinear Structural Engineering: With Unique Theories and Methods to Solve Effectively Complex Nonlinear Problems* (strony 22-23). New York: Springer.

Gengnagel, C., Hernández, E. i Alpermann, H. (2014). *Active Bending in Hybrid Structures.* Germany, Berlin: Departement of Structural Design and Technology [KET] Faculty of Architecture, University of the Arts Berlin.

Ghasempourabadi, M., Mahmoudabadi, V., Bahar, O. i Mahdavinejad, M. (2012). *Assessment of behavior of two-shelled domes in Iranian traditional architecture: the Charbaq School, Isfahan, Iran.* Tehran, Iran: Witpress.

Gobrick. (1995). *Technical Notes 31 -Brick Masonry Arches.* Reston,Virginia.

Gomez-Ferrer, M. (2009). *The Origins of Tile Vaulting in Valencia Vol. 24 pp. 31-44.* The Construction History Society.

Goss, V. A. (2003). *Snap buckling, writhing AND loop formation in twisted rods.* London, UK: Center for Nonlinear Dynamics University College .

Grasp. (2023, May 10). *What Is Finite Element Analysis? Why to Do FEA?* Pobrano z lokalizacji Grasp Engineering: https://www.graspengineering.com/hello-world-2/

Hang, X. Z., Gao2, W., Xia, Y., Wang, X., Luo, Y., Su, J., . . . Yuan, P. F. (2019). *DESIGN AND ANALYSIS OF BENDING-ACTIVE FORMWORK FOR SHELL STRUCTURES BASED ON 3D-PRINTING TECHNOLOGY.* Asia: Association for Computer-Aided Architectural Design Research.

Huerta, S. (2006). *Structural Design in the Work of Gaudi.* Madrid, Spain: Department of Structural Design, Escuela Ticnica Superior de Arquitecrura, Universidad Politecnica de Madrid.

Jacques Heyman, M. P. (1982). *The Masonry Arch.* J. Heyman/Ellis Horwood Ltd.

Jagoe, G. A. (2021). *Autoclaved Aerated Concrete Tile Vaults for Lightweight Floor Systems.* Notre Dame, Indiana, United States: Massachusetts Institute of Technology, University of Notre Dame.

Jigme , D., Zahra, T., Thambiratnam, D. i Lee, D. (2021). *Strength assessment of old masonry arch bridges through moderate destructive testing methods.* ScienceDirect.

Knippers, J. (2013). *From Model Thinking to Process Design.* AD Architectural Design.

Lee, T.-U. (2019). *Elastic Energy Behaviours of Curved-crease.* Australia: University of Queensland, Australia.

Levien, R. (2008). *The elastica: a mathematical history.* California: University of California at Berkeley.

Levien, R. L. (2009). *From Spiral to Spline: Optimal Techniques in Interactive Curve Design.* California, USA: Electrical Engineering and Computer Sciences University of California at Berkeley.

Li, H. (2023, April 22). *Timoshenko-Ehrenfest Beam theory*. Pobrano z lokalizacji Encyclopedia: https://encyclopedia.pub/entry/30338

Liddell, I. (2015). *Frei Otto and the development of gridshells.* United Kingdom: Elsevier.

Lienhard, J. (2014). *Bending-Active Structures .* Stuggart, Germany: University of Stuttgart.

Lienhard, J. i Knippers, J. (2013). *Considerations on the Scaling of Bending-Active Structures.* Germany: International Journal of Space Structures Vol. 28 No. 3&4 2013.

Lienhard, J. i Knippers, J. (2013). *International Journal of Space Structures.* 5 Wates Way, Brentwood, Essex CM15 9TB, United Kingdom: MULTI-SCIENCE PUBLISHING CO. LTD.

Lienhard, J., Schleicher, S. i Knippers, J. (2011). *Bending-active Structures – Research Pavilion ICD/ITKE.* London, UK: International Symposium of the IABSE-IASS Symposium, Taller Longer Lighter.

LIUTI, A., MAZZOLA, C. i ZANELLI, A. (2018). *Where design meets construction: a review of bending active.* Milan, Italy: Proceedings of the IASS Symposium 2018.

López, D. L. (2012). *Structural Analysis of Tile Vaulting: Method and Variables.* Barcelona, Spain: Department d'Estructures de l'Edificació Universitat Politècnica de Catalunya.

Lusas. (2023, May 17). *LUSAS Analyst / Analyst Plus Overview*. Pobrano z lokalizacji Lusas: https://www.lusas.com/products/analyst.html

Mallia, A. (2018). *Contemporary Architectural Tectonics; The Role of Stone in the Maltese Islands.* Malta: University of Malta.

Mathworks. (2023, May 10). *What Is Finite Element Analysis (FEA)?* Pobrano z lokalizacji Mathworks: https://de.mathworks.com/discovery/finite-element-analysis.html

McElwain, W. (2014). *Grasshopper3d*. Pobrano z lokalizacji Grasshopper algorithmic modeling for rhino: https://www.grasshopper3d.com/forum/topics/a-script-for-elastic-bending-aka-the-elastica-curve

Mirante, L. (2015). *Auxetic Structures: Towards bending-active architectural applications by Mirante Lorenzo.* Milan, Italy: Politecnico di Milano, Facoltà di Architettura e Società.

(2004). *Mortar in Tension.* University of Warwick, United Kingdom: https://warwick.ac.uk/fac/sci/eng/research/grouplist/structural/dtu/pubs/rn/build/still_2004/still_11-2-04.pdf.

Naboni, R. (2016). *Embedding auxetic properties in designing active-bending gridshells .* Milan, Italy: XX Congress of the Iberoamerican Society of Digital Graphics.

Nguyen, A. (2017). *Comparative Spectral Analysis of Flexible Structure Models: the Euler-Bernoulli Beam model, the Rayleigh Beam model, and the Timoshenko Beam Model.* Semantic Scholar.

Oki, H. (2023, May 31). *Bamboo rising: Vo Trong Nghia reimagines an ancient 'green steel'*. Pobrano z lokalizacji Foreground: https://www.foreground.com.au/parks-places/bamboo-rising-vo-trong-nghia-reimagines-an-ancient-green-steel/

Otto, F., Fritz, J., Greiner, S., Gab, S., Hennicke, J., Reiner, R., . . . Voigt, H. (1985). *IL 31 Bambus Bamboo.* Stuggart: Klaus Dunkelberg.

Pacheco , Q. i Piña, E. (2007). *The elastic rod.* Mexico: Revista Mexicana de Física.

Reddy, J. (2009). *An Introduction to the Finite Element Method.* Texas, USA: McGraw-Hill Medical Publishing.

Repointing stone and brick. (2023, May 18). Pobrano z lokalizacji Department for Communities: https://www.communities-ni.gov.uk/technical-note-repointing-stone-and-brick#:~:text=Galleted'%20stone%20joints-,Description,'snecked'%20pieces%20of%20stone.

Solanki, K. J. (2023, May 28). *Catalan Vaulting – a masonry construction technique*. Pobrano z lokalizacji Archweb: https://www.archweb.com/en/design/page/catalan-vaulting/#:~:text='Catalan%20Vaulting'%20also%20known%20as,the%20region%20of%20Catalunya%2C%20Spain.

Svirin, A. (2023, May 21). *Equation of Catenary*. Pobrano z lokalizacji Math24: https://math24.net/equation-catenary.html

The Bernoulli-Euler Beam Theory . (2023, April 22). Pobrano z lokalizacji Learn About Structures: https://learnaboutstructures.com/Bernoulli-Euler-Beam-Theory

The Different Kinds of Mortar. (2023, May 18). Pobrano z lokalizacji Stone Arch Bridges: https://stonearchbridges.com/2022/06/17/the-different-kinds-of-mortar/

Tonna, J. (1971). *Form-making in Maltese Culture.* Malta: University of Malta.

Valiente, A. (2004). *An experiment in nonlinear beam theory.* Departamento de Ciencia de Materiales, Escuela Te´cnica Superior de Ingenieros de Caminos, Canales y Puertos, Universidad Politecnica de Madrid, Ciudad Universitaria, s/n, 28040-Madrid, Spain: American Journal of Physics 72, 1008–1012.

Vella, H. C. (1980). *The earliest description of Malta (Lyons 1536) / by Jean Quintin d'Autun.* Sliema, Malta: DeBono Enterprises.

Vella, I. M. (2019). *A Stereotomic Approach to Regional Digital Architecture.* Malta: University of Malta.

Zhang, X., Gao, W., Xia, Y., Wang, X., Luo, Y., Su, J., . . . Yuan, P. F. (2019). *Design and analysis of bending-active formwork for shell structures based on 3d-printing technology.* Hong Kong, China: The Association for Computer-Aided Architectural Design Research in Asia.

7. Appendix I: Geometrical properties of the Arch

Masonry Arch

Calculation Sheets

Job Title: The Relationship between the span, rise, radius and centre of a circle
Worked by: Rebecca Mifsud

Date : 11/05/23

1. Stage 1: Deciding the parameters of the Shallow Arch

Desired Span	s	3	m
Desired Rise	h	0.1	m

At low values of curvature, the elastica could be approximated to a segment of a circle

2. Arriving to the Radius (r) and Circle Centre Coordinates (a,b) from 3 points on a curve

a. 3 Known Points on the Segment of the Circle

	x	y	Units
Point A (start of arch segment)	0	0	m
Point B (end of arch segment)	3	0	m
Point C (rise of arch segment)	1.5	0.1	m

b. Equation of a Circle

$$r^2 = (x-a)^2 + (y-b)^2$$

Where the unknowns are:

r	radius of circle
a	x-coordinate of the centre of a centre
b	y-coordinate of the centre of a centre

c. Writing the 3 Simultaneous Equations from the 3 points on the Circle

	RHS of Equation (x-a)^2 + (y-b)^2		LHS of Equation r^2	
Equation 1	127.6899972	=	127.6896993	r^2 = (0-a)^2 + (0-b)^2
Equation 2	127.6899972	=	127.6896993	r^2 = (3-a)^2 + (0-b)^2
Equation 3	127.6899972	=	127.6896993	r^2 = (1.5-a)^2 + (0.1-b)^2

d. Finding the r, a and b values

r	11.29998669	m
a	1.5	m
b	-11.19999987	m

3. Finding the length of the segment of the arch = Flat Formwork Original Length

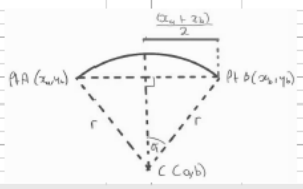

a. Finding the angle, Θ1

By Trigonometry:

sin(θ1) = ((xa+xb)/2) / r1

x-coordinate of point a	xa	0	m
x-coordinate of point b	xb	3	m
opposite	(xa+xb)/2	1.5	m
hypotenuse	r	11.3	m

Masonry Arch

Calculation Sheets

Job Title: The Relationship between the span, rise, radius and centre of a circle
Worked by: Rebecca Mifsud

Date : 11/05/23

Half the Angle	Θ1	7.6282	degrees
Angle of Segment	Θ1,total	15.256	degrees

Flat formwork Span = Segment of circle length = l = (θ/360) x 2πr

Therefore flat formwork length	l	3.0089	m

4. Stage 2: Elastically Deformed formwork to form an arch

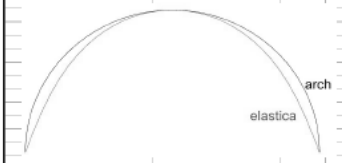

I. Actual Geometry (elastica)

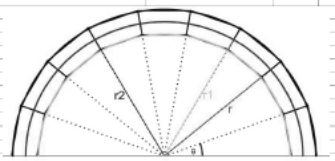

II. Assumed Geometry

Assumptions:
a. Assuming that the axis of rotation is within the bottom side of the geometry since the horizontal axial force shall be applied at that location

b, The formed arch is a parabola as it follow the elastica curve. Yet this will be approximated to a semicircle since the rise is low and in order to have equal and modular voussiers

a. Arc radial length	l	3.0089	m

5. Voussier Depth

Voussier Depth Assumption	*Vd*	*0.3*	*m*

6. Determining the inner and outer radii, r1 and r2

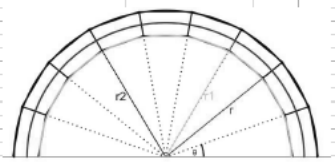

a. Voussier Depth

Vd = 0.2R or assumed	Vd	0.3	m

b. Number of voussiers

Number of voussiers	N	15	amount	*(needs to be odd)*

Masonry Arch

Calculation Sheets

Job Title: The Relationship between the span, rise, radius and centre of a circle
Worked by: Rebecca Mifsud

Date : 11/05/23

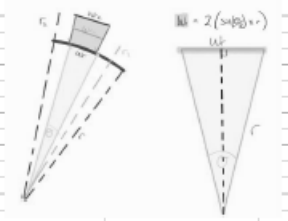

c. Inner Radius	r	11.3	m
Central Circumference	lr	3.0089	m
Angle of 1 voussoir	Θ	1.0171	degrees
Width per voussier	wr	0.2006	m
d. Central Radius	r1	11.45	m
Central Circumference	lr1	3.0488	m
Angle of 1 voussoir	Θ	1.0171	degrees
Width per voussier	wr1	0.2033	m
e. Outer Radius	r2	11.6	m
Outer Circumference	lr2	3.0888	m
Angle of 1 voussoir	Θ	1.0171	degrees
Width per voussier	wr2	0.2059	m

8. Appendix II: Data of Study 8

a. Simplified Approach

Central Displacement due to Loading (mm)			
Applied Loads	**10mm rod**	**20mm rod**	**30mm rod**
V1	18.5296	1.05863	0.176651
V1 - V2	66.2725	3.74855	0.612045
V1 - V3	123.667	6.86067	1.07176
V1 - V4	166.263	8.88821	1.26514
V1 - V5	171.659	8.45923	0.930339
V1 - V6	126.491	4.77144	-0.0803271
V1 - V7	33.4151	-1.97227	-1.71478
V1 - V8	-24.247	-6.05078	-2.67532

10mm Rod — Vertical Displacement due to Loading

Node Number	V1	V1-V2	V1-V3	V1-V4	V1-V5	V1-V6	V1-V7	V1-V8
1	-7.81727	-22.8998	-36.1127	-42.3077	-39.6185	-28.7436	-12.2199	-2.9551
2	-15.0825	-51.5521	-87.086	-105.655	-100.918	-74.1029	-31.8642	-7.99281
3	-13.2128	-48.7467	-92.0601	-120.109	-119.978	-90.9588	-41.097	-12.3996
4	-6.19504	-24.7645	-52.8138	-79.8789	-88.7309	-72.8998	-37.5811	-16.2836
5	2.68915	7.42623	7.5576	-1.29435	-15.5644	-23.6016	-22.2682	-19.57
6	10.8749	37.6901	66.7096	82.5407	74.5035	43.0242	0.48596	-22.0982
7	16.5237	58.7624	108.624	143.943	145.276	102.738	22.8392	-23.6986
8	18.5296	66.2725	123.667	166.263	171.659	126.491	33.4151	-24.247
9	16.5237	58.7624	108.624	143.943	145.276	102.738	22.8392	-23.6986
10	10.8749	37.6901	66.7096	82.5407	74.5035	43.0242	0.48596	-22.0982
11	2.68915	7.42623	7.5576	-1.29435	-15.5644	-23.6016	-22.2682	-19.57
12	-6.19504	-24.7645	-52.8138	-79.8789	-88.7309	-72.8998	-37.5811	-16.2836
13	-13.2128	-48.7467	-92.0601	-120.109	-119.978	-90.9588	-41.097	-12.3996
14	-15.0825	-51.5521	-87.086	-105.655	-100.918	-74.1029	-31.8642	-7.99281
15	-7.81727	-22.8998	-36.1127	-42.3077	-39.6185	-28.7436	-12.2199	-2.9551

20mm Rod — Vertical Displacement due to Loading

Node Number	V1	V1-V2	V1-V3	V1-V4	V1-V5	V1-V6	V1-V7	V1-V8
1	-0.500375	-1.47509	-2.35177	-2.80641	-2.71939	-2.13086	-1.1955	-0.666183
2	-0.974712	-3.34885	-5.72015	-7.08012	-7.02363	-5.6171	-3.265	-1.92004
3	-0.870086	-3.24799	-6.19825	-8.27356	-8.65249	-7.27416	-4.62284	-3.06678
4	-0.454636	-1.8146	-3.88991	-6.01211	-7.08265	-6.67488	-5.08875	-4.07498
5	0.0870225	0.143513	-0.235421	-1.30596	-2.82256	-4.02724	-4.69404	-4.90853
6	0.588529	1.99506	3.37339	3.78116	2.57648	-0.183728	-3.68896	-5.53285
7	0.935359	3.28747	5.93879	7.52492	6.85812	3.35289	-2.54786	-5.91971
8	1.05863	3.74855	6.86067	8.88821	8.45923	4.77144	-1.97227	-6.05078
9	0.935359	3.28747	5.93879	7.52492	6.85812	3.35289	-2.54786	-5.91971
10	0.588529	1.99506	3.37339	3.78116	2.57648	-0.183728	-3.68896	-5.53285
11	0.0870225	0.143513	-0.235421	-1.30596	-2.82256	-4.02724	-4.69404	-4.90853
12	-0.454636	-1.8146	-3.88991	-6.01211	-7.08265	-6.67488	-5.08875	-4.07498
13	-0.870086	-3.24799	-6.19825	-8.27356	-8.65249	-7.27416	-4.62284	-3.06678
14	-0.974712	-3.34885	-5.72015	-7.08012	-7.02363	-5.6171	-3.265	-1.92004
15	-0.500375	-1.47509	-2.35177	-2.80641	-2.71939	-2.13086	-1.1955	-0.666183

30mm Rod — Vertical Displacement due to Loading

Node Number	V1	V1-V2	V1-V3	V1-V4	V1-V5	V1-V6	V1-V7	V1-V8
1	-0.102693	-0.305691	-0.495471	-0.607287	-0.616548	-0.530042	-0.377057	-0.288731
2	-0.202999	-0.702907	-1.22041	-1.55411	-1.62114	-1.43124	-1.06055	-0.842851
3	-0.18978	-0.707283	-1.36942	-1.88452	-2.08572	-1.95553	-1.58358	-1.35372
4	-0.111816	-0.44552	-0.960618	-1.52036	-1.90065	-2.00992	-1.89937	-1.80267
5	-0.009261	-0.076288	-0.277484	-0.65777	-1.16123	-1.6284	-2.00492	-2.17232
6	0.0865053	0.276409	0.406594	0.297315	-0.169861	-0.973805	-1.94248	-2.44781
7	0.15296	0.523675	0.895631	1.00619	0.629672	-0.339004	-1.80061	-2.61784
8	0.176651	0.612045	1.07176	1.26514	0.930339	-0.0803271	-1.71478	-2.67532
9	0.15296	0.523675	0.895631	1.00619	0.629672	-0.339004	-1.80061	-2.61784
10	0.0865053	0.276409	0.406594	0.297315	-0.169861	-0.973805	-1.94248	-2.44781
11	-0.009261	-0.076288	-0.277484	-0.65777	-1.16123	-1.6284	-2.00492	-2.17232
12	-0.111816	-0.44552	-0.960618	-1.52036	-1.90065	-2.00992	-1.89937	-1.80267
13	-0.18978	-0.707283	-1.36942	-1.88452	-2.08572	-1.95553	-1.58358	-1.35372
14	-0.202999	-0.702907	-1.22041	-1.55411	-1.62114	-1.43124	-1.06055	-0.842851
15	-0.102693	-0.305691	-0.495471	-0.607287	-0.616548	-0.530042	-0.377057	-0.288731

b. The Middle Approach

Central Displacement due to Loading (mm)			
Applied Loads	**10mm rod**	**20mm rod**	**30mm rod**
V1	8.11434	0.582562	0.096328
V1 - V2	18.2476	1.97984	0.321662
V1 - V3	25.9407	3.56542	0.55459
V1 - V4	30.4915	4.59383	0.647958
V1 - V5	31.4493	4.40598	0.469465
V1 - V6	27.8158	2.57028	-0.0557325
V1 - V7	15.3214	-0.918269	-0.901498
V1 - V8	-10.6816	-3.07339	-1.3973

10mm Rod — Vertical Displacement due to Loading

Node Number	V1	V1-V2	V1-V3	V1-V4	V1-V5	V1-V6	V1-V7	V1-V8
1	-3.71699	-7.38631	-9.02287	-9.39151	-9.02588	-8.09244	-6.27029	-2.02563
2	-6.9913	-16.5525	-19.949	-21.0875	-23.5925	-21.2617	-16.2885	-5.08467
3	-6.03713	-15.1865	-23.6388	-28.7149	-29.4727	-27.4131	-21.3579	-7.12347
4	-2.83595	-7.64298	-13.7443	-19.9489	-23.3866	-23.5937	-19.7547	-8.71984
5	1.11389	1.61142	0.0221226	-3.6461	-8.17945	-11.2494	-11.8222	-9.61945
6	4.72516	10.0712	12.9211	12.9249	10.1281	5.05364	-0.802332	-10.3422
7	7.22292	16.0578	22.3617	25.5298	25.2483	20.8363	10.2516	-10.5765
8	8.11434	18.2476	25.9407	30.4915	31.4493	27.8158	15.3214	-10.6816
9	7.22292	16.0578	22.3617	25.5298	25.2483	20.8363	10.2516	-10.5765
10	4.72516	10.0712	12.9211	12.9249	10.1281	5.05364	-0.802332	-10.3422
11	1.11389	1.61142	0.0221226	-3.6461	-8.17945	-11.2494	-11.8222	-9.61945
12	-2.83595	-7.64298	-13.7443	-19.9489	-23.3866	-23.5937	-19.7547	-8.71984
13	-6.03713	-15.1865	-23.6388	-28.7149	-29.4727	-27.4131	-21.3579	-7.12347
14	-6.9913	-16.5525	-19.949	-21.0875	-23.5925	-21.2617	-16.2885	-5.08467
15	-3.71699	-7.38631	-9.02287	-9.39151	-9.02588	-8.09244	-6.27029	-2.02563

20mm Rod — Vertical Displacement due to Loading

Node Number	V1	V1-V2	V1-V3	V1-V4	V1-V5	V1-V6	V1-V7	V1-V8
1	-0.283445	-0.822646	-1.30489	-1.55728	-1.51751	-1.19859	-0.667943	-0.359603
2	-0.537573	-1.78669	-3.02464	-3.74054	-3.72964	-3.00566	-1.7393	-0.997254
3	-0.478712	-1.7129	-3.23185	-4.31056	-4.52701	-3.82643	-2.41437	-1.56744
4	-0.245376	-0.950601	-2.02312	-3.12274	-3.68394	-3.47746	-2.63076	-2.08217
5	0.051602	0.082507	-0.12097	-0.678594	-1.4453	-2.04924	-2.38242	-2.49586
6	0.325884	1.05752	1.75437	1.95292	1.35472	-0.0268287	-1.83568	-2.81823
7	0.515267	1.73729	3.08651	3.88842	3.57501	1.82841	-1.21647	-3.00705
8	0.582562	1.97984	3.56542	4.59383	4.40598	2.57028	-0.918269	-3.07339
9	0.515267	1.73729	3.08651	3.88842	3.57501	1.82841	-1.21647	-3.00705
10	0.325884	1.05752	1.75437	1.95292	1.35472	-0.0268287	-1.83568	-2.81823
11	0.051602	0.082507	-0.12097	-0.678594	-1.4453	-2.04924	-2.38242	-2.49586
12	-0.245376	-0.950601	-2.02312	-3.12274	-3.68394	-3.47746	-2.63076	-2.08217
13	-0.478712	-1.7129	-3.23185	-4.31056	-4.52701	-3.82643	-2.41437	-1.56744
14	-0.537573	-1.78669	-3.02464	-3.74054	-3.72964	-3.00566	-1.7393	-0.997254
15	-0.283445	-0.822646	-1.30489	-1.55728	-1.51751	-1.19859	-0.667943	-0.359603

30mm Rod — Vertical Displacement due to Loading

Node Number	V1	V1-V2	V1-V3	V1-V4	V1-V5	V1-V6	V1-V7	V1-V8
1	-0.058166	-0.170415	-0.274685	-0.336082	-0.341263	-0.293795	-0.20954	-0.160775
2	-0.11213	-0.375097	-0.644808	-0.818859	-0.854404	-0.756092	-0.56304	-0.449363
3	-0.103944	-0.373246	-0.713503	-0.979455	-1.08473	-1.01983	-0.830175	-0.712523
4	-0.060908	-0.234166	-0.499565	-0.788484	-0.986017	-1.04594	-0.99387	-0.946703
5	-0.004779	-0.03972	-0.144527	-0.341939	-0.602014	-0.846551	-1.04669	-1.13669
6	0.0475028	0.145593	0.210199	0.150126	-0.0941197	-0.512432	-1.01692	-1.28098
7	0.0837377	0.2753	0.463408	0.514759	0.315437	-0.187715	-0.943587	-1.36752
8	0.096328	0.321662	0.55459	0.647958	0.469465	-0.0557325	-0.901498	-1.3973
9	0.0837377	0.2753	0.463408	0.514759	0.315437	-0.187715	-0.943587	-1.36752
10	0.0475028	0.145593	0.210199	0.150126	-0.0941197	-0.512432	-1.01692	-1.28098
11	-0.004779	-0.03972	-0.144527	-0.341939	-0.602014	-0.846551	-1.04669	-1.13669
12	-0.060908	-0.234166	-0.499565	-0.788484	-0.986017	-1.04594	-0.99387	-0.946703
13	-0.103944	-0.373246	-0.713503	-0.979455	-1.08473	-1.01983	-0.830175	-0.712523
14	-0.11213	-0.375097	-0.644808	-0.818859	-0.854404	-0.756092	-0.56304	-0.449363
15	-0.058166	-0.170415	-0.274685	-0.336082	-0.341263	-0.293795	-0.20954	-0.160775

c. The True Approach

Central Displacement due to Loading (mm)			
Applied Loads	**10mm rod**	**20mm rod**	**30mm rod**
V1	-0.005804	0.0022183	0.00302314
V1 - V2	0.0080517	0.0263973	0.016196
V1 - V3	0.127006	0.0844336	0.008579
V1 - V4	0.430288	0.0333232	-0.119085
V1 - V5	0.489155	-0.4326	-0.390437
V1 - V6	-1.29482	-1.09866	-0.694416
V1 - V7	-2.84006	-1.56153	-0.95038
V1 - V8	-0.109525	-0.080226	-0.0617524

10mm Rod — Vertical Displacement due to Loading

Node Number	V1	V1-V2	V1-V3	V1-V4	V1-V5	V1-V6	V1-V7	V1-V8
1	-0.004459	-0.019086	-0.0436876	-0.0769012	-0.111258	-0.130125	-0.136398	-0.00602104
2	-0.015549	-0.072523	-0.166437	-0.29342	-0.425739	-0.501469	-0.531352	-0.0274774
3	-0.018656	-0.113104	-0.278244	-0.491868	-0.715546	-0.847332	-0.9049	-0.0483784
4	-0.017222	-0.107106	-0.366658	-0.689093	-1.0063	-1.19795	-1.28912	-0.0679456
5	-0.013626	-0.073214	-0.255561	-0.775136	-1.29827	-1.55442	-1.68581	-0.084865
6	-0.009726	-0.033308	-0.0781571	-0.316993	-1.29254	-1.91165	-2.09112	-0.0978853
7	-0.006851	-0.003075	0.0704457	0.211645	-0.137544	-1.93863	-2.50863	-0.106073
8	-0.005804	0.0080517	0.127006	0.430288	0.489155	-1.29482	-2.84006	-0.109525
9	-0.006851	-0.003075	0.0704457	0.211645	-0.137544	-1.93863	-2.50863	-0.106073
10	-0.009726	-0.033308	-0.0781571	-0.316993	-1.29254	-1.91165	-2.09112	-0.0978853
11	-0.013626	-0.073214	-0.255561	-0.775136	-1.29827	-1.55442	-1.68581	-0.084865
12	-0.017222	-0.107106	-0.366658	-0.689093	-1.0063	-1.19795	-1.28912	-0.0679456
13	-0.018656	-0.113104	-0.278244	-0.491868	-0.715546	-0.847332	-0.9049	-0.0483784
14	-0.015549	-0.072523	-0.166437	-0.29342	-0.425739	-0.501469	-0.531352	-0.0274774
15	-0.004459	-0.019086	-0.0436876	-0.0769012	-0.111258	-0.130125	-0.136398	-0.00602104

20mm Rod — Vertical Displacement due to Loading

Node Number	V1	V1-V2	V1-V3	V1-V4	V1-V5	V1-V6	V1-V7	V1-V8
1	-0.003498	-0.014939	-0.0309696	-0.0471805	-0.0565731	-0.0648122	-0.073631	-0.00516038
2	-0.011328	-0.05279	-0.113737	-0.173947	-0.209714	-0.241635	-0.275987	-0.0196182
3	-0.012824	-0.080753	-0.190614	-0.292367	-0.355291	-0.412733	-0.474973	-0.0350353
4	-0.010134	-0.071995	-0.242373	-0.412535	-0.504042	-0.590149	-0.683981	-0.0496091
5	-0.00598	-0.042018	-0.172943	-0.476182	-0.656609	-0.774067	-0.903596	-0.062288
6	-0.001823	-0.008164	-0.0533413	-0.287358	-0.739117	-0.963699	-1.13332	-0.0720167
7	0.0011484	0.0171332	0.0464786	-0.0610021	-0.54692	-1.11155	-1.37143	-0.0780824
8	0.0022183	0.0263973	0.0844336	0.0333232	-0.4326	-1.09866	-1.56153	-0.0802258
9	0.0011484	0.0171332	0.0464786	-0.0610021	-0.54692	-1.11155	-1.37143	-0.0780824
10	-0.001823	-0.008164	-0.0533413	-0.287358	-0.739117	-0.963699	-1.13332	-0.0720167
11	-0.00598	-0.042018	-0.172943	-0.476182	-0.656609	-0.774067	-0.903596	-0.062288
12	-0.010134	-0.071995	-0.242373	-0.412535	-0.504042	-0.590149	-0.683981	-0.0496091
13	-0.012824	-0.080753	-0.190614	-0.292367	-0.355291	-0.412733	-0.474973	-0.0350353
14	-0.011328	-0.05279	-0.113737	-0.173947	-0.209714	-0.241635	-0.275987	-0.0196182
15	-0.003498	-0.014939	-0.0309696	-0.0471805	-0.0565731	-0.0648122	-0.073631	-0.00516038

30mm Rod — Vertical Displacement due to Loading

Node Number	V1	V1-V2	V1-V3	V1-V4	V1-V5	V1-V6	V1-V7	V1-V8
1	-0.002706	-0.010328	-0.0197217	-0.0264556	-0.0313858	-0.0378028	-0.0441284	-0.0041582
2	-0.008484	-0.037698	-0.0715874	-0.0967777	-0.115619	-0.140084	-0.164331	-0.0153045
3	-0.009287	-0.056448	-0.12038	-0.162775	-0.196523	-0.239944	-0.283275	-0.0270647
4	-0.007123	-0.050189	-0.153049	-0.231845	-0.280761	-0.3455	-0.410354	-0.0382832
5	-0.003678	-0.029865	-0.120356	-0.27551	-0.369061	-0.466132	-0.545105	-0.04806
6	-0.002708	-0.007047	-0.0608129	-0.222012	-0.484138	-0.572107	-0.687062	-0.055561
7	0.0021522	-0.009969	-0.0105838	-0.149833	-0.411013	-0.67296	-0.837314	-0.0602111
8	0.0030231	0.016196	0.008579	-0.119085	-0.390437	-0.694416	-0.95038	-0.0617524
9	0.0021522	-0.009969	-0.0105838	-0.149833	-0.411013	-0.67296	-0.837314	-0.0602111
10	-0.002708	-0.007047	-0.0608129	-0.222012	-0.484138	-0.572107	-0.687062	-0.055561
11	-0.003678	-0.029865	-0.120356	-0.27551	-0.369061	-0.466132	-0.545105	-0.04806
12	-0.007123	-0.050189	-0.153049	-0.231845	-0.280761	-0.3455	-0.410354	-0.0382832
13	-0.009287	-0.056448	-0.12038	-0.162775	-0.196523	-0.239944	-0.283275	-0.0270647
14	-0.008484	-0.037698	-0.0715874	-0.0967777	-0.115619	-0.140084	-0.164331	-0.0153045
15	-0.002706	-0.010328	-0.0197217	-0.0264556	-0.0313858	-0.0378028	-0.0441284	-0.0041582

9. Appendix III: Data of Study 9

a. 10mm Rod Formwork

Load Factor vs Displacement

Load factor	Load (N/mm)	Negative Displacement (mm)	Positive Displacement (mm)	
10	10	-0.218411	0.218411	
20	20	-0.524835	0.524835	
28.4515	28.4515	-0.772397	0.772397	
37.9007	37.9007	-1.06099	1.06099	
45.8866	45.8866	-1.36392	1.36392	
54.8152	54.8152	-1.74528	1.74528	
64.7976	64.7976	-2.28534	2.28534	
74.7976	74.7976	-2.9396	2.9396	
84.7976	84.7976	-3.75028	3.75028	
94.7976	94.7976	-4.80833	4.80833	
104.798	104.798	-6.0365	6.0365	
114.798	114.798	-119.075	119.075	
124.798	124.798	-2.27E+03	2271.55	FAILURE
134.798	134.798	-2.27E+05	227213	
144.798	144.798	-4.17E+06	4168560	

Load Factor vs Stress (SX)

Load factor	Load (N/mm)	Compressive Stress (N/mm2)	
10	10	1.66083	
20	20	3.92186	
28.4515	28.4515	5.77967	
37.9007	37.9007	8.00349	
45.8866	45.8866	9.10537	
54.8152	54.8152	10.3553	
64.7976	64.7976	12.118	
74.7976	74.7976	13.7769	
84.7976	84.7976	15.4051	
94.7976	94.7976	16.8326	
104.798	104.798	17.9063	
114.798	114.798	-6242.42	
124.798	124.798	5535300	FAILURE
134.798	134.798	-67972900	
144.798	144.798	-13719100	

Load Factor vs Reaction at the Support

Load factor	Load (N/mm)	Horizontal Reaction of Left Support (N)	
10	10	2.17E+04	
20	20	4.91E+04	
28.4515	28.4515	6.54E+04	
37.9007	37.9007	8.67E+04	
45.8866	45.8866	1.04E+05	
54.8152	54.8152	1.21E+05	
64.7976	64.7976	1.44E+05	
74.7976	74.7976	1.68E+05	
84.7976	84.7976	1.89E+05	
94.7976	94.7976	2.01E+05	
104.798	104.798	2.10E+05	
114.798	114.798	2.73E+07	
124.798	124.798	2.18E+11	FAILURE
134.798	134.798	9.08E+12	
144.798	144.798	-3.57E+16	

b. 20mm Rod Formwork

Load Factor vs Displacement

Load factor	Load (N/mm)	Negative Displacement (mm)	Positive Displacement (mm)	
10	10	-0.204977	0.204977	
20	20	-0.494914	0.494914	
29.1287	29.1287	-0.737581	0.737581	
39.1287	39.1287	-1.01431	1.01431	
48.2574	48.2574	-1.30356	1.30356	
57.3861	57.3861	-1.64428	1.64428	
67.3861	67.3861	-2.0921	2.0921	
77.3861	77.3861	-2.61536	2.61536	
87.3861	87.3861	-3.22686	3.22686	
97.3861	97.3861	-3.94296	3.94296	
106.515	106.515	-4.72388	4.72388	
116.515	116.515	-5.78059	5.78059	
126.515	126.515	-6.83E+00	6.82797	
136.515	136.515	-5.37E+00	5.36945	FAILURE
146.515	146.515	-7.98E+05	798286	

Load Factor vs Stress (SX)

Load factor	Load (N/mm)	Compressive Stress (N/mm2)	
10	10	1.58263	
20	20	3.76383	
29.1287	29.1287	5.60996	
39.1287	39.1287	7.78388	
48.2574	48.2574	9.02164	
57.3861	57.3861	10.1505	
67.3861	67.3861	11.5595	
77.3861	77.3861	12.9023	
87.3861	87.3861	14.3363	
97.3861	97.3861	15.7086	
106.515	106.515	16.8158	
116.515	116.515	17.8219	
126.515	126.515	18.4113	
136.515	136.515	-3.95893	FAILURE
146.515	146.515	-1758740000	

Load Factor vs Reaction at the Support

Load factor	Load (N/mm)	Horizontal Reaction of Left Support (N)	
10	10	2.03E+04	
20	20	4.33E+04	
29.1287	29.1287	5.78E+04	
39.1287	39.1287	7.78E+04	
48.2574	48.2574	9.57E+04	
57.3861	57.3861	1.12E+05	
67.3861	67.3861	1.31E+05	
77.3861	77.3861	1.50E+05	
87.3861	87.3861	1.69E+05	
97.3861	97.3861	1.85E+05	
106.515	106.515	1.95E+05	
116.515	116.515	2.01E+05	
126.515	126.515	1.78E+05	
136.515	136.515	1.24E+05	FAILURE
146.515	146.515	-4.94E+12	

c. 30mm Rod Formwork

Load Factor vs Displacement

Load factor	Load (N/mm)	Negative Displacement (mm)	Positive Displacement (mm)	
10	10	-0.19155	0.19155	
20	20	-0.454731	0.454731	
30	30	-0.697675	0.697675	
40	40	-0.942321	0.942321	
50	50	-1.20448	1.20448	
60	60	-1.5196	1.5196	
70	70	-1.89269	1.89269	
80	80	-2.31658	2.31658	
90	90	-2.80496	2.80496	
100	100	-3.35588	3.35588	
102.5	102.5	-3.51575	3.51575	
107.5	107.5	-3.83845	3.83845	
117.5	117.5	-4.54E+00	4.53566	
127.5	127.5	-5.34E+00	5.33596	
137.5	137.5	-6.29E+00	6.29141	
147.5	147.5	-7.01E+00	7.01402	
150	150	2.17E+01	-21.7102	FAILURE

Load Factor vs Stress (SX)

Load factor	Load (N/mm)	Compressive Stress (N/mm2)	
10	10	1.5052	
20	20	3.5351	
30	30	5.4313	
40	40	7.3084	
50	50	8.8121	
60	60	9.7487	
70	70	11.0241	
80	80	12.2777	
90	90	13.5393	
100	100	14.7706	
102.5	102.5	15.0680	
107.5	107.5	15.6524	
117.5	117.5	16.7274	
127.5	127.5	17.5967	
137.5	137.5	18.2468	
147.5	147.5	18.6230	
150	150	-62.5035	FAILURE

Load Factor vs Reaction at the Support

Load factor	Load (N/mm)	Horizontal Reaction of Left Support (N)	
10	10	1.91E+04	
20	20	3.76E+04	
30	30	4.90E+04	
40	40	6.56E+04	
50	50	8.15E+04	
60	60	9.65E+04	
70	70	1.12E+05	
80	80	1.27E+05	
90	90	1.44E+05	
100	100	1.59E+05	
102.5	102.5	1.62E+05	
107.5	107.5	1.67E+05	
117.5	117.5	1.74E+05	
127.5	127.5	1.79E+05	
137.5	137.5	1.68E+05	
147.5	147.5	9.37E+04	
150	150	-9.47E+06	FAILURE

10. Appendix IV: Data of Study 10

a. Traditional arch with mortar joint

Load Factor vs Displacement

Load factor	Load (N/mm)	Negative Displacement (mm)	Positive Displacement (mm)	
1	1	-0.0236931	0.0236931	
2	2	-0.0473897	0.0473897	
3	3	-0.0710898	0.0710898	
4	4	-0.094958	0.094958	
5	5	-0.119896	0.119896	
6	6	-0.146402	0.146402	
7	7	-0.176934	0.176934	
8	8	-0.214077	0.214077	
9	9	-0.290411	0.290411	
10	10	-0.364809	0.364809	
11	11	-6.10703	6.10703	
12	12	620.91	-620.91	
13	13	-5.22E+03	5223.41	FAILURE
14	14	1.58E+04	-15779.7	
15	15	-7.67E+03	7667.59	

Load Factor vs Stress (SX)

Load factor	Load (N/mm)	Compressive Stress (N/mm2)	
1	1	0.16886	
2	2	0.337738	
3	3	0.506636	
4	4	0.676081	
5	5	0.849007	
6	6	1.02721	
7	7	1.22076	
8	8	1.41523	
9	9	1.68421	
10	10	1.91856	
11	11	14.9344	
12	12	-168.273	
13	13	638.402	FAILURE
14	14	-998.492	
15	15	-10205.4	

Load Factor vs Reaction at the Support

Load factor	Load (N/mm)	Horizontal Reaction of Left Support (N)	
1	1	2.28E+03	
2	2	4.56E+03	
3	3	6.84E+03	
4	4	9.16E+03	
5	5	1.16E+04	
6	6	1.29E+04	
7	7	1.43E+04	
8	8	1.63E+04	
9	9	2.09E+04	
10	10	6.72E+04	
11	11	1.17E+06	
12	12	-6.07E+11	
13	13	4.38E+08	FAILURE
14	14	4.57E+08	
15	15	-2.57E+09	

b. Arch with steel joint

Load Factor vs Displacement

Load factor	Load (N/mm)	Negative Displacement (mm)	Positive Displacement (mm)	
5	5	-0.108536	0.108536	
10	10	-0.225561	0.225561	
15	15	-0.401569	0.401569	
20	20	-0.545852	0.545852	
25	25	-0.692067	0.692067	
30	30	-0.845046	0.845046	
35	35	-1.00918	1.00918	
40	40	-1.19779	1.19779	
45	45	-1.41206	1.41206	
50	50	-1.6324	1.6324	
55	55	-1.88924	1.88924	
60	60	-2.18177	2.18177	
65	65	-2.51E+00	2.51293	
70	70	-2.89E+00	2.88585	
75	75	-3.31E+00	3.30601	
80	80	-3.80E+00	3.80027	
85	85	-4.40E+00	4.40263	
90	90	-5.22E+00	5.21732	
95	95	-6.30E+00	6.29683	
100	100	5.85E+00	-5.8463	FAILURE

Load Factor vs Stress (SX)

Load factor	Load (N/mm)	Compressive Stress (N/mm2)	
5	5	0.502053	
10	10	1.04769	
15	15	1.97451	
20	20	2.72588	
25	25	3.44417	
30	30	4.18278	
35	35	4.94077	
40	40	6.00598	
45	45	7.56582	
50	50	8.69066	
55	55	9.48004	
60	60	10.0969	
65	65	10.7471	
70	70	11.3733	
75	75	12.0359	
80	80	12.8072	
85	85	13.8057	
90	90	15.1433	
95	95	16.7464	
100	100	-305.761	FAILURE

Load Factor vs Reaction at the Support

Load factor	Load (N/mm)	Horizontal Reaction of Left Support (N)	
5	5	1.09E+04	
10	10	2.40E+04	
15	15	4.17E+04	
20	20	5.16E+04	
25	25	6.43E+04	
30	30	7.67E+04	
35	35	8.87E+04	
40	40	9.98E+04	
45	45	1.11E+05	
50	50	1.21E+05	
55	55	1.34E+05	
60	60	1.46E+05	
65	65	1.59E+05	
70	70	1.72E+05	
75	75	1.83E+05	
80	80	1.92E+05	
85	85	1.97E+05	
90	90	1.92E+05	
95	95	1.88E+05	
100	100	-6.47E+04	FAILURE

c. 20mm Rod Formwork

Load Factor vs Displacement

Load factor	Load (N/mm)	Negative Displacement (mm)	Positive Displacement (mm)	
10	10	-0.204977	0.204977	
20	20	-0.494914	0.494914	
29.1287	29.1287	-0.737581	0.737581	
39.1287	39.1287	-1.01431	1.01431	
48.2574	48.2574	-1.30356	1.30356	
57.3861	57.3861	-1.64428	1.64428	
67.3861	67.3861	-2.0921	2.0921	
77.3861	77.3861	-2.61536	2.61536	
87.3861	87.3861	-3.22686	3.22686	
97.3861	97.3861	-3.94296	3.94296	
106.515	106.515	-4.72388	4.72388	
116.515	116.515	-5.78059	5.78059	
126.515	126.515	-6.83E+00	6.82797	
136.515	136.515	-5.37E+00	5.36945	FAILURE
146.515	146.515	-7.98E+05	798286	

Load Factor vs Stress (SX)

Load factor	Load (N/mm)	Compressive Stress (N/mm2)	
10	10	1.58263	
20	20	3.76383	
29.1287	29.1287	5.60996	
39.1287	39.1287	7.78388	
48.2574	48.2574	9.02164	
57.3861	57.3861	10.1505	
67.3861	67.3861	11.5595	
77.3861	77.3861	12.9023	
87.3861	87.3861	14.3363	
97.3861	97.3861	15.7086	
106.515	106.515	16.8158	
116.515	116.515	17.8219	
126.515	126.515	18.4113	
136.515	136.515	-3.95893	FAILURE
146.515	146.515	-1758740000	

Load Factor vs Reaction at the Support

Load factor	Load (N/mm)	Horizontal Reaction of Left Support (N)	
10	10	2.03E+04	
20	20	4.33E+04	
29.1287	29.1287	5.78E+04	
39.1287	39.1287	7.78E+04	
48.2574	48.2574	9.57E+04	
57.3861	57.3861	1.12E+05	
67.3861	67.3861	1.31E+05	
77.3861	77.3861	1.50E+05	
87.3861	87.3861	1.69E+05	
97.3861	97.3861	1.85E+05	
106.515	106.515	1.95E+05	
116.515	116.515	2.01E+05	
126.515	126.515	1.78E+05	
136.515	136.515	1.24E+05	FAILURE
146.515	146.515	-4.94E+12	

11. Appendix V: Data of Study 11

Study 11: Real life Application for a 5KN/m2 Live load

	Job Title: : A comparative analysis between Finite element analysis and Heyman's Funicular Polygon	Date : 01/06/23
Calculation Sheets	Worked by: Rebecca Mifsud	Sheet 1 of 1

1. Determining the Applied Load (KN/m)

Dead Load	a. Density of Materials (KN/m3)	b. Thickness (m)	c. Width (m)	Unfactored UDL Load (KN/m)	Factored UDL Load (KN/m)
Reconstituted Stone	22.5	0.24	0.25	1.35	1.8225
Torba	1.15	0.15	0.25	0.043125	0.05821875
Tiles	15	0.01	0.25	0.0375	0.050625

Live Load	a. Load (KN/m2)	NA	c. Width (m)	Unfactored UDL Load (KN/m)	Factored UDL Load (KN/m)
Category C	5		0.25	1.25	1.875

Total Load	Unfactored UDL Load (KN/m)	Factored UDL Load (KN/m)
	2.680625	3.80634375

2. Dividing the Load in Point Loads for the Heyman Analysis

Number of Voussoirs	15	KN
Span	3	m
Point Load / Voussoir	0.76126875	KN

Funicular Polygons for the Horizontal reactions of 10-30KN

a. Horizontal Reaction of 10KN

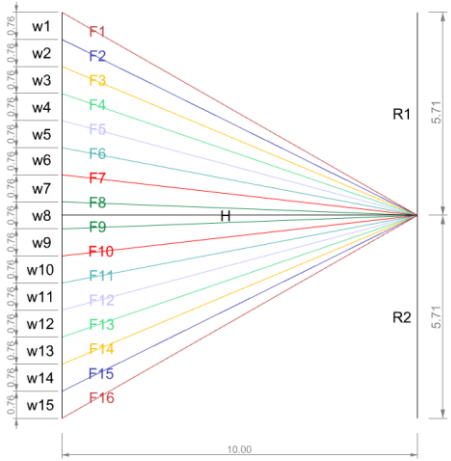

b. Horizontal Reaction of 15KN

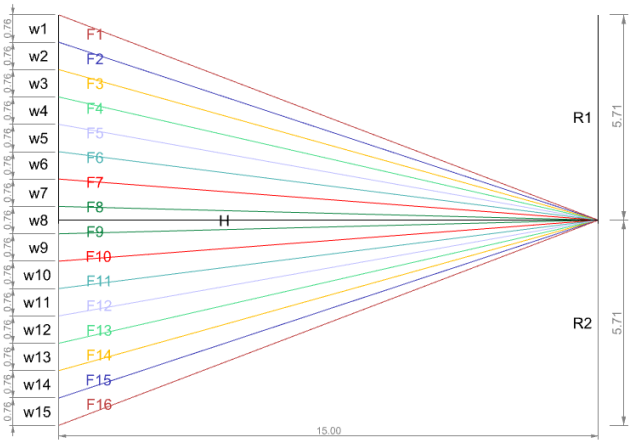

c. Horizontal Reaction of 20KN

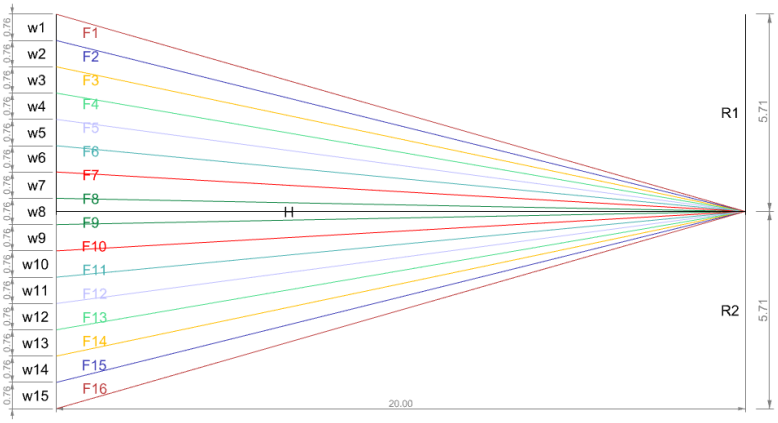

d. Horizontal Reaction of 25KN

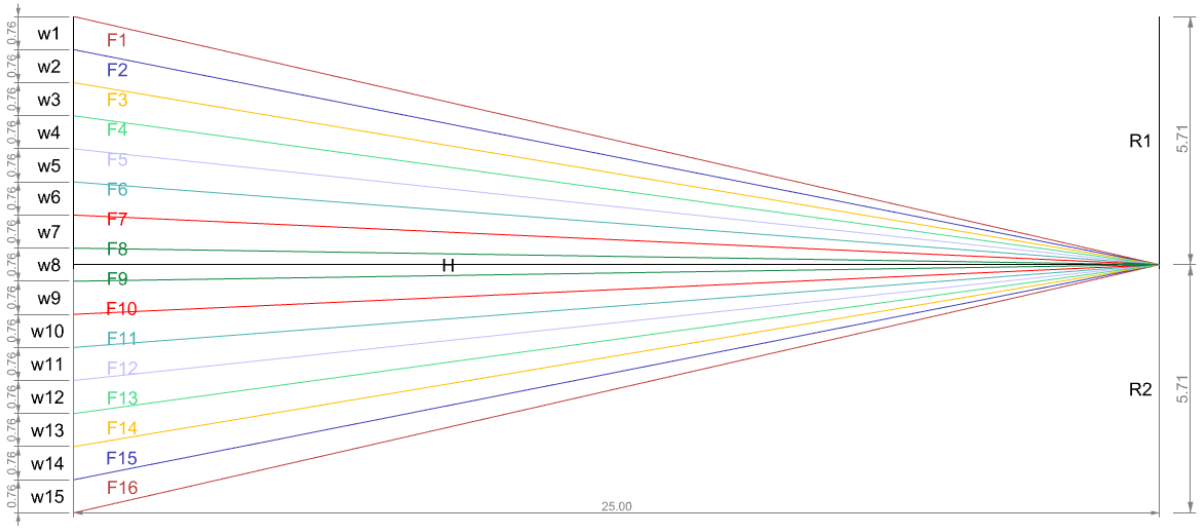

e. Horizontal Reaction of 30KN